Copy
RM L9G07

NACA RM L9G07

CLASSIFICATION CHANGED
TO UNCLASSIFIED
By authority of N.A.C.A. per letter from 1374 Date 4/13/53
4/13/53

RESEARCH MEMORANDUM

ANALYTICAL AND EXPERIMENTAL INVESTIGATION OF 90° SUPERSONIC TURNING PASSAGES SUITABLE FOR SUPERSONIC COMPRESSORS OR TURBINES

By Luke L. Liccini

Langley Aeronautical Laboratory
Langley Air Force Base, Va.

CLASSIFIED DOCUMENT

This document contains classified information affecting the National Defense of the United States within the meaning of the Espionage Act, USC 50:31 and 32. Its transmission or the revelation of its contents in any manner to an unauthorized person is prohibited by law. Information so classified may be imparted only to persons in the military and naval services of the United States, appropriate civilian officers and employees of the Federal Government who have a legitimate interest therein, and to United States citizens of known loyalty and discretion who of necessity must be informed thereof.

NATIONAL ADVISORY COMMITTEE
FOR AERONAUTICS

WASHINGTON
September 12, 1949

UNCLASSIFIED

NASA Technical Library
3 1176 01436 7610

NACA RM L9G07

NATIONAL ADVISORY COMMITTEE FOR AERONAUTICS

RESEARCH MEMORANDUM

ANALYTICAL AND EXPERIMENTAL INVESTIGATION OF 90° SUPERSONIC TURNING PASSAGES SUITABLE FOR SUPERSONIC COMPRESSORS OR TURBINES

By Luke L. Liccini

SUMMARY

Four 90° two-dimensional turning passages designed by the method of characteristics were tested at an inlet Mach number of 1.71. The measured losses varied from 5 to 15 percent of the inlet stagnation pressure. The smallest loss was obtained for a passage in which separation on the convex surface was minimized through the introduction of a favorable pressure gradient.

INTRODUCTION

Reference 1 presents several schemes of supersonic compressors, one of which would give high values of compression ratio if supersonic turning and diffusing problems related to the rotor and stator design could be solved. For such a compressor, the stream enters the rotor at a relative supersonic velocity and undergoes a large change of direction in the rotor. Leaving the rotor, the air then enters the stator at a high supersonic velocity and is diffused in the stator to subsonic velocity. A more detailed analysis of this type of compressor is presented in reference 2. The analysis in reference 2 shows that with a variable-geometry stator, a stage compression ratio of the order of 6 to 10 may be obtained with an adiabatic efficiency ranging from 75 to 80 percent, provided that a turning angle of the order of 90° can be accomplished in the rotor without large losses for an entrance Mach number of about 1.70. In view of the interesting possibilities indicated by the analysis of reference 2, a preliminary investigation was conducted at the Langley Aeronautical Laboratory in order to determine criterions for the design of an efficient supersonic rotor

UNCLASSIFIED

passage employing a 90° turn. It may be noted that the problem of an efficient turn of this magnitude arises also in the design of turbines with relative supersonic entrance velocities.

In the present investigation, four turning-passage designs having different aerodynamic design criterions were analyzed and tested by means of the stationary cascade technique. For the design conditions of the rotor considered, all of the waves generated by the blades are contained inside the passage (reference 2), and no interference exists between different passages; therefore, in the cascade tests, only a single passage was reproduced in order to simulate the conditions of the rotor. For each passage, the velocity distribution and the losses in stagnation pressure were measured at the exit. Because of the large curvature, the boundary-layer effects were expected to be large; however, the nature and magnitude of these effects were not known beforehand and were taken into consideration as the tests proceeded.

Reference 2 shows that a compression in the rotor rather than an expansion is desirable. For some practical velocity diagrams, in rotor passages with constant span, the exit velocity is larger than the entrance velocity; therefore, as stated in reference 2, use of a converging annulus is desirable to achieve compression in the rotor. For this reason, in this preliminary investigation, tests were also made in which the span was decreasing along the passage.

The analysis of reference 2 indicates that the possibility of obtaining, at the starting conditions, variation of entrance velocity and rotational speed of the supersonic compressor considered depends upon the flow in the vicinity of the sharp leading edge of the rotor blade when a detached shock is present in front of the blade. Additional tests were thus made with the blade set at high angles of attack that may correspond to operating conditions other than the design condition.

Because of the many variables involved and because no previous similar experimental results were available, this investigation has been directed toward understanding the general phenomena related to the problem rather than toward developing specific blade designs. The information obtained, however, can be applied directly to blade designs of practical interest and can be used in different velocity diagrams and for different values of turning angle.

[redacted]

SYMBOLS

c	blade chord (fig. 1)
h	distance between blades normal to stream (fig. 1)
m	mass flow
p	static pressure
s	blade spacing (fig. 1)
t	maximum thickness of blade
A	area normal to the stream
M	Mach number
P	stagnation pressure
V	velocity
α	angle of attack, degrees
δ	deviation of flow from stream direction, degrees
T	temperature ($^{\circ}$F, absolute)
c/s	solidity
t/c	thickness ratio

Subscripts:

o	absolute inlet stagnation condition
1	entrance condition
2	exit condition
av	average condition
A	atmospheric condition

[redacted]

AERODYNAMIC DESIGN OF THE EXPERIMENTAL TURNING PASSAGES

In the design of a channel to represent a blade passage that can be used in a supersonic compressor of the type discussed in the INTRODUCTION, preliminary considerations indicated that the following requirements should generally be fulfilled for the design operating conditions of the compressor: The air that enters the passage at supersonic speed must change direction very rapidly in order to avoid high solidity in the rotor blades; the shape of the convex and concave surfaces of the passage must give a blade shape of practical thickness; the disturbances in the flow produced by the passage must be confined inside the passage; the exit velocity must be of the same order of magnitude as the entrance velocity, or possibly smaller; and the blade spacing at the entrance and exit must be equal in order to give sharp-edge blades.

These requirements impose some limitations on the passage design and also fix some of the parameters that must be investigated in a further analysis. For example, the blade chord relative to the blade spacing (fig. 1) for a given turning angle is a function of the difference in stream velocity between the two curved surfaces of the passage, and the blade solidity decreases as the difference in stream velocity between the convex and concave surfaces of the passage increases. The thickness ratio of the blade corresponding to the passage is a function of the curvature of the passage, of the velocity distribution along the passage, and of the stagger angle.

Because the axial velocity is usually subsonic (subsonic flow in front of the rotor) in all the passages considered the convex surface was designed parallel to the relative stream direction in the zone of the leading edge. Only when the entrance velocity component in a normal direction to the plane of rotation is larger than the speed of sound can waves be produced at the leading edge of the convex surface. If, therefore, a wedge of finite physical dimensions is to be obtained at the leading edge of the blade, the concave surface at the leading edge must be inclined to the undisturbed stream direction. If no disturbances are to be transmitted upstream from the passage (the disturbances in the flow produced by the passage must be confined inside the passage), the shock must start at the leading edge of the concave surface, and, therefore, must be inside the passage.

In the design of the turning passage, the characteristics system was used to determine the flow field in the passage. When compression waves were introduced, the flow still was assumed to be potential flow. This assumption was considered justified because the Mach number variation in the passage was small in most cases.

[redacted]

The detailed considerations in the design of the four turning passages and wedge model investigated are discussed in the following sections. The coordinates of the blades represented by the various turning-passage models are given in table I and the primary geometrical parameters of the blades are summarized in table II.

Model 1.- Model 1 was considered a preliminary design which could be tested to give an indication of the basic aerodynamic phenomena that would aid in the development of succeeding designs. The turn was very gradual and resulted in a rather thin blade which may be of little interest for practical considerations.

Figure 2(a) presents the theoretical Mach number distribution at the convex and concave surfaces as a function of the percent of chord for model 1. In figure 3(a) the same Mach number distribution is given as a function of the surface angle along the passage.

The characteristics net for model 1 is shown in figure 4. For the design of this model, the following arbitrary conditions were chosen: At a design entrance Mach number of 1.71 the leading edge of the concave surface was designed to produce a 4° shock; the leading edge of the convex surface was designed to be parallel to the stream direction; compression waves were produced at the concave surface and expansion waves at the convex surface; the initial shock wave and the subsequent compression waves were reflected at the convex surface as expansion waves; and the intensity of the expansion and compression waves was fixed in order to obtain a constant difference in velocity between the two surfaces corresponding to an expansion from $M = 1.50$ to $M = 1.99$.

Along the concave surface the velocity at the 12-percent-chord station reached a minimum of $M = 1.50$ and remained constant to the 83-percent-chord station. (See figs. 2(a) and 3(a).) At this station, expansion waves from the convex surface were neutralized. In this way, the velocity at the 100-percent-chord station was increased to $M = 1.71$. At the convex surface the velocity was increased at first and attained a value of $M = 1.99$ at the 23-percent-chord station and remained constant to the 83-percent-chord station. From the 83-percent to the 100-percent-chord station only the compression waves from the concave surface were neutralized, and the velocity decreased to $M = 1.71$. It may be noted that the cross section of the channel remained constant from the 23-percent to the 83-percent-chord station. For the design conditions, the Mach number at the exit was uniform and equal to the entrance Mach number. The area ratio A_2/A_1 for this design condition was 1.00.

In order to investigate the effects of small positive and negative pressure gradients along the passage, tests were made with different area ratios ranging from 0.96 to 1.29. The area ratios (and stagger

[redacted]

angles) were varied by moving the concave surface in a direction parallel to the undisturbed stream; thus a gradual increase and decrease was introduced in cross-sectional area along the passage. Because the convex surface near the leading edge was parallel to the stream direction, the passage can be used for blade designs of rotors with different velocity diagrams. In figure 5 some possible blade designs are shown, and the principal geometric parameters are shown in table II.

Model 2.- The characteristics net for model 2 is presented in figure 6. In order to increase the thickness ratio and decrease the solidity as compared with those for model 1, the following different design conditions were chosen: A 10° shock instead of a 4° shock was introduced at the leading edge of the concave surface and thus more expansion waves were introduced at the convex surface in front of the shock in order to facilitate the reflection of the shock; also, the difference between the velocities at the two surfaces was made larger than for model 1.

At the concave surface the Mach number behind the shock was 1.36 and increased to 1.50 at the 15-percent-chord station. (See figs. 2(b) and 3(b).) From the 15-percent-chord station to the 85-percent-chord station the Mach number remained constant. From the 85-percent to the 100-percent-chord station the expansion waves from the convex surface were neutralized, and the Mach number at the concave surface increased to 1.77. At the convex surface, expansion waves were produced up to the 17-percent-chord station where the Mach number reached a value of 2.21. The shock from the leading edge of the concave surface met the convex surface at this station, and the value of the Mach number dropped to 1.64; however, more expansions were introduced behind the 17-percent-chord station, and the Mach number increased to a value of 2.13 at the 38-percent-chord station. From the 38-percent to the 70-percent-chord station, the Mach number remained constant. From the 70-percent to the 100-percent-chord station, the compression waves from the concave surface were neutralized, and the Mach number decreased to a value of 1.77. The design Mach number at the exit was uniform and was selected to be slightly larger than the entrance Mach number to compensate for the boundary-layer growth along the convex surface as observed in tests of model 1. It may be noted that the cross section of the channel remained constant from the 38-percent to the 70-percent-chord station. For the design conditions the area ratio A_2/A_1 was 1.077.

Tests were made for various values of area ratio (ranging from 1.028 to 1.421), obtained in the same manner as for model 1. Also because the convex surface was designed parallel to the stream direction in the region of the leading edge, the passage can be used for blade designs of rotors with different velocity diagrams. In figure 7 some possible blade designs are shown, and the principal geometric parameters are shown in table II.

Model 3.- For models 1 and 2 the cross section of the channel was maintained about constant over a large part of the passage. In model 3 a contraction of the channel was introduced. This contraction permitted the thickness ratio of the blade to be increased and also introduced a favorable pressure gradient along the convex surface in the region where the flow tended to separate as observed in tests of models 1 and 2. This pressure gradient remained favorable until 70° turning was accomplished. (See figs. 2(c) and 3(c).)

The characteristics net for model 3 is presented in figure 8. A 10° shock was produced at the leading edge of the concave surface. This shock was followed by compression waves, and the Mach number decreased to a value of 1.14 at the 20-percent-chord station and remained constant to the 50-percent-chord station. (See figs. 2(c) and 3(c).) From the 50-percent to the 100-percent-chord station the Mach number was increased gradually to a value of 1.76 at the 100-percent-chord station. At the leading edge of the convex surface, a straight section was extended to the 5-percent-chord station, after which expansions were introduced and the Mach number increased to a value of 2.13 at the 23-percent-chord station. The shock wave from the leading edge of the concave surface met the convex surface at this point, and the Mach number dropped to a value of 1.50. More expansions were gradually introduced, and the Mach number increased to a maximum value of 2.04 at the 60-percent-chord station and then gradually decreased to a value of 1.76 at the 100-percent-chord station. The Mach number at the exit was uniform.

In this design the blade has a much larger thickness ratio than the preceding blades, and the solidity is smaller. (See table II.) The concave surface was not moved in tests of model 3. The design area ratio A_2/A_1 is 1.208. Figure 9 illustrates a possible blade design represented by model 3.

Model 4.- If the expansion in front of the shock along the convex surface is very large, the curvature of the blade increases, the solidity decreases, and the thickness ratio of the blade increases. Model 4 was therefore designed to determine the effect of a large increase in the initial rate of expansion and total expansion along the convex surface ahead of the zone in which compression waves produced by the concave surface meet the concave surface and, therefore, in this manner determine the effect of a large curvature on the separation that was observed to occur in this zone.

The characteristics net for model 4 is shown in figure 10(a). In model 4 a strong shock of 15° was introduced at the leading edge of the concave surface that reduced the speed from $M = 1.71$ to $M = 1.35$, and further compression reduced the Mach number to 1.07 at the 10-percent-chord station. (See figs. 2(d) and 3(d).) The Mach number

[redacted]

then gradually increased until, at the 100-percent-chord station, a value of 1.75 was reached. At the convex surface a strong expansion was introduced, and the maximum theoretical Mach number attained is 3.70 at the 25-percent-chord station. In the actual flow a local separation was expected to occur which would reduce the local expansion. The expansion was followed by a zone of compression in which the velocity decreased to a value of 1.70 at the 35-percent-chord station. From the 35-percent to the 100-percent-chord station the Mach number was gradually increased to a value of 2.08, which value is higher than that necessary for the concave surface to compensate for the expected large separation. In the actual case, the boundary layer effectively changes the curvature on the convex surface, and, therefore, the expansion would be expected to be less.

After the tests of the original configuration (fig. 10(a)), model 4 was slightly modified in order to decrease the zone of separation obtained in the tests. In figure 10(b) the characteristics net for the modified configuration tested is presented. In this characteristics net, a zone of local separation at a point ahead of the shock reflection has been assumed in order to analyze the effects of the separation on the local expansion in the zone ahead of the shock. The maximum Mach number ahead of the shock at the convex surface is 2.34 and decreases to 2.25 behind the shock along the convex surface. (See figs. 2(e) and 3(e).) From the 30-percent to the 80-percent-chord station the Mach number remained constant and then decreased to a value of 2.15 at the 100-percent-chord station. The Mach number after the compression (along the concave surface) was 1.04 and then increased to 1.94 at the 100-percent-chord station. Blade profiles corresponding to the passage of figures 10(a) and 10(b) are shown in figure 11.

Variable-span models.- Model 2 was used to investigate the effect of a contraction of the annulus of the rotor in a spanwise direction. In the first configuration (shown in fig. 12) the fairing introduced along one side wall starting at the 30-percent-chord station gave a gradual spanwise contraction. The fairing was so chosen that the area ratio A_2/A_1 was equal to 1.00. A second fairing configuration (fig. 13) was made in order to determine the effect of a spanwise pressure gradient such as would be expected in the actual rotor. In this design, the variation of area along the passage was introduced by filling one of the corners of the passage between the convex surface and one side wall. This filling started at the 30-percent-chord station and gradually increased in size so that at the exit of the passage the area ratio $\frac{A_2}{A_1} = 1.016$.

Model used for detached shock.- For some starting conditions of the compressor scheme described in reference 2, variations in entrance

[redacted]

velocity and rotational speed may occur and, for a rotor passage such as that considered herein, a detached shock will be produced in front of the blade by one of the blade surfaces. For this case of detached shock, it is of interest to determine whether the velocity at the other surface of the blade, along which expansion would occur, produces the same order of Mach number that would exist if the shock wave were attached at the lower surface. Previous experience has shown this to be the case for moderate flow deviations beyond that for shock attachment (reference 3); however, no evidence is available as to whether this result would hold for much larger flow deviation resulting in a very strong detached shock; therefore, tests were made with a wedge at high angles of attack.

The concave surface block of model 2 was used in the tests of a wedge with detached shock. The upper surface of this block was arbitrarily shaped for test convenience. The lower surface was designed in accordance with the previous explanation for model 2.

APPARATUS AND TEST METHODS

The tests of the turning passages were made in one of the blowdown jets of the Langley Gas Dynamics Section. The apparatus consisted of a nozzle and a model especially adapted to simulate the passage between rotor blades. High-pressure air was throttled to the desired stagnation pressure in the settling chamber and discharged through a two-dimensional nozzle and a turning passage to the atmosphere. The test section of this nozzle had a span of 2 inches and a height of 1.5 inches. A pressure survey made at the test section indicated the measured Mach number to be uniform at a value of 1.71. Figure 14 is a photograph of model 2 mounted in the test setup. Figure 15 is a more detailed photograph of the same setup. Both photographs were made with one side wall removed.

The models of the turning passages were constructed of two metal blocks, each separately supported to the side walls in such a way that a change in the relative positions of the surfaces could be easily obtained by moving the concave surface. In the test setup, a "bleed-off" is provided at the entrance of the passage to prevent the boundary layer at the top and bottom of the nozzle from entering the passage. (See fig. 15.) The boundary layer along the side walls was not eliminated and thus entered the passage. In the actual rotor, boundary layer exists at the surfaces between the roots and between the tips of the blade sections, which correspond to the side walls in the cascade setup. The surface between the root sections rotates with the blades, and it follows that the velocity component influencing the boundary layer at this surface is the same as was indicated by the

cascade tests. The surface between the tip sections does not rotate with the rotor, and the velocity component influencing the boundary layer is the axial velocity. In the cascade tests, however, the velocity component is the relative velocity component, which is larger than the axial velocity and, therefore, the boundary-layer effects of the cascade tests are slightly exaggerated compared with those of the actual rotor.

The variation of Reynolds number of these tests was small and the average value based on the chord of the passage was 9.16×10^6. The span of each turning passage was 2 inches. The ratio of blade chord to span was much greater than would be considered in the design of a rotor, and, therefore, the effect of the boundary layer on the side walls may again be somewhat exaggerated in these tests. A large span was not possible in the experimental apparatus used; however, the large value of the chord facilitated the test measurements of the aerodynamic properties of the passage.

Conventional schlieren photographs and shadowgraphs were obtained of the flow along the passage in addition to the pressure survey at the exit of each passage. The pressure surveys for models 1, 2, and 3 were taken in a zone where the velocity was expected to be uniform from the nonviscous theoretical considerations. The pressure survey for model 4 was taken in a zone of nonuniform flow. The characteristics net for model 4 was made without canceling the compression and expansion waves because of the large expected boundary-layer separation which would annul any theoretical calculations of the flow.

In model 1 a survey of static and total pressures was made at one station by using a fixed rake placed at the 50-percent-span station. It was found in tests of model 1 that the boundary layer collected in the center of the span and that a single fixed rake could not be expected to indicate a sufficiently accurate average of the flow in the passage. For tests of model 2, the survey of static and total pressures was made at two stations by using two fixed rakes, one placed at the 50-percent-span station, and one placed at the 10.15-percent-span station of the passage. The position of the rakes and a schematic drawing of the setup for models 1 and 2 are shown in figure 16.

Because of the uncertainty of the stream direction at the exit, the static pressure for model 2 was also determined by placing the static tubes at a slight inclination to the axis of the passage and parallel to the surface. No appreciable difference was obtained. Because a large variation of stagnation-pressure recovery and of Mach number along the span was found in the tests of model 2, the survey in models 3 and 4 was made at three spanwise stations. In order to obtain pressure data close to the surfaces, two types of movable rakes

having opposite positions of static- and total-pressure tubes were used, together with the fixed rakes previously used. In this way, a larger number of points were measured for each station investigated, and a more accurate measure of the spanwise distribution of pressure was obtained. The position of the surveys for models 3 and 4 are shown in figure 17.

In all tests the value of the static pressure at the entrance of the passage could be changed by changing the stagnation pressure, and since the flow of the passage discharges into the atmosphere, compression or expansion waves can be produced at the exit of the passage by changing the test stagnation pressure. The existence of compression waves or expansion waves at the exit of the passage can change somewhat the phenomena in the boundary layer upstream in the passage and also the extent of the separation region. In practical applications for steady conditions the static pressure outside of each section of the rotor should probably be equal to the average static pressure at the exit of the section considered (reference 2). In the tests of models 1, 3, and 4, the static pressure was therefore maintained about equal to the average static pressure at the exit. For model 2, some tests were made with different values of exit pressure to determine the importance of this parameter. Because its value was not known before the tests, the static pressure at the exit of the passage in all the tests of models 1, 3, and 4 was not exactly equal to the atmospheric pressure. The exit static pressure is a function of the exit Mach number, which, relative to the theoretical value, is influenced by the boundary layer. Before each test a preliminary estimate was made, and when the difference between the estimated pressure and average final pressure measured was large, the inlet pressure was adjusted to give the correct exit pressure.

From the measured static pressure and the pressure indicated by a pitot tube, the local values of Mach number were obtained. The stagnation pressure was then determined from the Mach number and pitot-tube pressures. The Mach number and stagnation pressure were used to calculate the average Mach number and the average stagnation pressure. The average stagnation pressure and the average Mach number were computed in reference to the unit mass flow and are given by the following expressions:

$$P_{2_{av}} = \frac{1}{m} \int_{A_2} P_2 \, dm$$

[redacted]

$$\frac{P_{2_{av}}}{P_o} = \frac{\int_{A_2}\left[M_2 \frac{P_2}{P_o}\frac{p_2}{P_o}\sqrt{\frac{T_o}{T_2}}\right]dh_2}{\int_{A_2}\left[M_2 \frac{p_2}{P_o}\sqrt{\frac{T_o}{T_2}}\right]dh_2}$$

$$M_{2_{av}} = \frac{1}{m}\int_{A_2} M_2 \, dm$$

$$\frac{M_{2_{av}}}{M_1} = \frac{\int_{A_2}\left[M_2 \frac{M_2}{M_1}\frac{p_2}{P_o}\sqrt{\frac{T_o}{T_2}}\right]dh_2}{\int_{A_2}\left[M_2 \frac{p_2}{P_o}\sqrt{\frac{T_o}{T_2}}\right]dh_2}$$

In the test with two rakes, the average values of Mach number ratio and pressure ratio were computed with the mass flow, calculated from measurements at each rake, considered as half of the total mass flow. In the tests with three rakes the mass flow measured by each rake, used in the average calculation among the rakes, was considered as a third of the total mass flow.

The wedge used in the detached-shock test was the concave surface block of model 2 and was tested in the same experimental setup by changing the inclination of the block with respect to the stream direction. Pressure measurements and shadowgraph observations of the flow were made along the upper surface of the block. The relation between the upper surface, nozzle blocks, and blade shape, as well as the general test setup, are shown in figure 18.

Model 2 was used for the test setup of the three-dimensional tests. Two fixed rakes, one at the 50-percent-span station and one at the 10.15-percent-span station were used for pressure measurements. The planes of survey for these tests were the same as for model 2, shown in figure 16.

RESULTS AND DISCUSSION

Model 1.- Figure 19 shows the exit Mach number distribution along the 50-percent-span station of the passage of model 1 for three positions of the concave surface corresponding to $\frac{A_2}{A_1} = 1.197$, 1.105, and 1.012; figure 20 presents the local stagnation-pressure-recovery distribution for the same three values.

The Mach number and stagnation-pressure distributions indicate that, in the zone near the convex surface, a separation occurs with subsonic flow. Also, from the schlieren observations, waves were found in the zone in which the pressure survey indicates a separation. It appears, therefore, that a nonuniform velocity distribution must also be expected across the span of the passage as a result of the boundary layer from the side walls; consequently, in tests of the other turning passages, the survey was conducted in more than one spanwise plane. The data for models 2, 3, and 4 show that a velocity gradient along the span does exist and that the boundary layer tends to collect at the 50-percent-span station. The midspan station is thus the station at which the largest losses are expected, and it follows that measurements made at this station do not represent the average values for the passage. These results, however, do give a conservative indication of the performance of this passage.

Figure 21 gives the ratio $\frac{M_{2_{av}}}{M_1}$ (the ratio of the average exit Mach number to entrance Mach number) plotted against area ratio $\frac{A_2}{A_1}$, and figure 22 presents the ratio $\frac{P_{2_{av}}}{P_o}$ (the average exit stagnation pressure to the entrance stagnation pressure) against the area ratio $\frac{A_2}{A_1}$. These figures show that the ratio $\frac{M_{2_{av}}}{M_1}$ increases with increase of area ratio $\frac{A_2}{A_1}$; whereas the stagnation-pressure recovery showed little variation, the maximum value of $\frac{P_{2_{av}}}{P_o}$ being 0.84.

The results from tests of model 1 thus show that a flow at a Mach number of 1.71 can be turned 90° with moderate losses in pressure recovery when the exit Mach number is of the same order as the entrance Mach number.

Model 2.- The exit Mach number distribution at the 50-percent-span station and at the 10.15-percent-span station of model 2 at the design

area ratio $\left(\frac{A_2}{A_1} = 1.077\right)$ is shown in figure 23 for three different entrance static-pressure ratios $\frac{p_1}{p_A}$ and, hence, for three different conditions at the exit of the passage. The ratios of static pressure of the stream to the atmospheric pressure $\frac{p_1}{p_A}$ are 1.28, 1.0, and 0.85, for the three conditions.

Figure 24 presents the static-pressure distribution and the stagnation-pressure-recovery distribution at the 50-percent-span station for which the variations obtained for the three values of $\frac{p_1}{p_A}$ considered were larger than at the 10.15-percent-span station. Figures 25 and 26 present the average exit Mach number and the stagnation-pressure recovery at the two stations as functions of the area ratio $\frac{A_2}{A_1}$ for the three values of $\frac{p_1}{p_A}$ considered. These figures show that the average exit Mach number varies considerably when the exit conditions of the passages change. When the entrance static-pressure ratio decreases or when $\frac{A_2}{A_1}$ increases, the separation on the convex surface increases and the Mach number decreases.

Figures 27 and 28 give the average Mach number ratio and average stagnation-pressure recovery for the three entrance static-pressure ratios plotted against the area ratio $\frac{A_2}{A_1}$. The values in figures 27 and 28 are an average of the two stations. Although the variation of the entrance static pressure affects the exit Mach number a large amount, the variation has little effect on the value of the stagnation-pressure recovery. In figures 27 and 28 a dotted line has been drawn that corresponds to the values of $\frac{M_{2_{av}}}{M_1}$ and $\frac{P_{2_{av}}}{P_o}$ for which the atmospheric pressure at the discharge is equal to the static pressure at the exit of the passage. The average maximum value of $\frac{P_{2_{av}}}{P_o}$ for model 2 shown in figure 28 is about 0.90 and occurs at the highest value of $\frac{p_1}{p_A}$.

Shadowgraphs of the flow in the passage for model 2 are shown in figures 29 and 30. From the shadowgraphs, the flow at the entrance of the passage appears to be similar to the flow given by the theoretical analysis. At the exit, separation occurs on the convex surface that changes the velocity distribution in the spanwise plane. From the shocks on the total-pressure rake tubes (short tubes are at the

[redacted]

10.15-percent-span station and long tubes are at the 50-percent-span station) it is possible to determine that the separation zone is thicker at the 50-percent-span station than at the 10.15-percent-span station of the model (at the 10.15-percent-span station the shocks are extended nearer to the convex surface than at the 50-percent-span station). These results are also shown from all the pressure distributions (figs. 23, 25, and 26), which indicate that the flow in the passage is far from two dimensional.

An explanation of the fact that the separated region tends to collect at the midspan of the passage can be deduced from the consideration of the centrifugal forces and the boundary-layer effects along the side walls (reference 4). For every section of the passage a negative gradient of velocity exists in the normal direction from the convex surface to the concave surface. (See, for example, fig. 6.) The negative gradient of velocity corresponds to a positive pressure gradient, which, outside of the boundary layer, balances the centrifugal forces. Because of the pressure gradient, the boundary layer on the side walls and on the concave surface, which has higher pressure, tends to move in toward the convex surface; therefore, all the boundary layer tends to collect at the middle of the convex surface. A schematic distribution of the boundary layer and the secondary flow involved is shown in figure 31. A different phenomena occurs in the actual rotor because centrifugal forces exist in the spanwise direction out toward the rotor blade tip and probably separation would tend to form near the root of the blade.

Model 3.- Figures 32, 33, and 34 show the Mach number distribution, the stagnation-pressure-recovery distribution, and the static-pressure distribution at the three spanwise stations considered for model 3. At the 50-percent-span station (fig. 32) the stream velocity tends to decrease near the convex surface in a manner similar to that of models 1 and 2; however, for model 3 the stream remains supersonic near the convex surface. The boundary-layer thickness at this spanwise station (shown by fig. 33) is approximately 0.30 inch from the convex surface. A comparison of Mach number distribution and stagnation-pressure distribution at the 50-percent-span station between model 3 (figs. 32 and 33) and model 2 (figs. 23(a) and 24(b)) shows that model 3 has a much higher velocity with smaller losses in pressure recovery near the convex surface than model 2.

The Mach number distribution at the 25-percent-span station (fig. 32) shows that near the convex surface a Mach number of 2.19 is attained which is the highest value obtained for the three stations. At this station, therefore, no separation is apparent, and the thickness of the boundary layer is very small. The Mach number distribution at the 10.15-percent-span station (fig. 32) shows a value of Mach number of 1.99 near the convex surface at the point corresponding to

the value of 2.19 at the 25-percent-span station. The Mach number distribution obtained shows that near the convex surface the velocity is still supersonic and, therefore, no strong separation effects exist.

The stagnation-pressure-recovery distribution (fig. 33) at the three spanwise stations follows that indicated by the Mach number distribution. The largest losses exist at the 50-percent-span station near the convex surface. The losses are somewhat less at the other two stations (fig. 33).

Figure 34 presents the static-pressure distribution at the three spanwise stations, and the static-pressure distribution appears to follow the indications of Mach number and stagnation-pressure-recovery distribution.

The stagnation-pressure recovery obtained from the average of the three stations for model 3 is 0.95, and the corresponding average exit Mach number ratio $\frac{M_{2_{av}}}{M_1}$ is 1.06. These results show that an appreciable gain in pressure recovery has been obtained with the introduction of a contraction in the passage and indicate that the introduction of a favorable pressure gradient in the zone of large curvature (fig. 3) has a large and favorable effect on the boundary layer at the convex surface and causes a large reduction of separation. A shadowgraph for model 3 is presented in figure 35.

Model 4.- Figures 36, 37, and 38 present Mach number distribution, stagnation-pressure-recovery distribution, and static-pressure distribution, respectively, at three spanwise stations for the original design of model 4 corresponding to the passage considered in figure 10(a). Figure 39(a) presents a shadowgraph of the flow. The results show that a large zone of separation occurs at the three stations. The height of separated flow is a maximum at the 50-percent-span station where large losses exist up to 0.80 inch from the convex surface (fig. 37). The zone of separation corresponds to large losses in stagnation pressure; however, the velocity in this zone is low and, therefore, the effect on the average pressure recovery for unit mass flow is not too large. An average stagnation-pressure recovery of 0.88 was obtained with this model, and the corresponding average Mach number ratio $\frac{M_{2_{av}}}{M_1}$ is 0.96.

Because of the large curvature of the convex surface, separation starts somewhat upstream of the zone in which the shock from the concave surface meets the convex surface (fig. 39(a)). The separation tends to contract the passage and reduces the local Mach number to values less than 1.0. In order to avoid this condition, a small change in stagger angle and curvature was introduced in the model and the tests were

[redacted]

repeated. The modified passage tested corresponds to the design shown in figure 10(b). The shadowgraph of flow in the modified passage (fig. 39(b)) indicates that an increase of local Mach number was obtained in the zone of separation. The average exit Mach number was 1.04 of the entrance Mach number. The separation was reduced; however, no gain in pressure recovery was obtained, and an average value of 0.88 was measured also for this configuration.

Variable-span models.- The fairing previously discussed and shown in figure 12 reduced the area ratio of model 2 from 1.24 to 1.00. The test results for model 2 with the fairing gave an average stagnation-pressure recovery of 0.84 and a corresponding average Mach number ratio of 0.80. These results are close to those obtained from the two-dimensional tests of model 2 for the same area ratio (figs. 27 and 28), and show that two-dimensional results can be used as a first-order indication of results to be expected for three-dimensional passages.

In an effort to simulate the large pressure gradient along the span in the same direction as the pressure gradient obtained in the passage of a rotor, the variation of passage cross section for the second three-dimensional test was obtained by filling one corner of the passage (fig. 13). The spanwise pressure gradient in the rotor depends primarily on the rotational velocity; therefore, the intensity of the pressure gradient in these tests (0.563 atmosphere per inch) may be smaller than that for an actual rotor (1.0 atmosphere per inch) but is an appreciable fraction of that for an actual rotor. Because the effect is important only in the boundary layer and because it was not possible for the experimental system to produce the dissymmetry all along the passage, the filling of the corner was gradual (fig. 13). The area ratio A_2/A_1 for this model was 1.016. For this condition an average stagnation-pressure recovery of 0.85 with an average Mach number equal to 0.90 of the entrance Mach number was obtained. These results are also in good agreement with the results obtained in the two-dimensional tests at $\frac{A_2}{A_1} = 1.016$.

Wedge with detached shock.- A photograph of the setup for study of the phenomena with detached shock is shown without flow in figure 40. The lower surface has a large inclination to the stream direction, and the deviation of the stream is larger than the maximum deviation for shock attachment for the stream Mach number (at $M = 1.71$, $\delta_{max} = 17.16$).

At the upper surface an expansion would be expected if no detached shock were produced by the lower surface. The shadowgraphs (figs. 41, 42, and 43) show the flow field for three angles of attack equal to 29.83°, 35°, and 40.08° at the lower surface of the wedge, and table III shows a comparison of the Mach number that would

[redacted]

be obtained without the presence of detached shock and the Mach number measured from the total-pressure and the static-pressure distribution along the upper surface. The shadowgraphs show that separation similar to the subsonic separation found for wedges in a subsonic stream exists with a vortex localized at the leading edge behind the detached shock. The separation is localized and the stream reattaches at the surface, an expansion is produced, and the local speed again becomes supersonic. The results of reference 3 indicate that, with normal shock close to the leading edge, the flow is still attached. The values of theoretical and measured Mach numbers in table III show that the presence of strong detached shock does not change appreciably the flow along the upper surface for the range of angles of attack tested.

CONCLUDING REMARKS

In order to turn a supersonic stream through a large angle in a passage of practical dimensions, the speed along the convex surface of the passage must be increased considerably with respect to the speed along the concave surface of the passage. If the static pressure at the exit is equal to the static pressure at the entrance, a compression of the flow must occur at the convex surface ahead of the passage exit and an expansion at the concave surface. The conditions for separation of the boundary layer depend to a large extent on the magnitude of the positive pressure gradient and the curvature of the convex surface. The possibility of separation increases if the exit static pressure is larger than the entrance static pressure and decreases for the opposite condition. The prevention of separation of the boundary layer at the convex surface is made more difficult by the necessity of having a shock at the leading edge of the concave surface because this shock meets the convex surface in the region of large curvature. The boundary-layer separation can be minimized by introducing a favorable pressure gradient along the convex surface in the zone of large curvature behind the shock.

Of the four 90° turning passages tested, the highest pressure recovery was obtained with a passage in which a favorable pressure gradient along the convex surface was introduced behind the point of shock reflection. A large contraction of the passage was used in order to permit the introduction of the favorable pressure gradient. The pressure loss for this design was 5 percent of the inlet stagnation pressure for a ratio of entrance to exit Mach number of 1.06. The passage contour corresponds to a practical compressor rotor blade having a thickness ratio of 0.12 and a solidity of 3.1.

Tests which were made to investigate the flow behind a detached shock at the leading edge of the concave surface of a turning passage

indicate that the flow at the surface on which expansion occurs is not changed appreciably by the presence of detached shock. (For an angle of attack of 40.1° the theoretical Mach number is 2.47 and the measured Mach number is 2.62.)

Langley Aeronautical Laboratory
National Advisory Committee for Aeronautics
Langley Air Force Base, Va.

REFERENCES

1. Kantrowitz, Arthur: The Supersonic Axial-Flow Compressor. NACA ACR L6D02, 1946.

2. Ferri, Antonio: Preliminary Analysis of Axial-Flow Compressors Having Supersonic Velocity at the Entrance of the Stator. NACA RM L9G06, 1949.

3. Ferri, Antonio: Experimental Results with Airfoils Tested in the High-Speed Tunnel at Guidonia. NACA TM 946, 1940.

4. Fluid Motion Panel of the Aeronautical Research Committee and Others: Modern Developments in Fluid Dynamics. Vol. I, S. Goldstein, ed., The Clarendon Press (Oxford), 1938.

[redacted]

TABLE I

ORDINATES OF BLADES TESTED

Station (percent chord)	Model 1 (percent chord)		Model 2 (percent chord)		Model 3 (percent chord)		Model 4			
							Original (percent chord)		Modified (percent chord)	
	Upper surface	Lower surface	Upper surface	Lower surface	Upper surface	Lower surface	Upper surface	Lower surface	Upper surface	Lower surface
0	0	0	0	0	0	0	0	0	0	0
5	4.95	4.54	4.62	3.32	5.60	3.71	6.81	5.22	6.55	4.27
10	9.78	8.74	8.70	6.46	10.45	7.08	12.61	8.84	12.20	7.62
20	17.79	15.83	15.55	12.09	20.65	12.74	21.30	14.49	20.05	12.80
30	23.06	19.83	19.66	15.63	27.04	16.66	25.65	17.39	25.84	15.85
40	26.21	22.23	22.04	17.99	30.50	19.13	27.54	18.70	28.20	17.38
50	27.14	23.30	23.04	18.82	30.94	19.81	27.54	18.70	28.66	17.68
60	26.55	22.33	22.48	18.28	28.77	19.20	25.07	17.10	26.52	16.46
70	23.62	19.90	20.22	16.36	24.29	16.98	21.10	14.49	21.80	13.87
80	18.45	15.87	15.92	12.70	18.02	13.05	14.78	10.58	15.24	10.52
90	10.44	8.98	9.14	7.76	9.79	7.31	7.94	5.70	7.77	5.79
100	0	0	0	0	0	0	0	0	0	0

TABLE II

VARIOUS BLADE CHARACTERISTICS

Model	Stagger angle (deg)	Chord (in.)	Thickness ratio t/c	Solidity c/s
1	45	6.56	0.0488	6.626
	55	6.56	.0488	5.248
	60	6.56	.0488	4.620
2	45	6.28	.0509	5.925
	55	6.28	.0509	4.906
	60	6.28	.0509	4.132
3	54	5.30	.1226	3.118
4	47	6.90	.0898	3.520
	49	6.56	.1089	3.094

TABLE III

COMPARISON OF THEORETICAL AND MEASURED MACH NUMBER

FOR THREE ANGLES OF ATTACK

α (deg)	δ (deg)	M (theoretical)	M (measured)
29.83	10.33	2.075	1.927
35.00	15.50	2.26	2.073
40.08	20.58	2.473	2.264

NACA

[redacted]

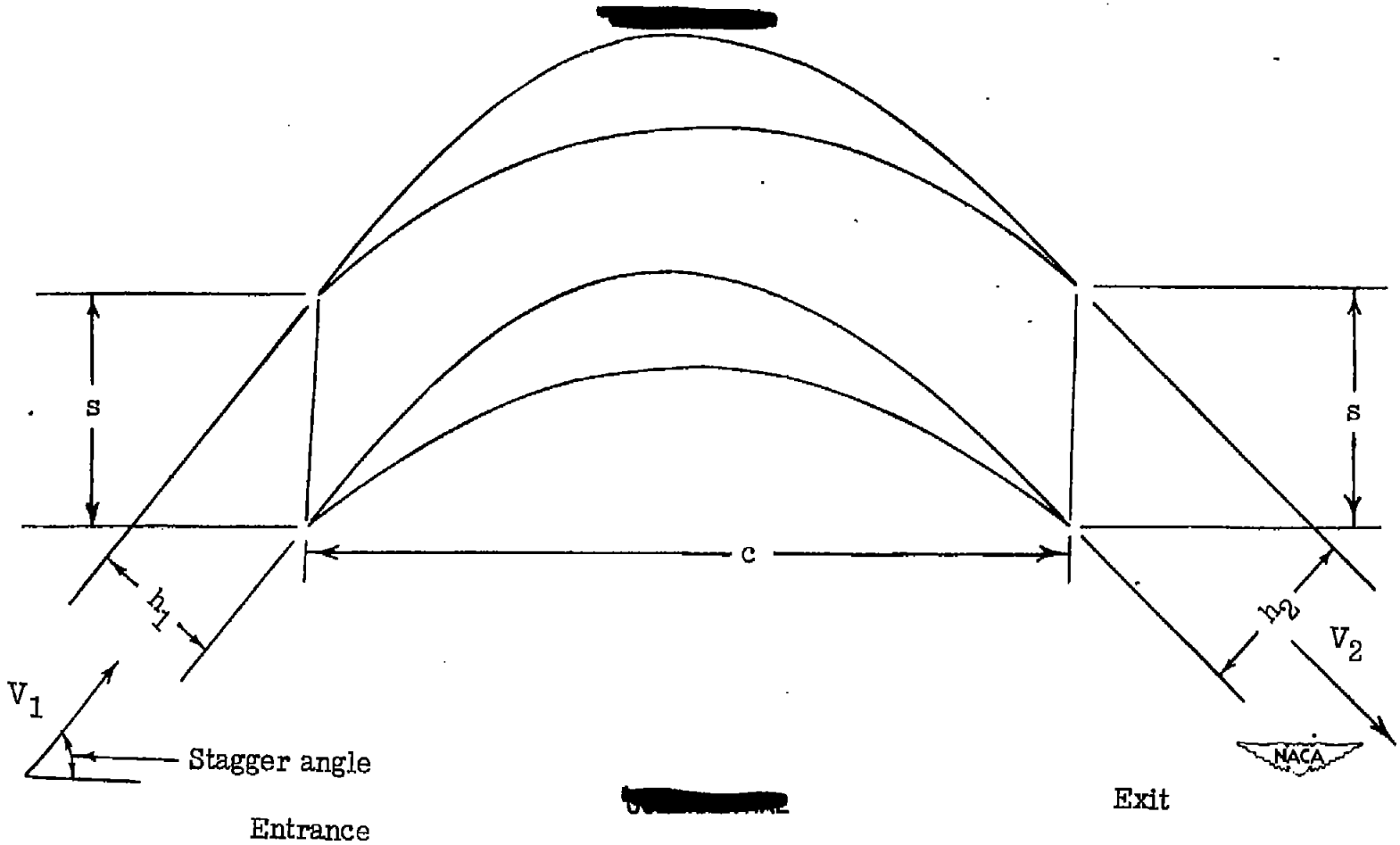

Figure 1.- Symbols defining blade geometry.

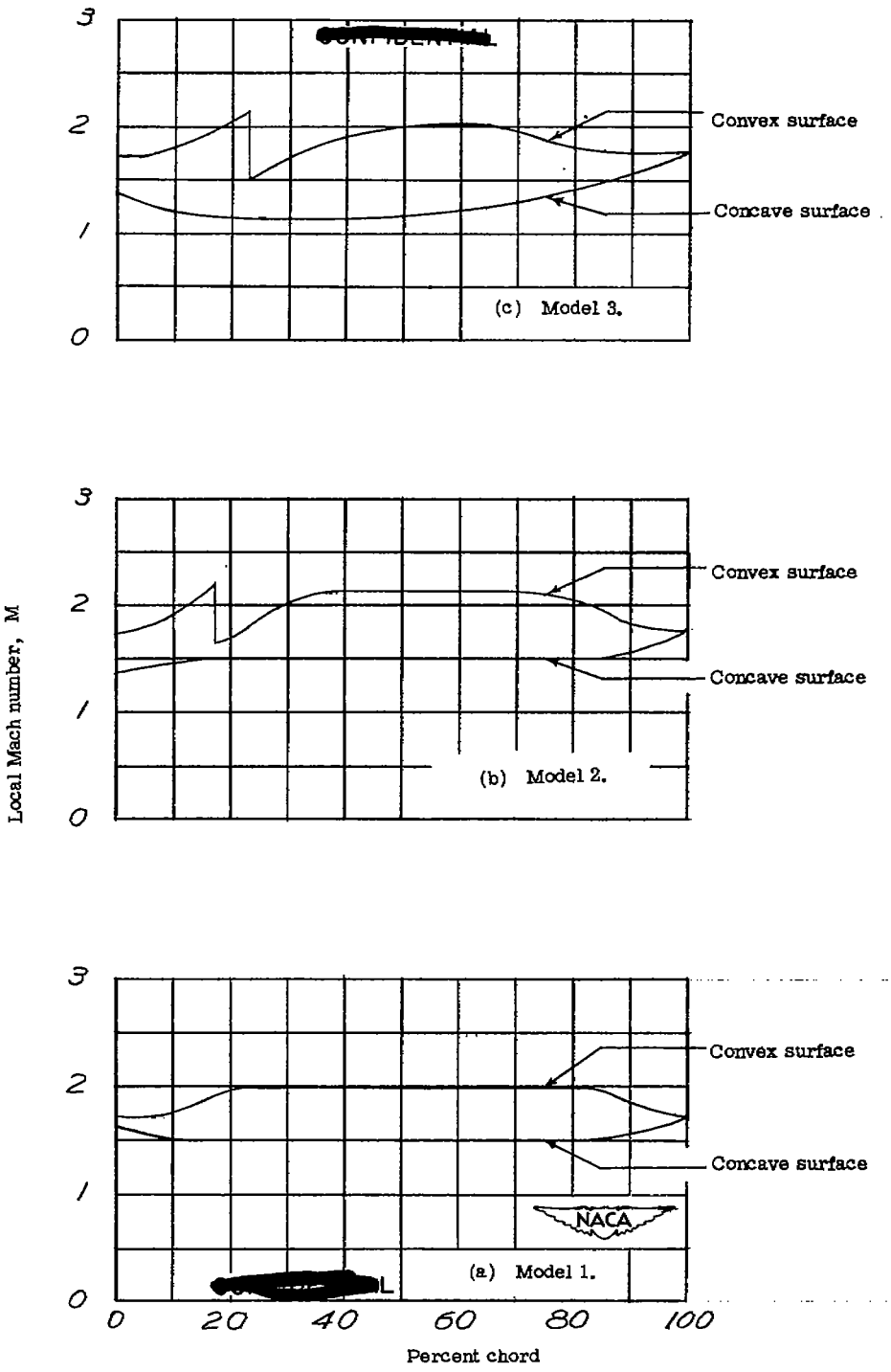

Figure 2.- The variation of local Mach number along the convex and concave surfaces with percent chord for the different models.

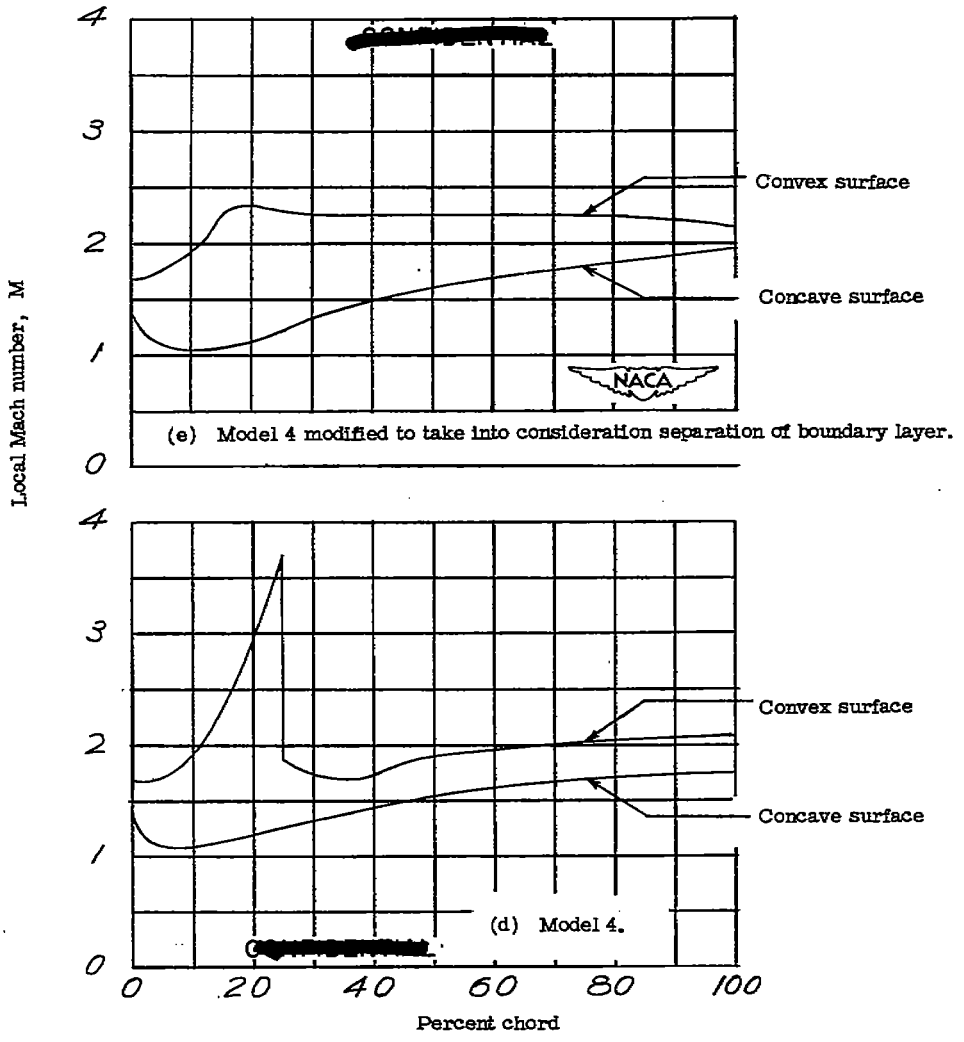

Figure 2.- Concluded.

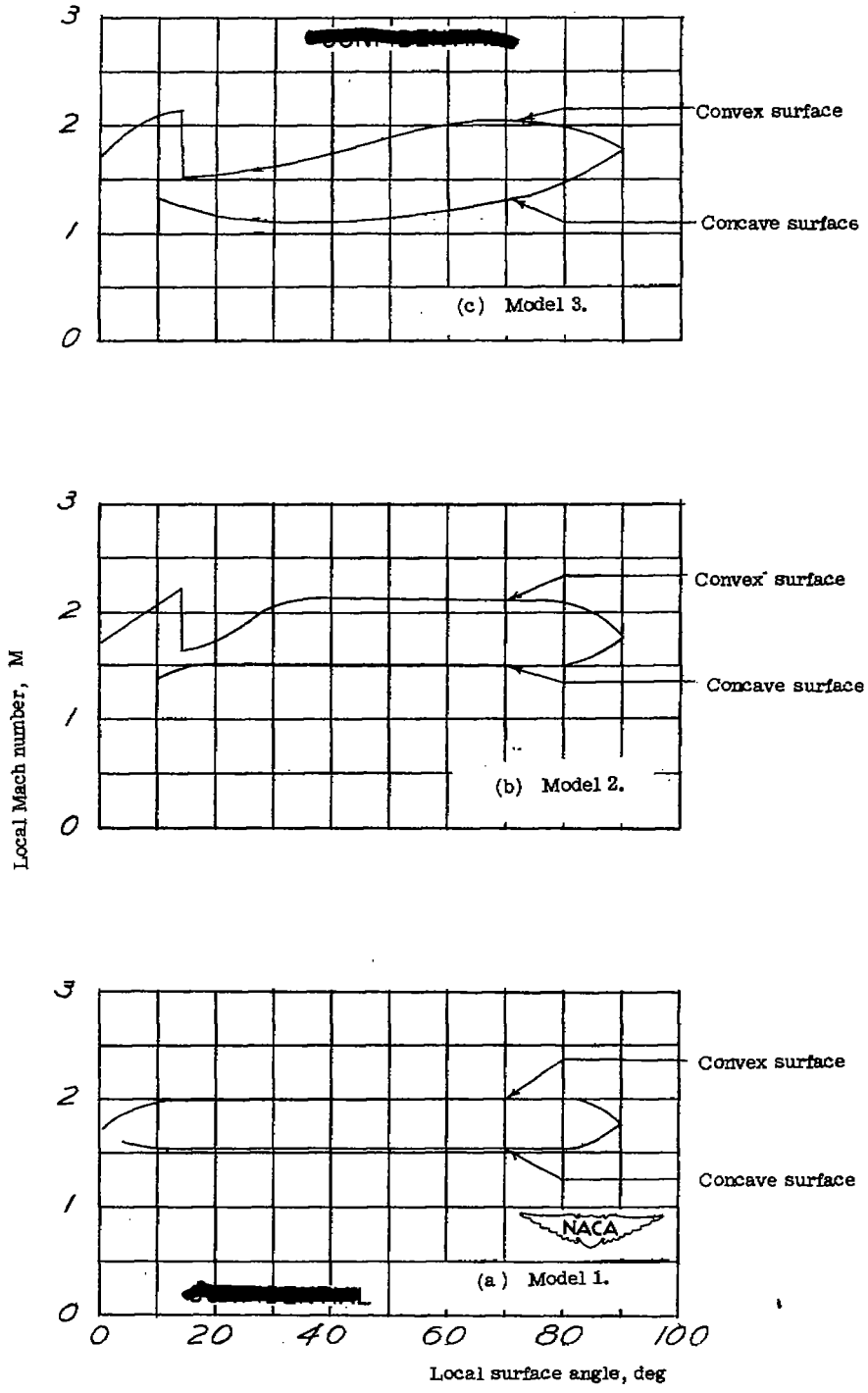

Figure 3.- Variation of local Mach number along the convex and concave surfaces with local surface angle for the different models.

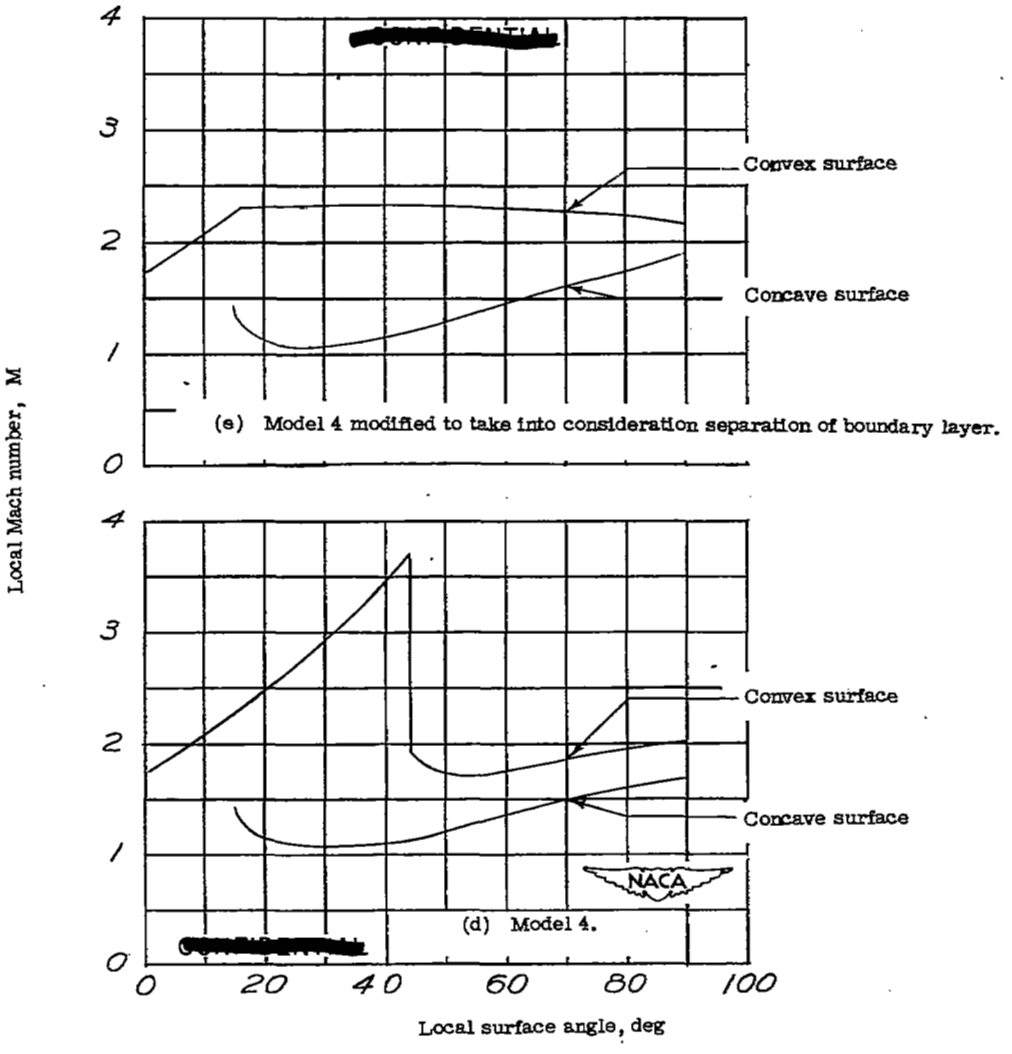

Figure 3.- Concluded.

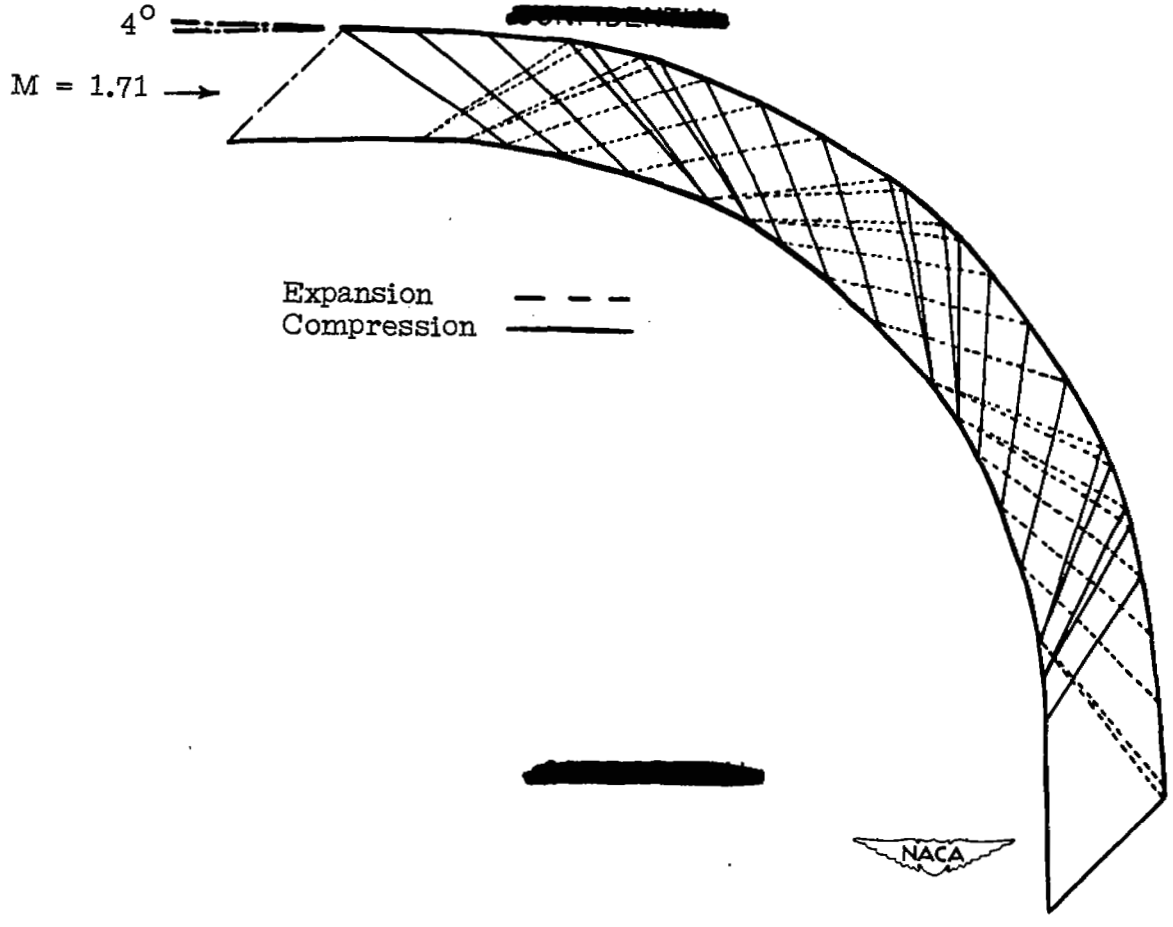

Figure 4.- Characteristics net for model 1.

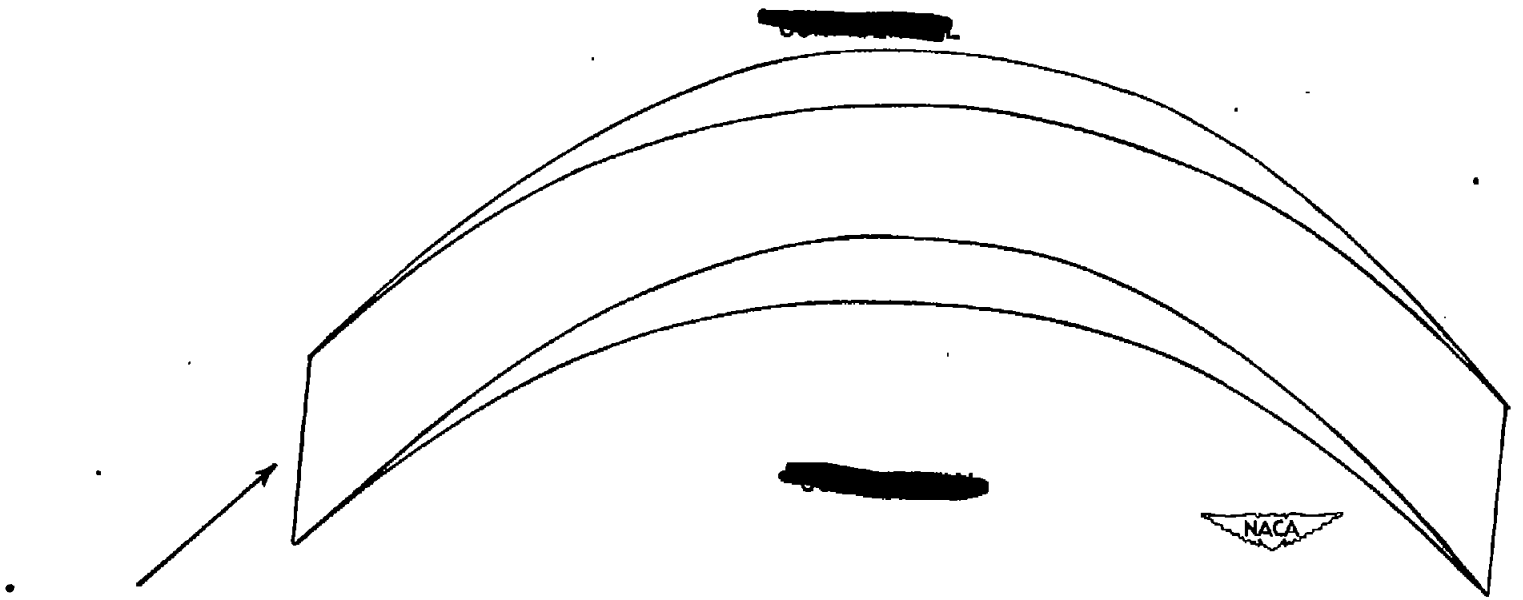

(a) Stagger angle, 45°.

Figure 5.- Possible blade shapes for model 1.

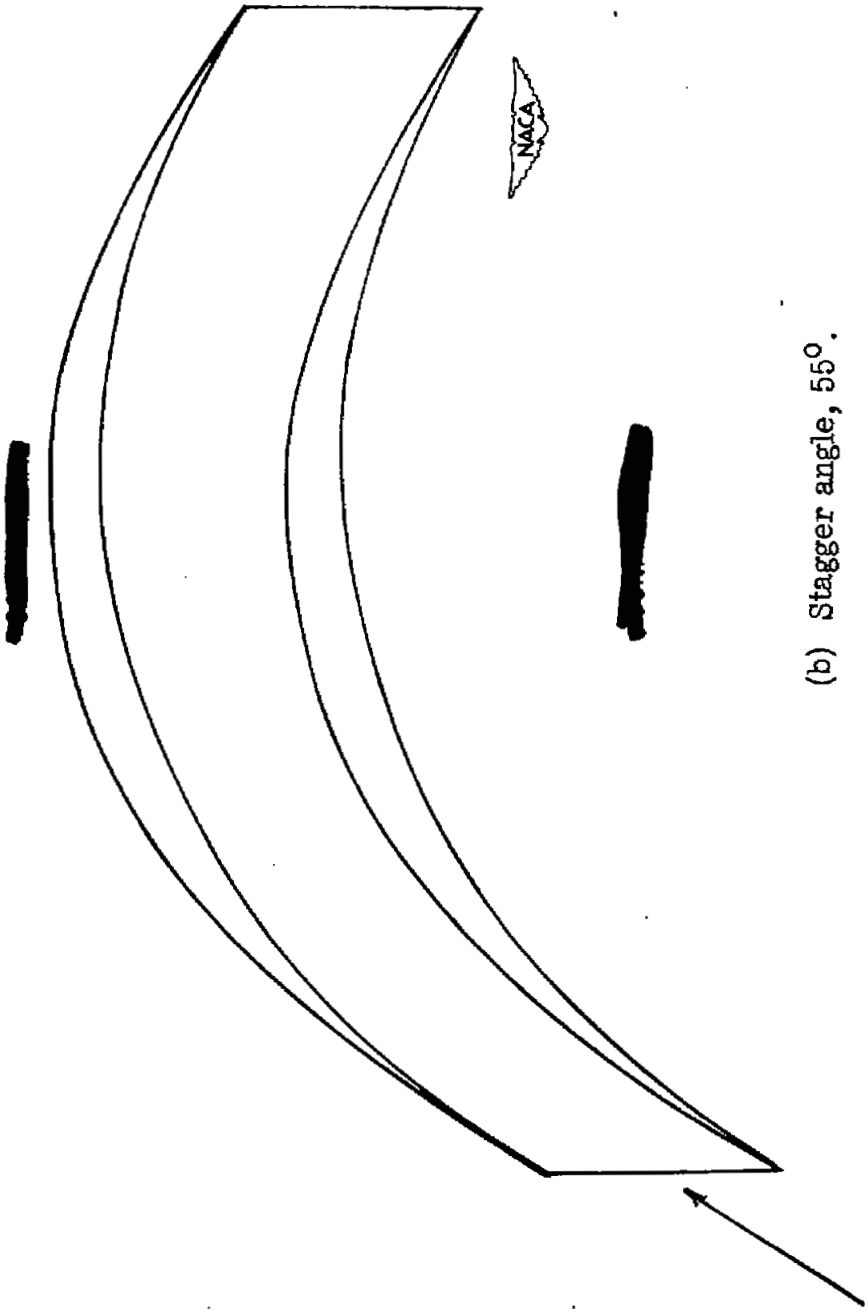

(b) Stagger angle, 55°.

Figure 5.- Continued.

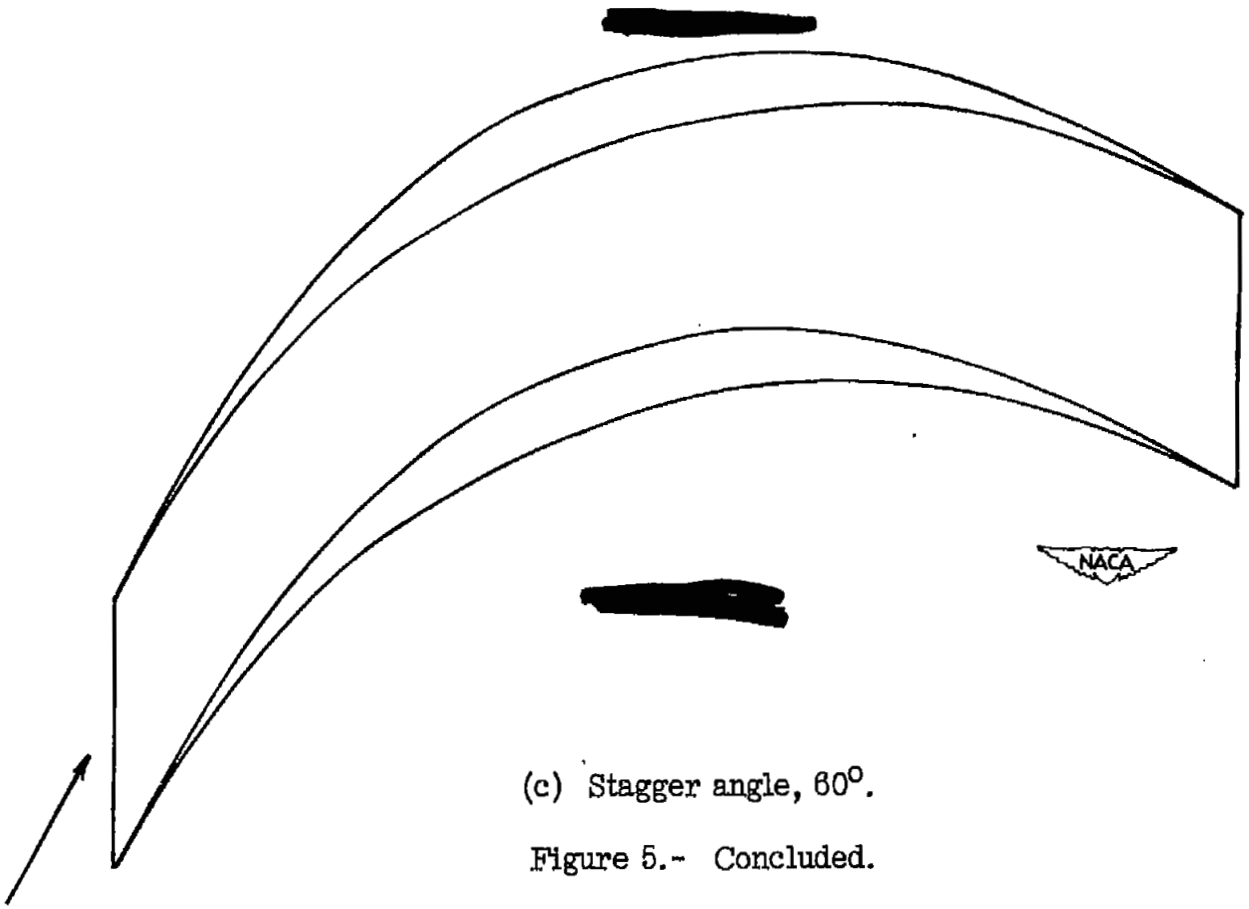

(c) Stagger angle, 60°.

Figure 5.- Concluded.

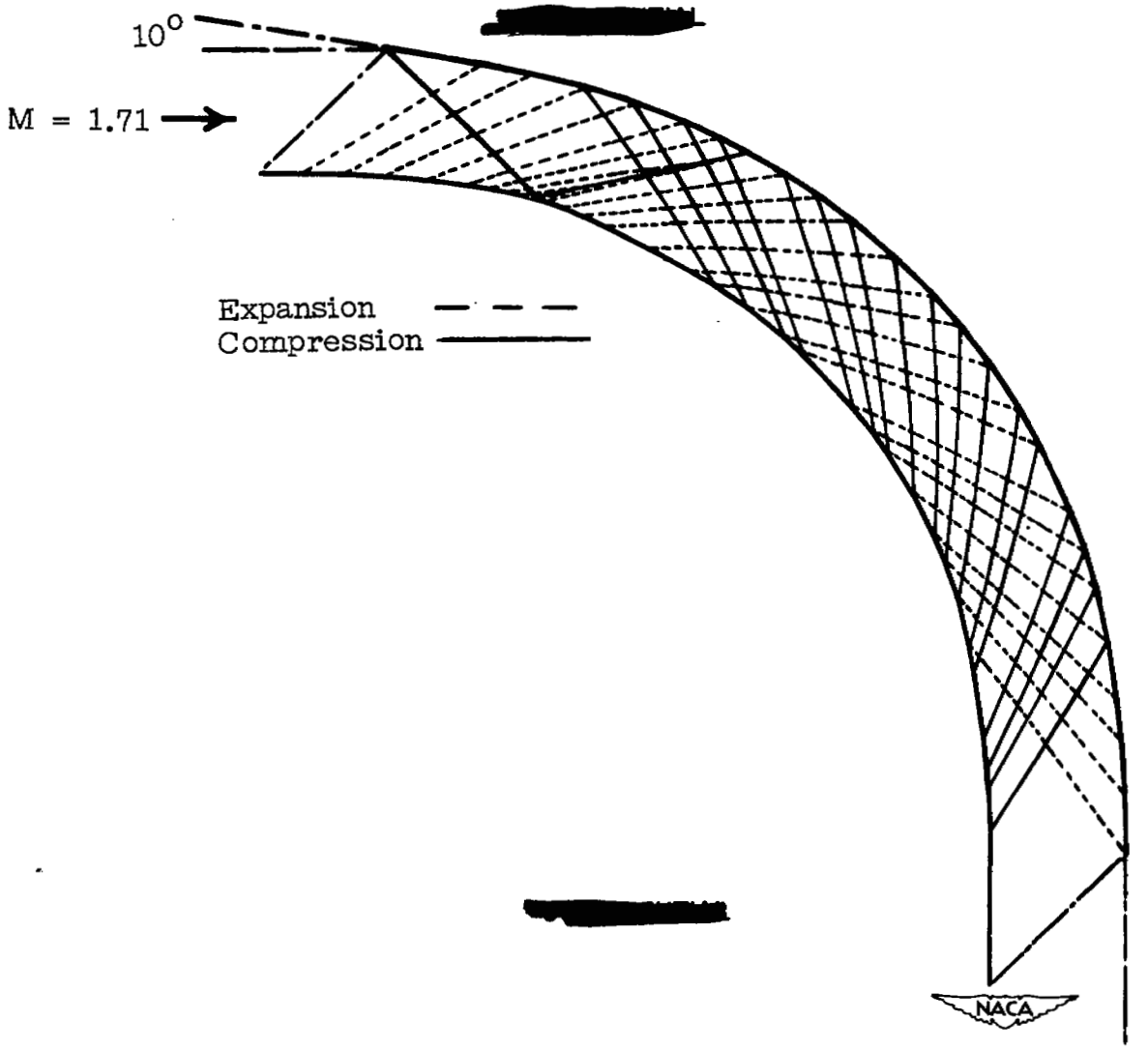

Figure 6.- Characteristics net for model 2.

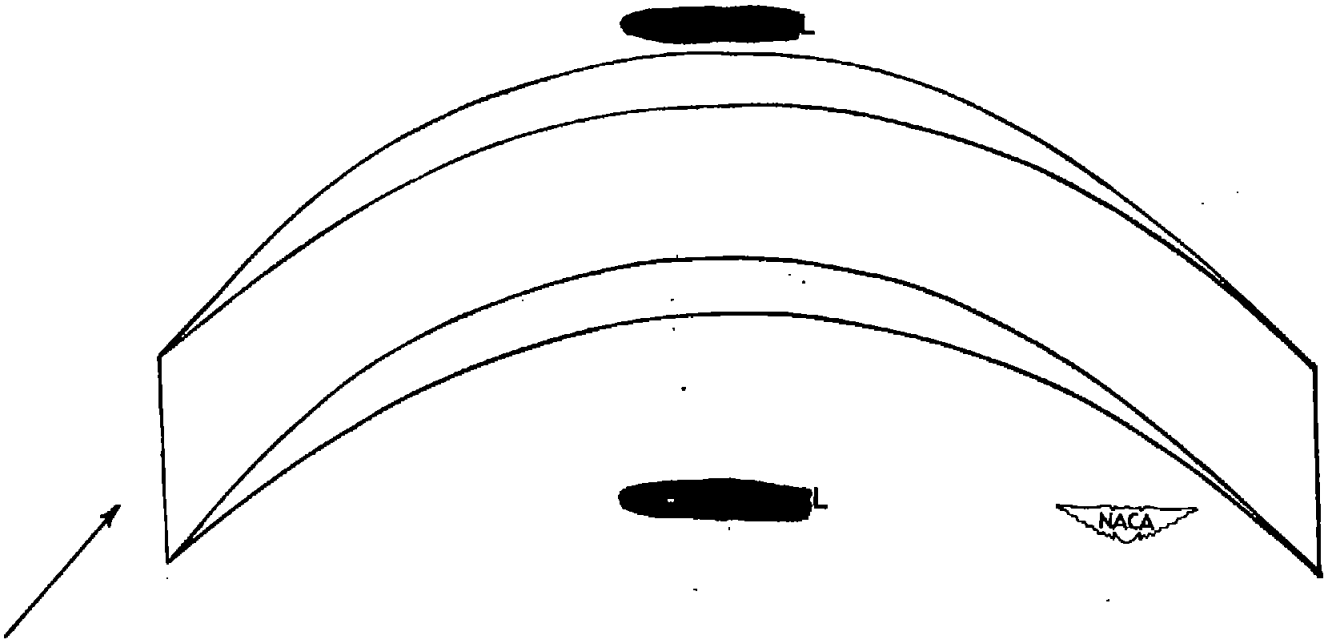

(a) Stagger angle, 45°.

Figure 7.- Possible blade shapes for model 2.

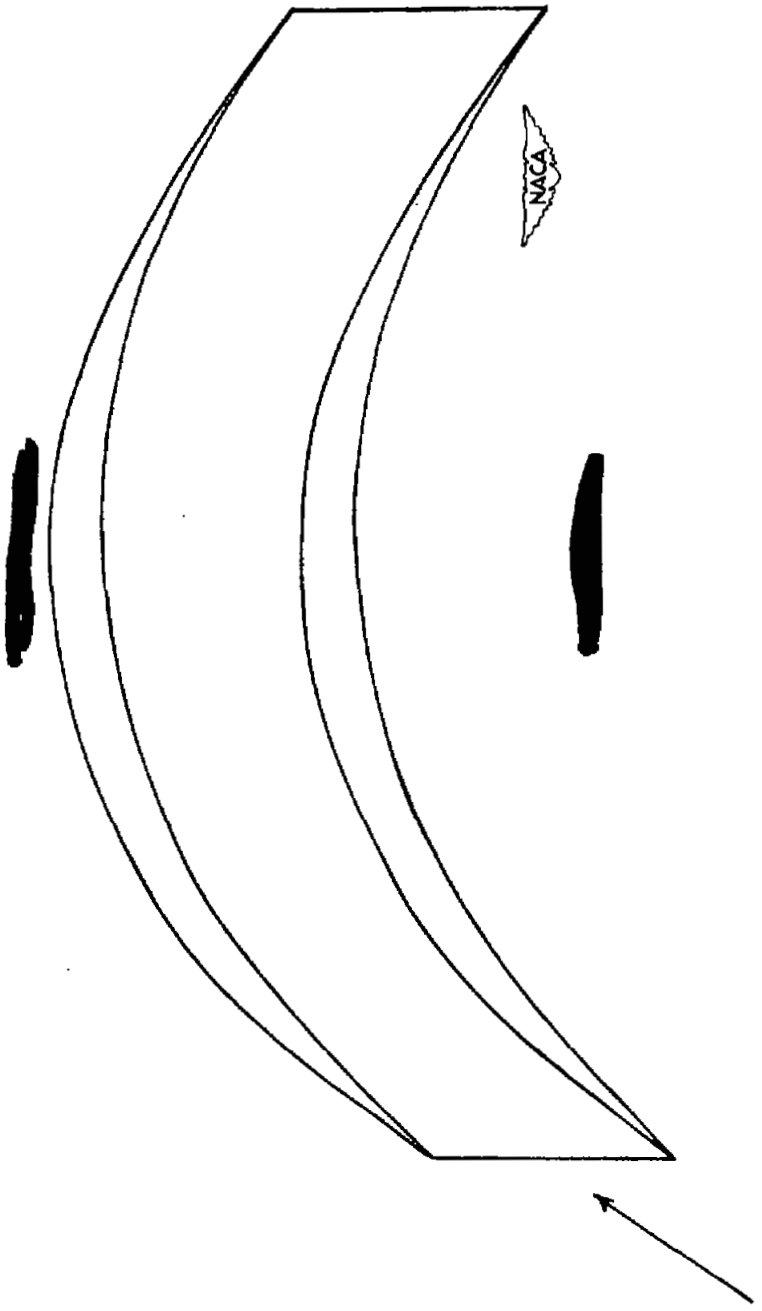

(b) Stagger angle, 55°.

Figure 7.- Continued.

(c) Stagger angle, 60°.

Figure 7.- Concluded.

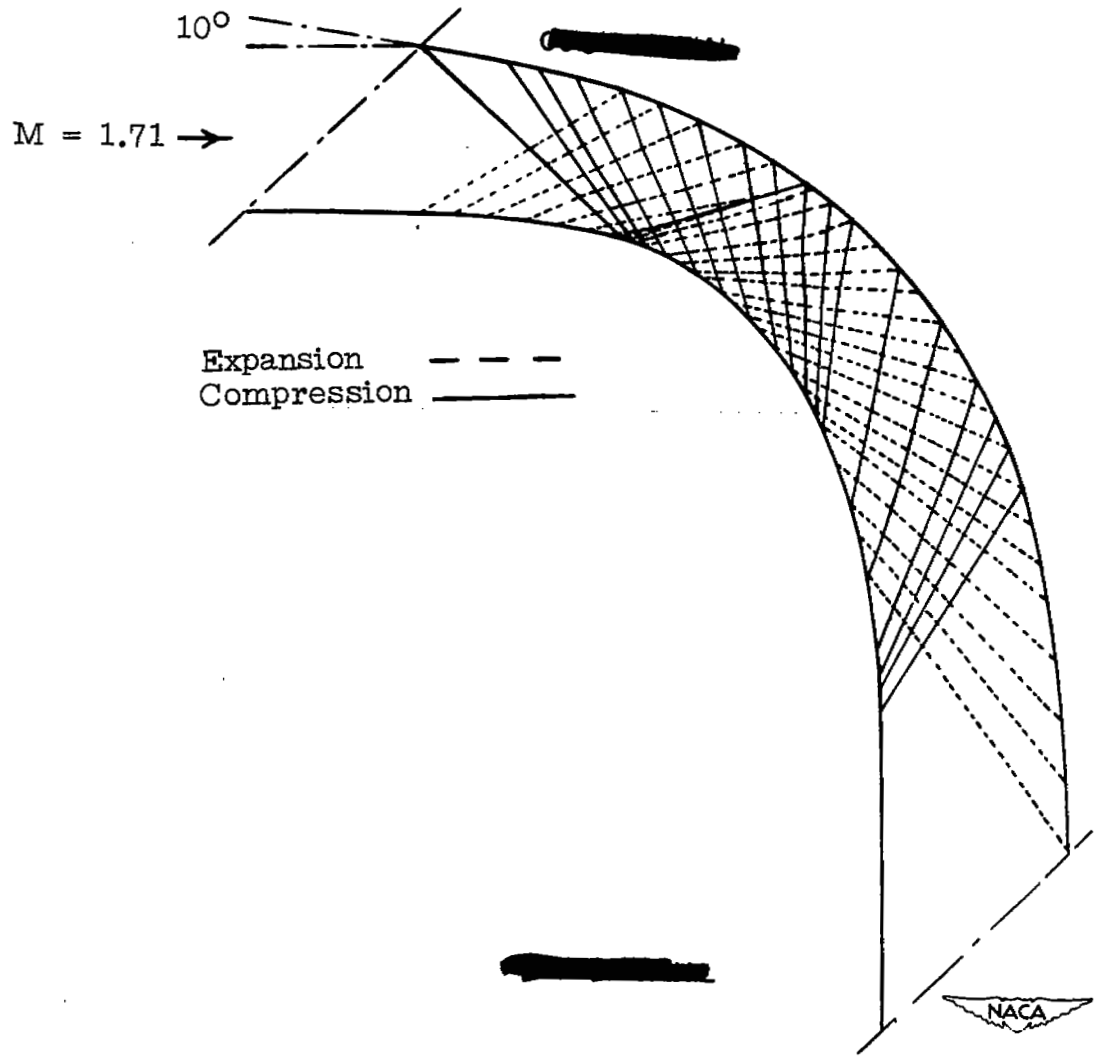

Figure 8.- Characteristics net for model 3.

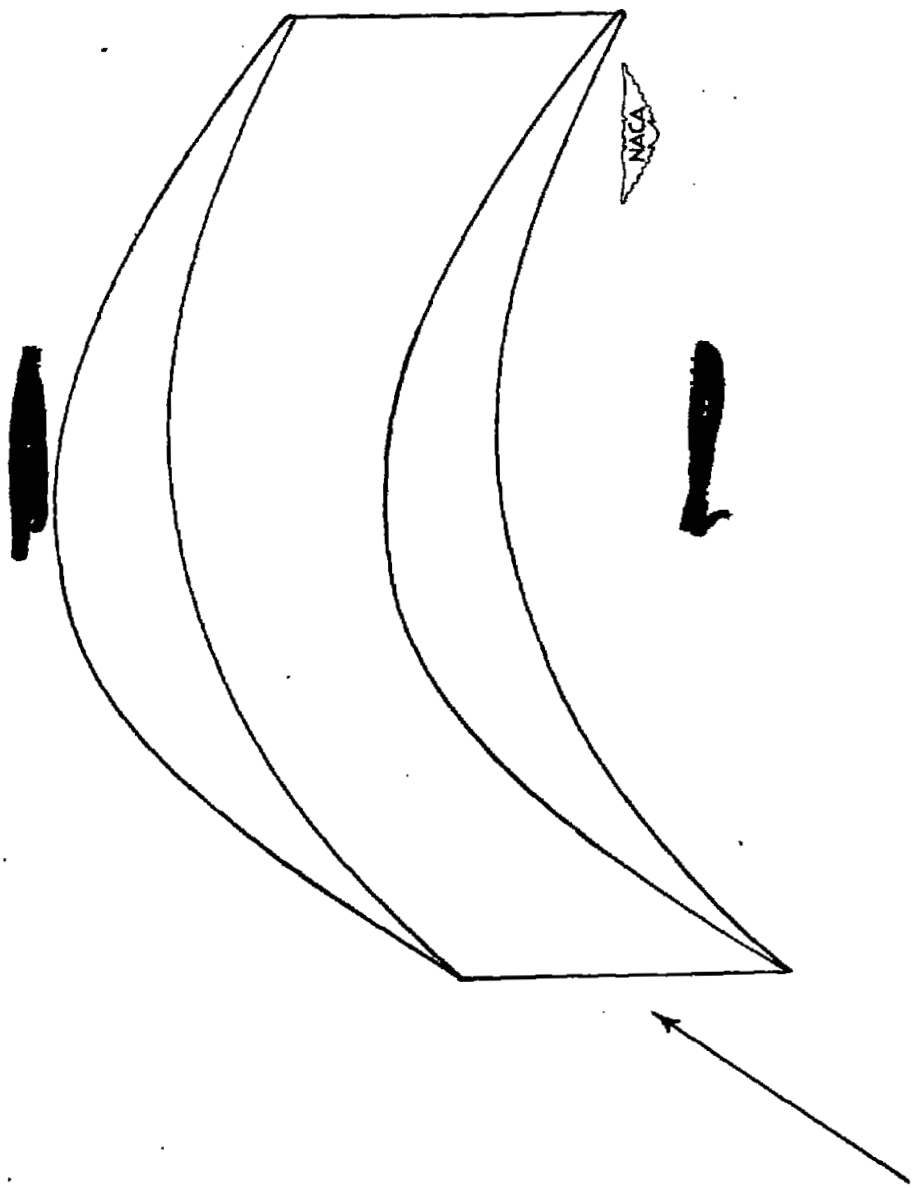

Figure 9.- Possible blade shape for model 3. Stagger angle, 54°.

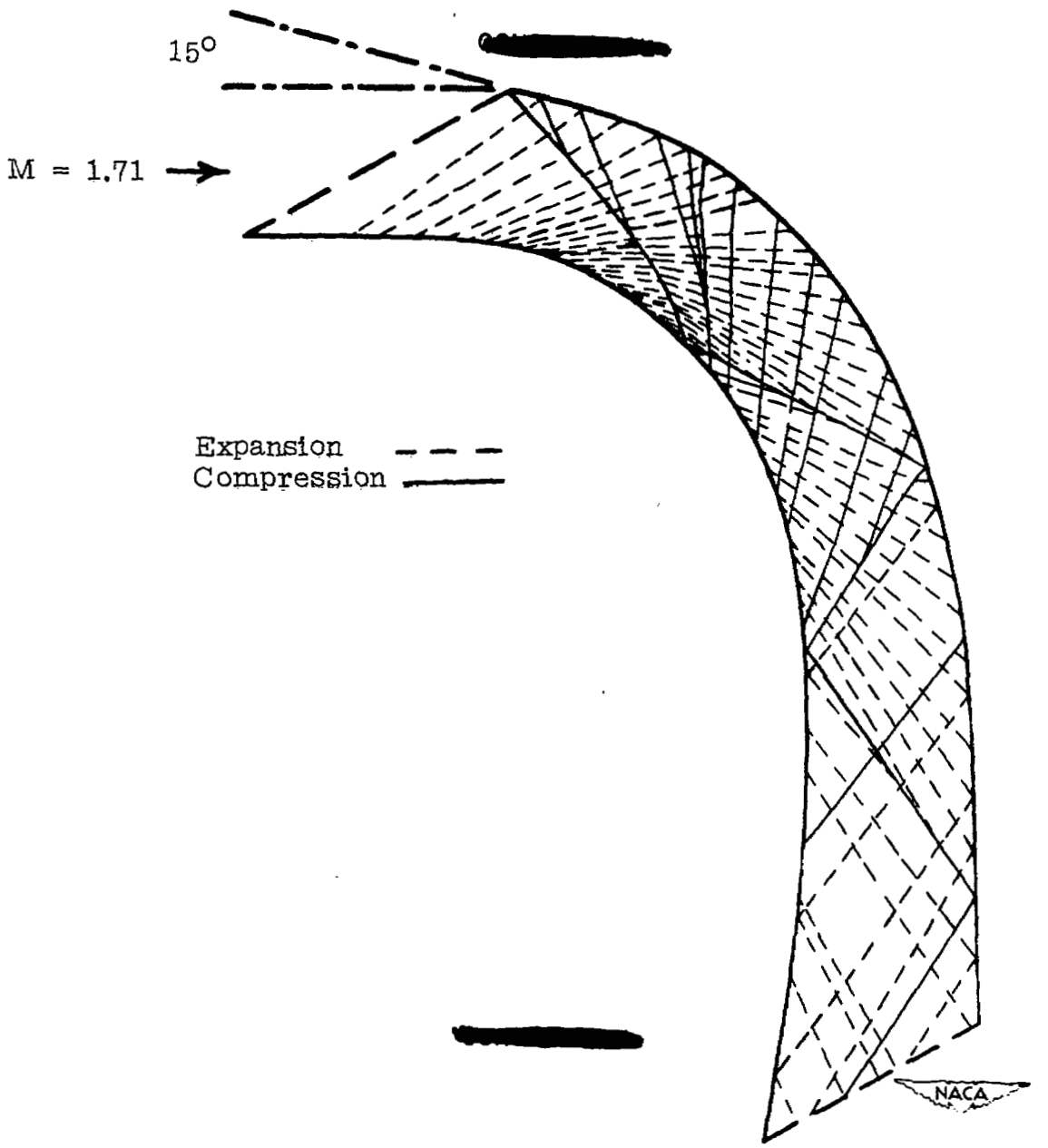

(a) No boundary-layer separation taken into consideration.

Figure 10.- Characteristics net for model 4.

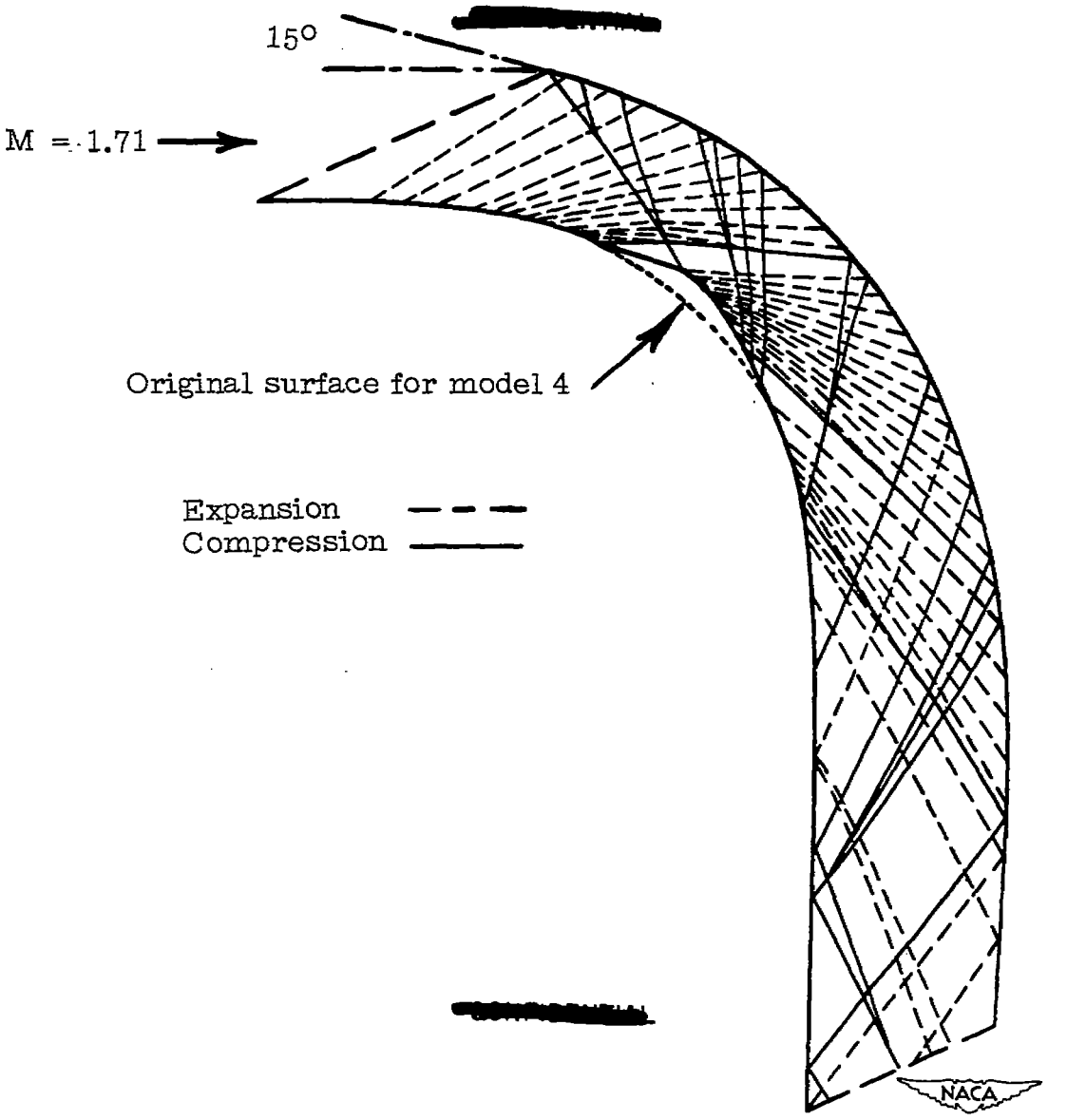

(b) Boundary-layer separation taken into consideration.

Figure 10.- Concluded.

(a) Blade corresponding to figure 10(a). Stagger angle, 47°.

Figure 11.- Possible blade shapes for model 4.

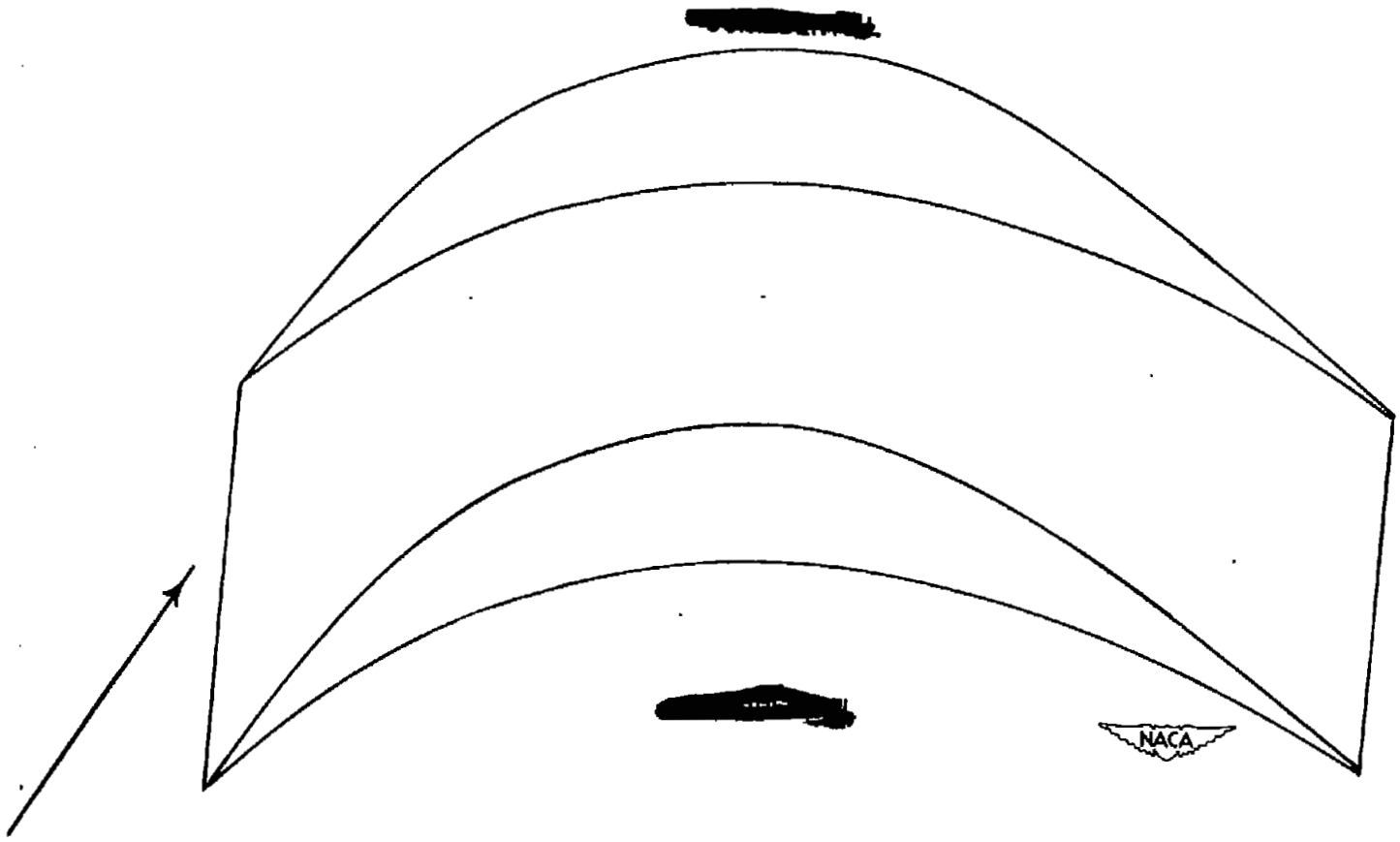

(b) Blade corresponding to figure 10(b). Stagger angle, 59°.

Figure 11.- Concluded.

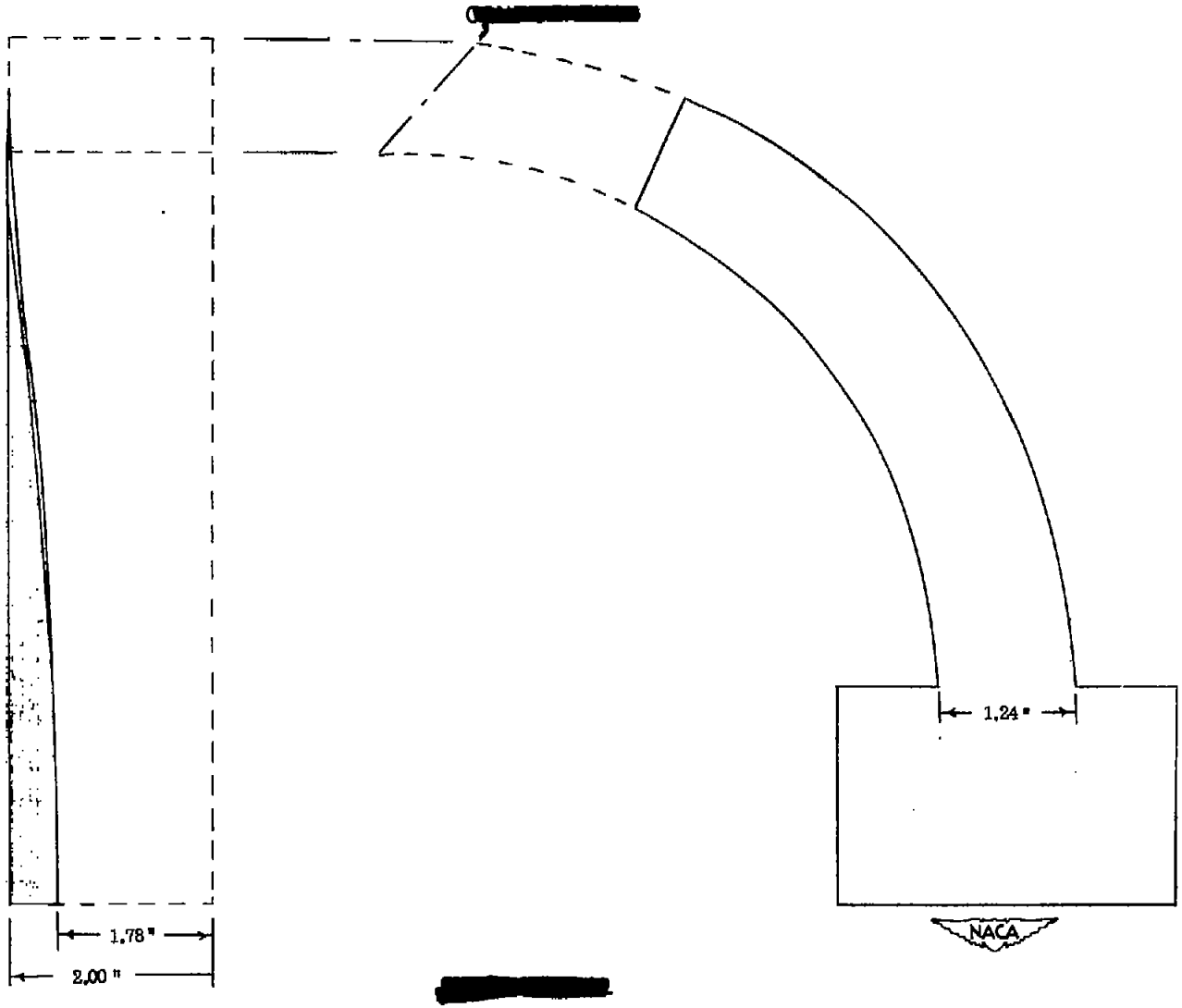

Figure 12.- Schematic setup for first variable-span model.

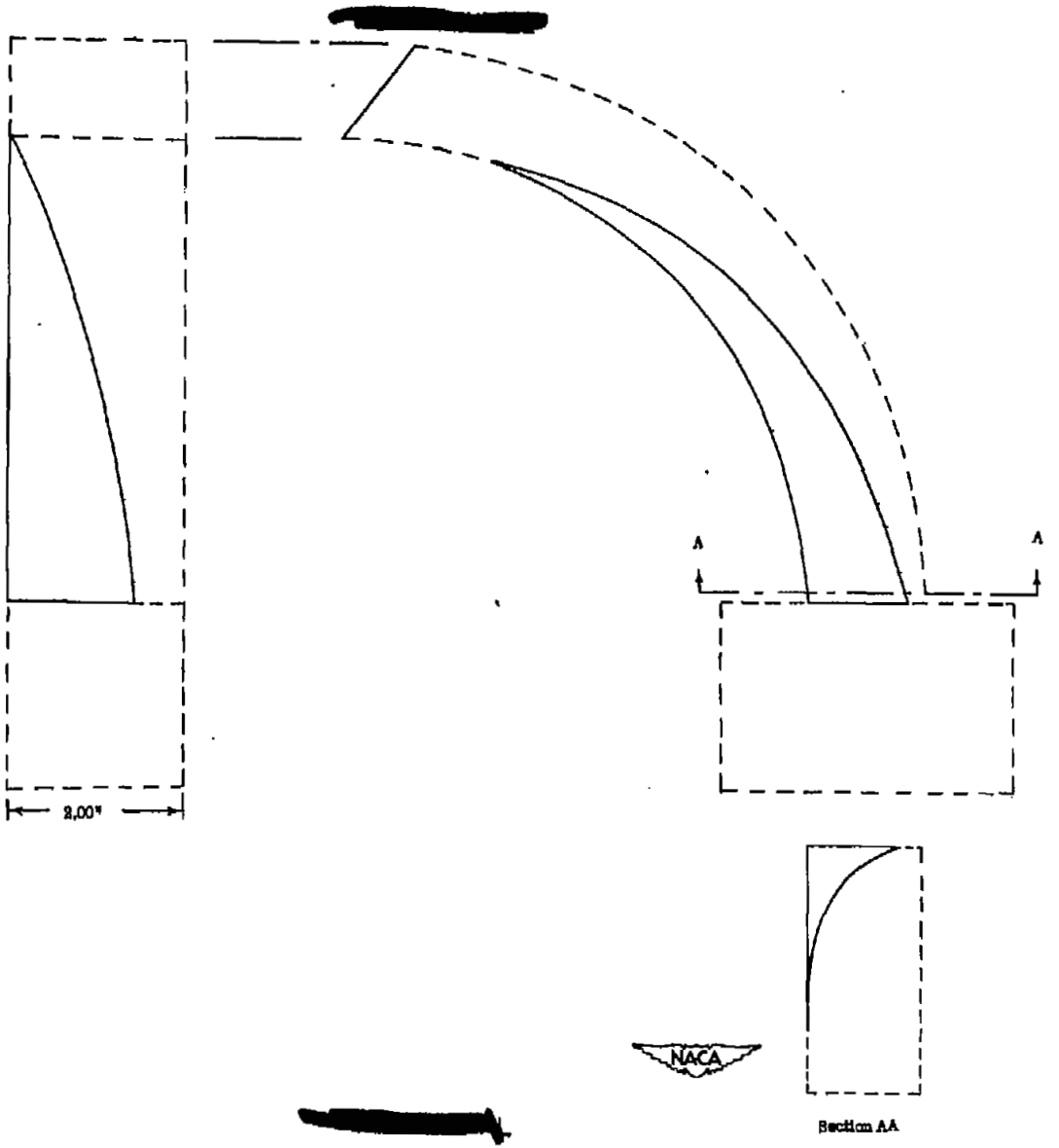

Figure 13.- Schematic setup for second variable-span model.

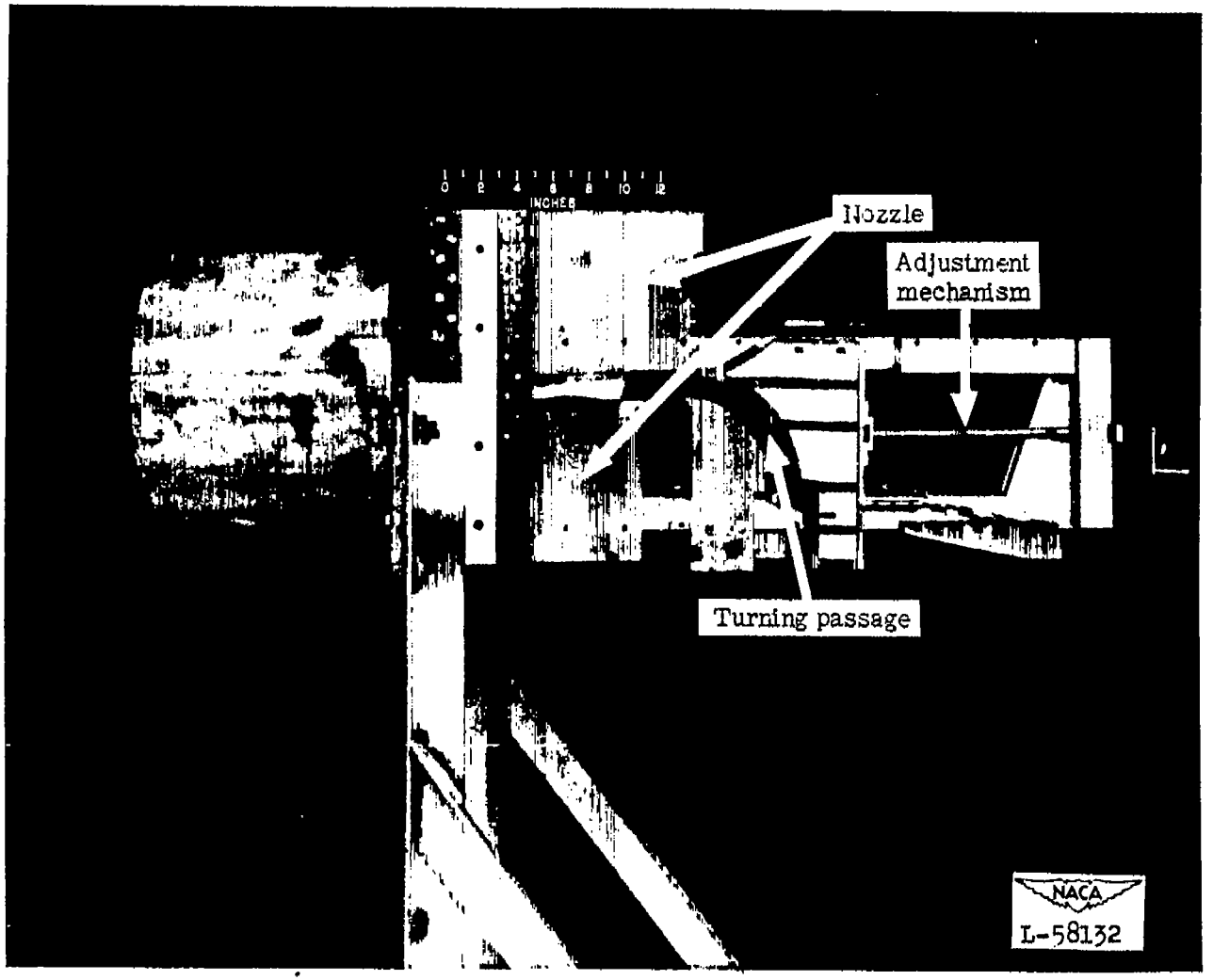

Figure 14.- Model mounted in test setup with one side wall removed.

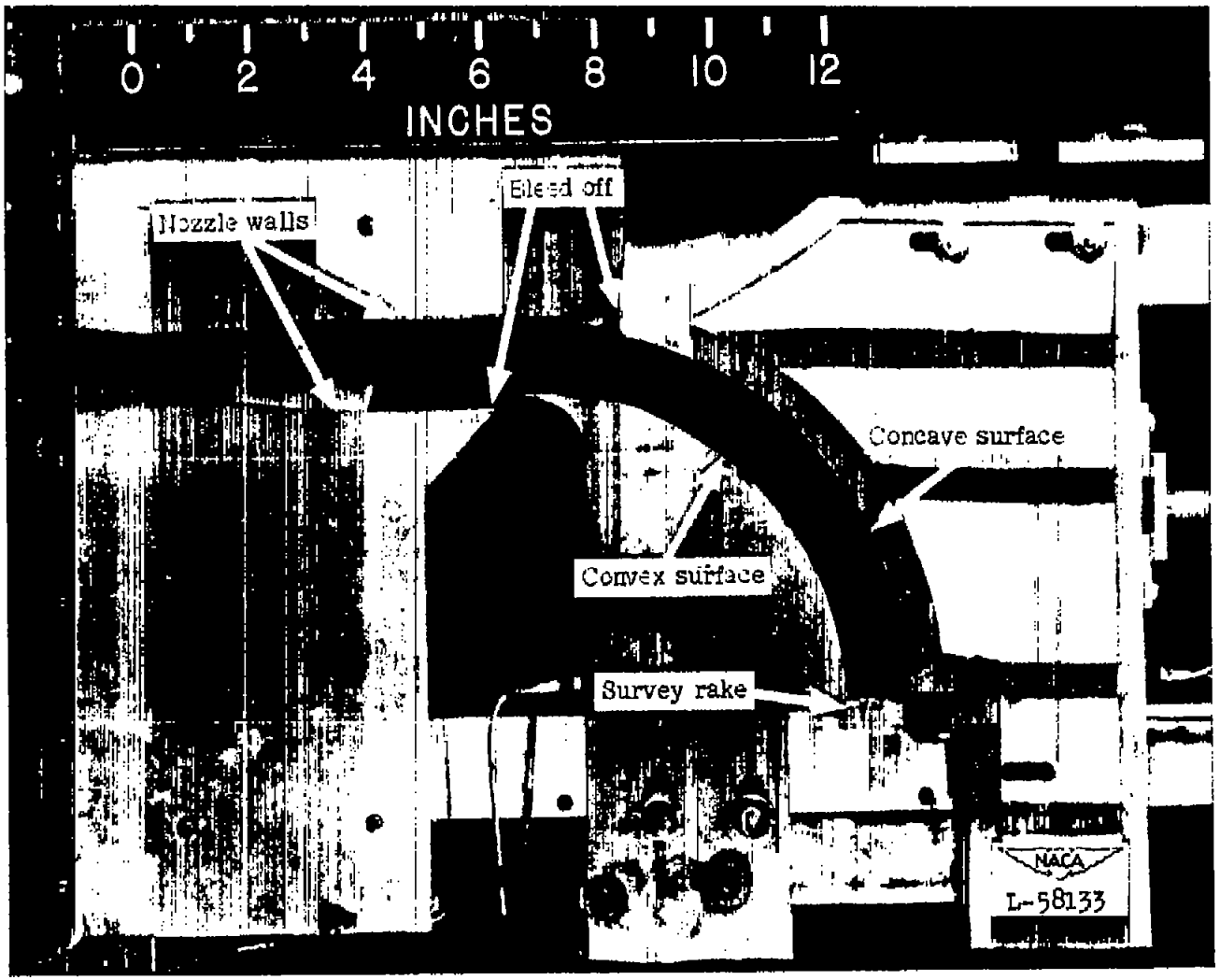

Figure 15.- Model mounted in test setup with one side wall removed.

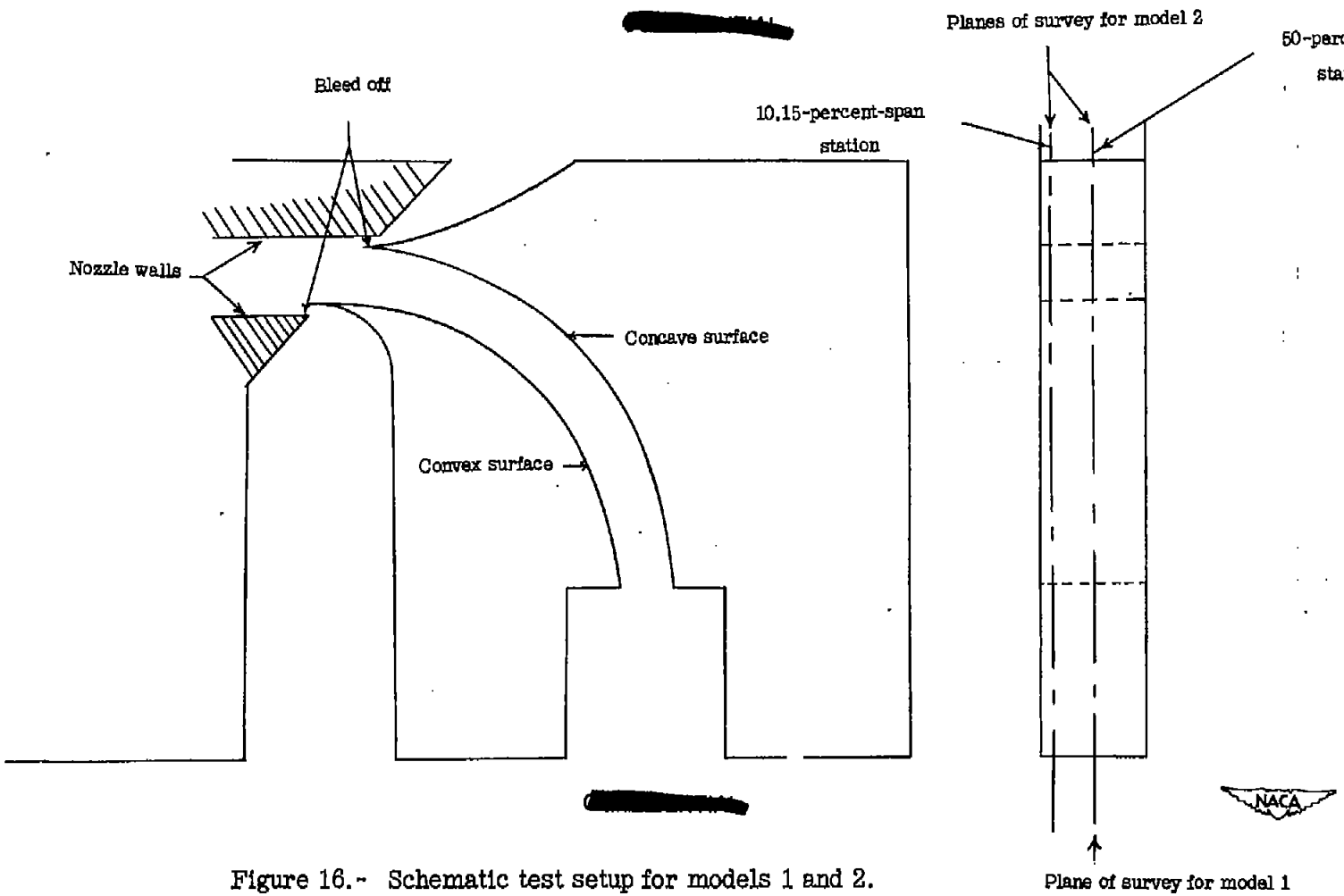

Figure 16.- Schematic test setup for models 1 and 2.

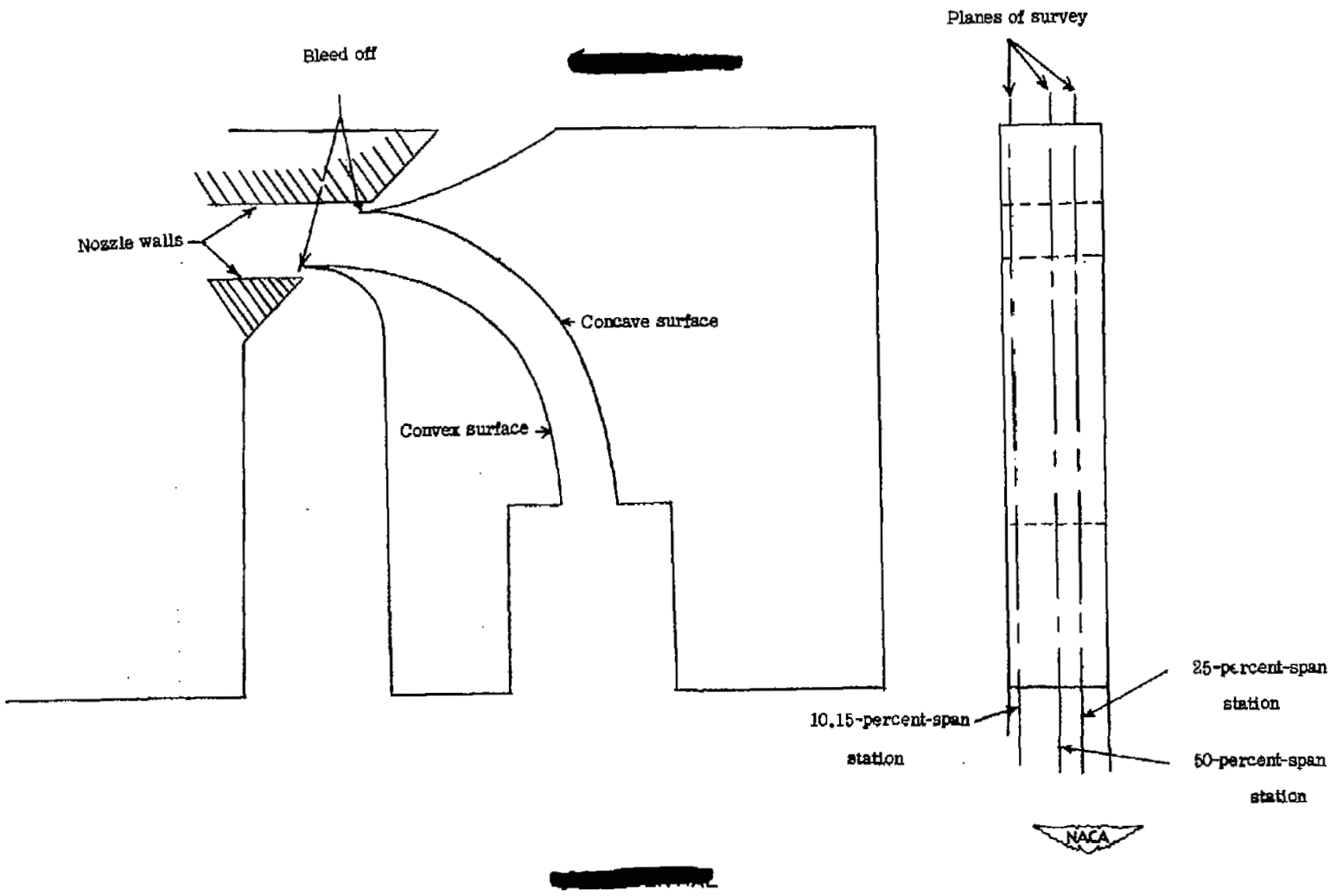

Figure 17.- Schematic test setup for models 3 and 4.

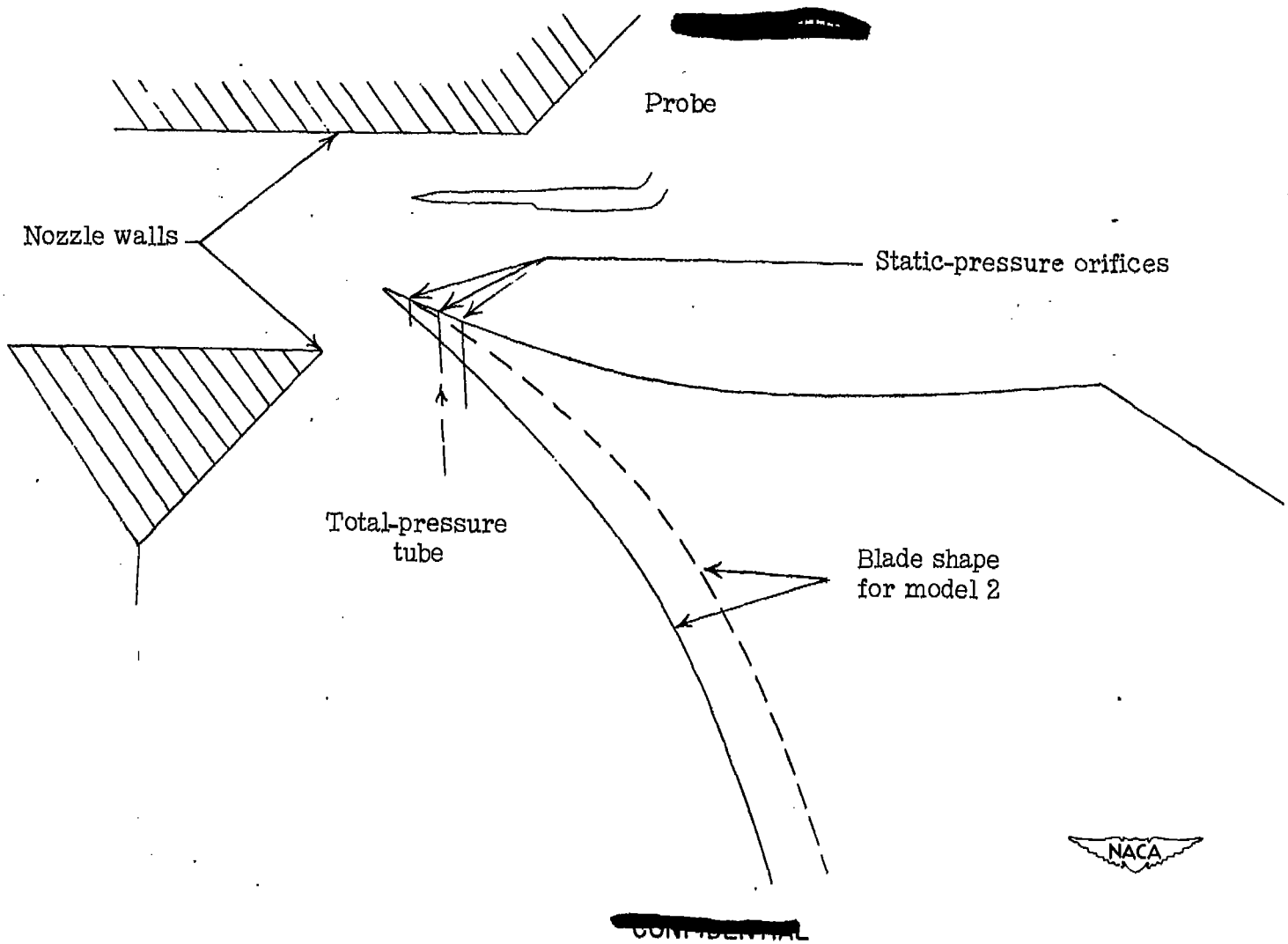

Figure 18.- Schematic test setup for model used for detached shock.

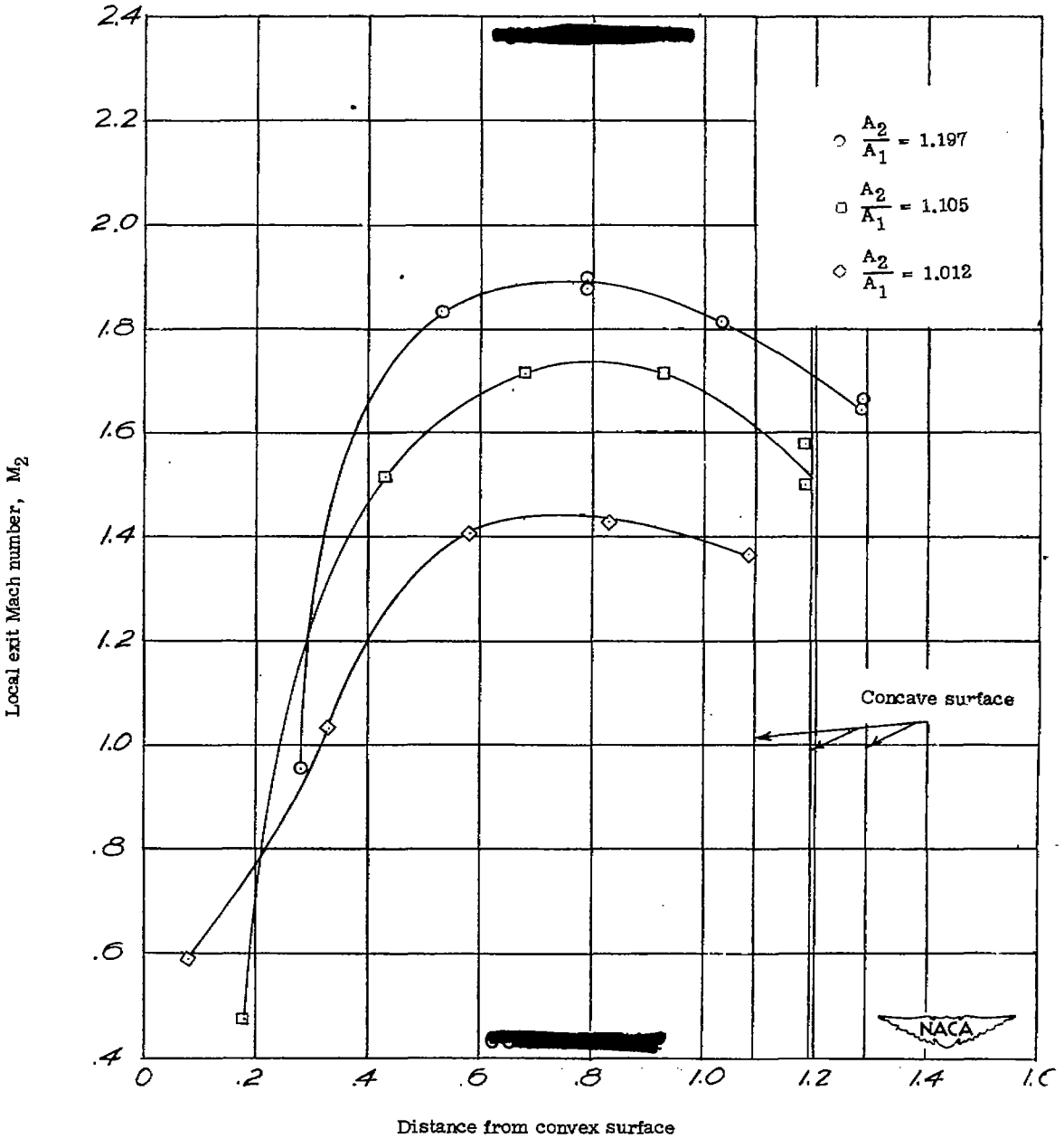

Figure 19.- The variation of local exit Mach number with distance from convex surface for three area ratios for model 1.

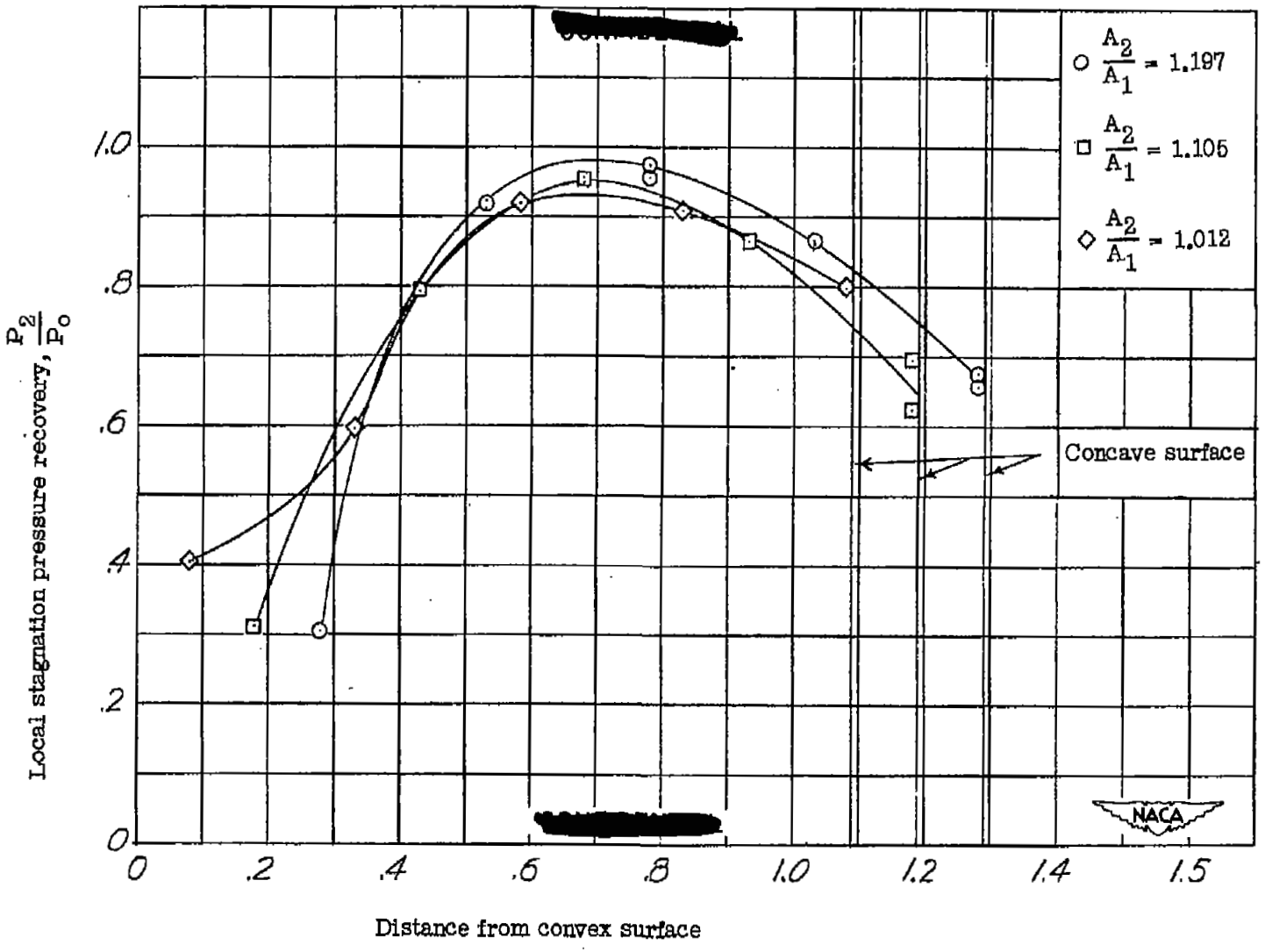

Figure 20.- The variation of the local stagnation-pressure recovery with distance from convex surface for three area ratios for model 1.

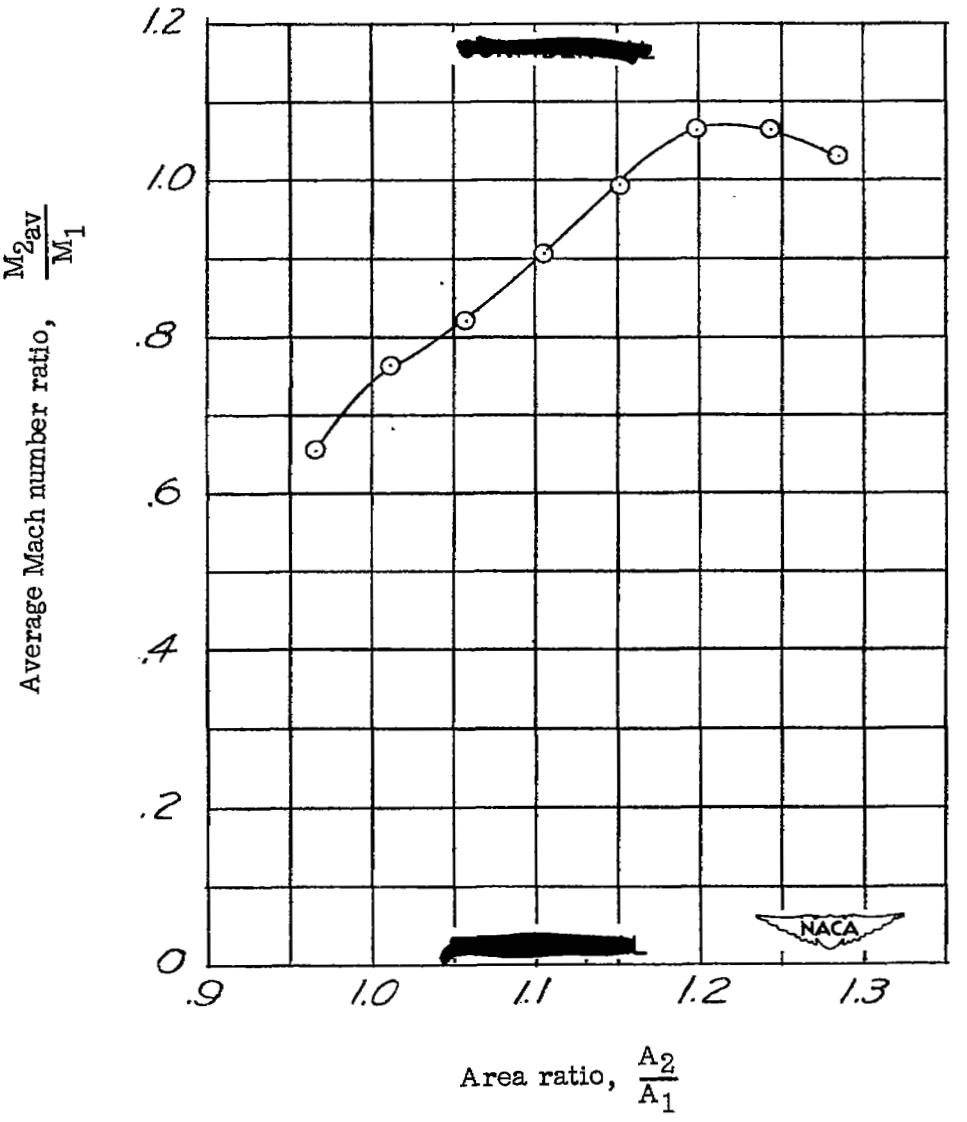

Figure 21.- The variation of the average Mach number ratio with area ratio for model 1.

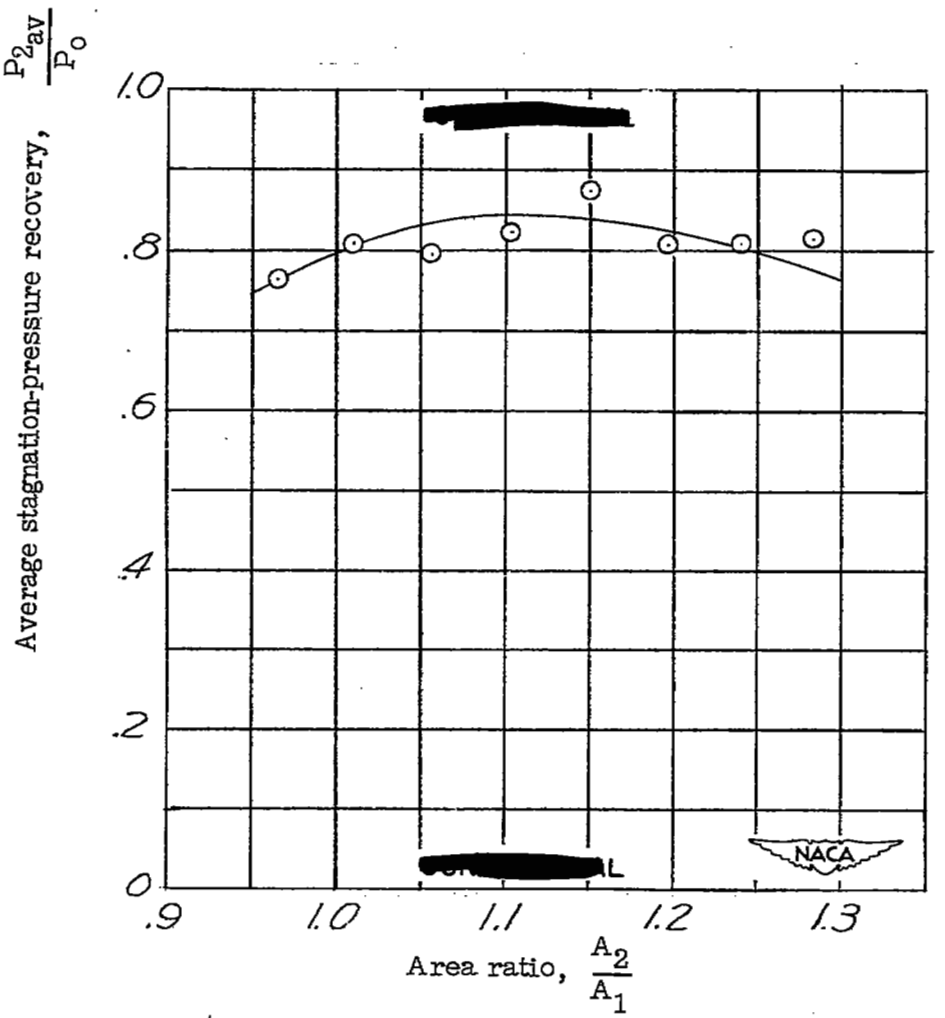

Figure 22.- The variation of the average stagnation-pressure recovery with area ratio for model 1.

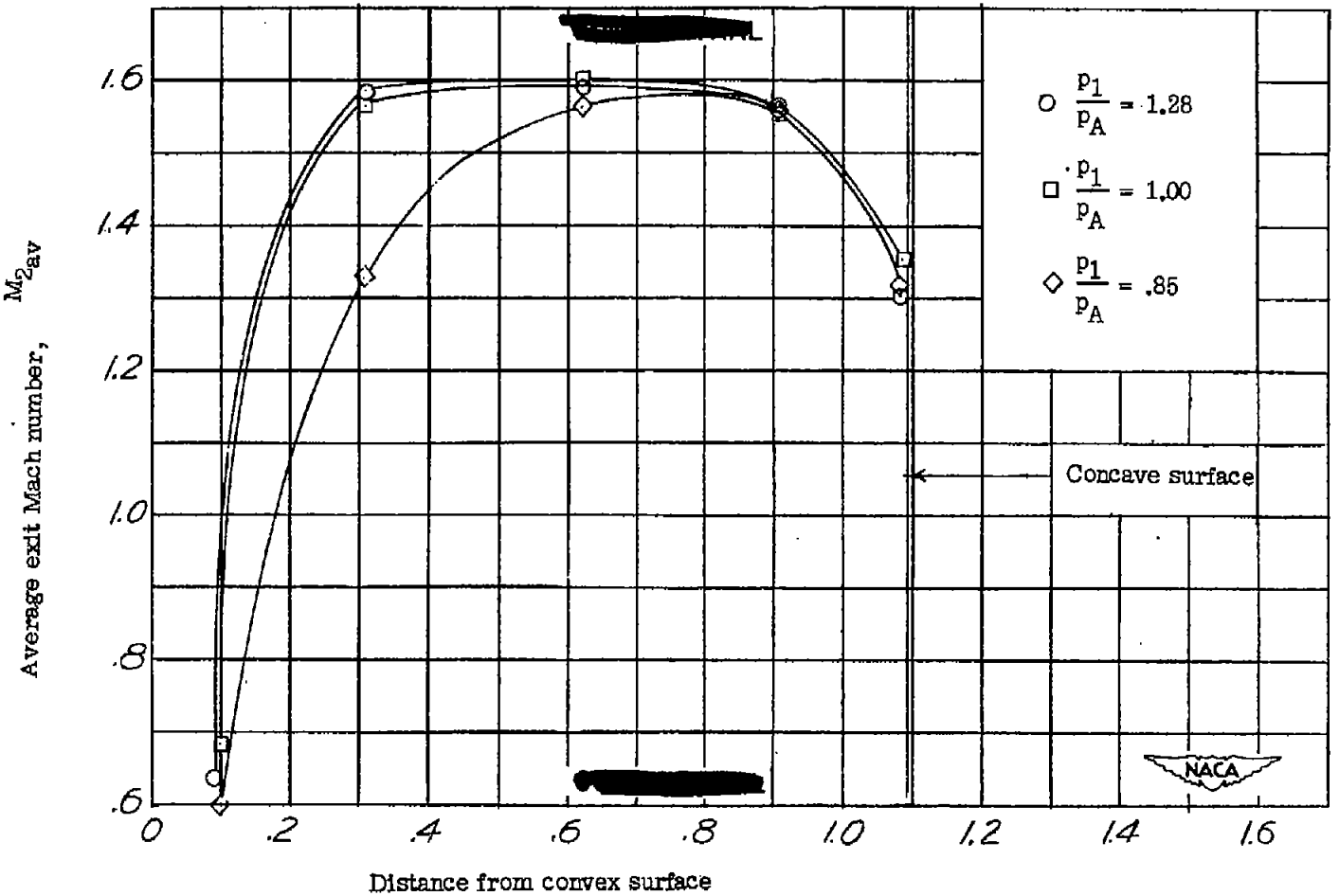

(a) 50-percent-span station.

Figure 23.- The variation of the average exit Mach number with distance from convex surface for three static-pressure ratios at an area ratio of 1.077 for model 2.

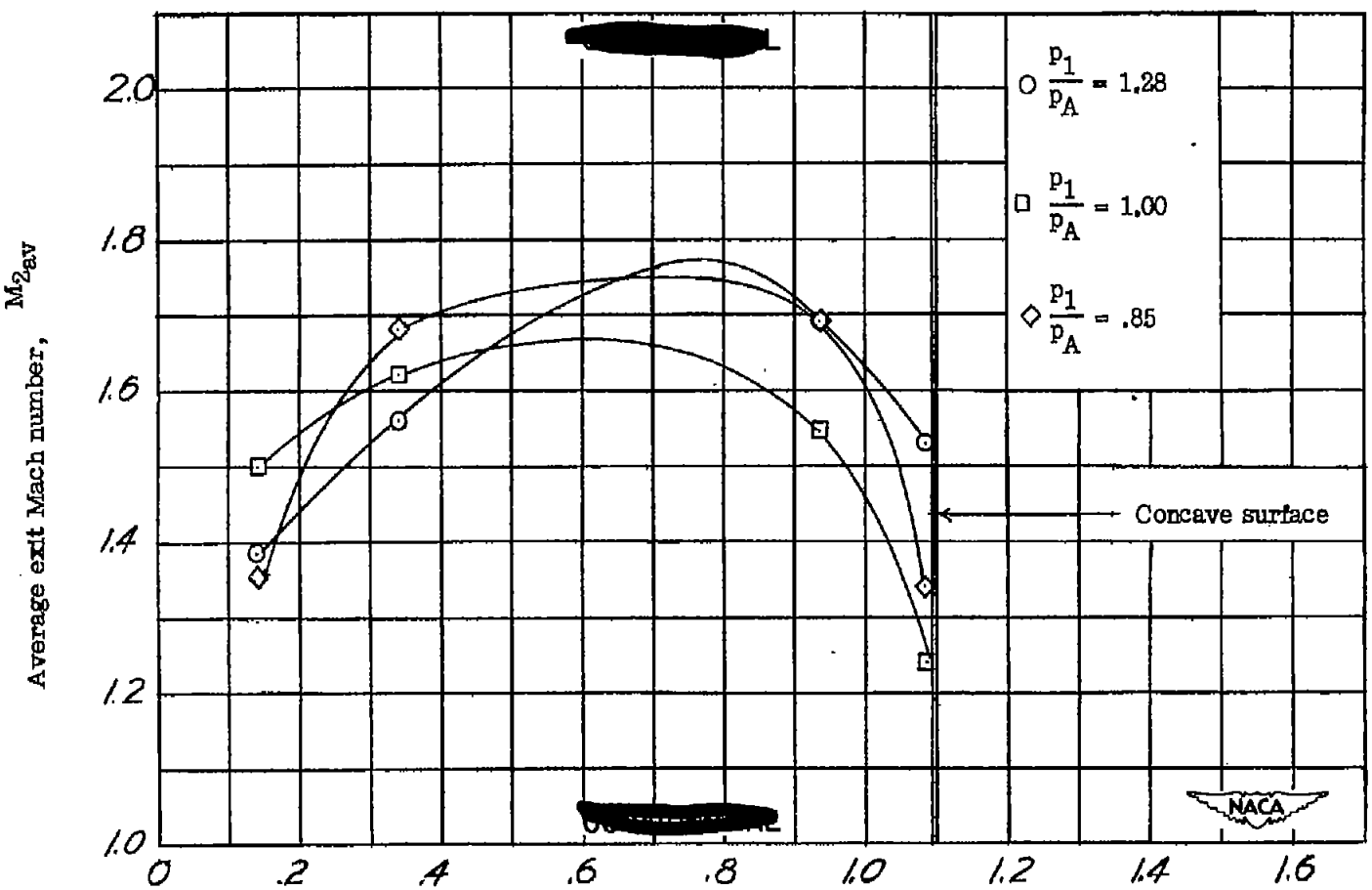

(b) 10.15-percent-span station.

Figure 23.- Concluded.

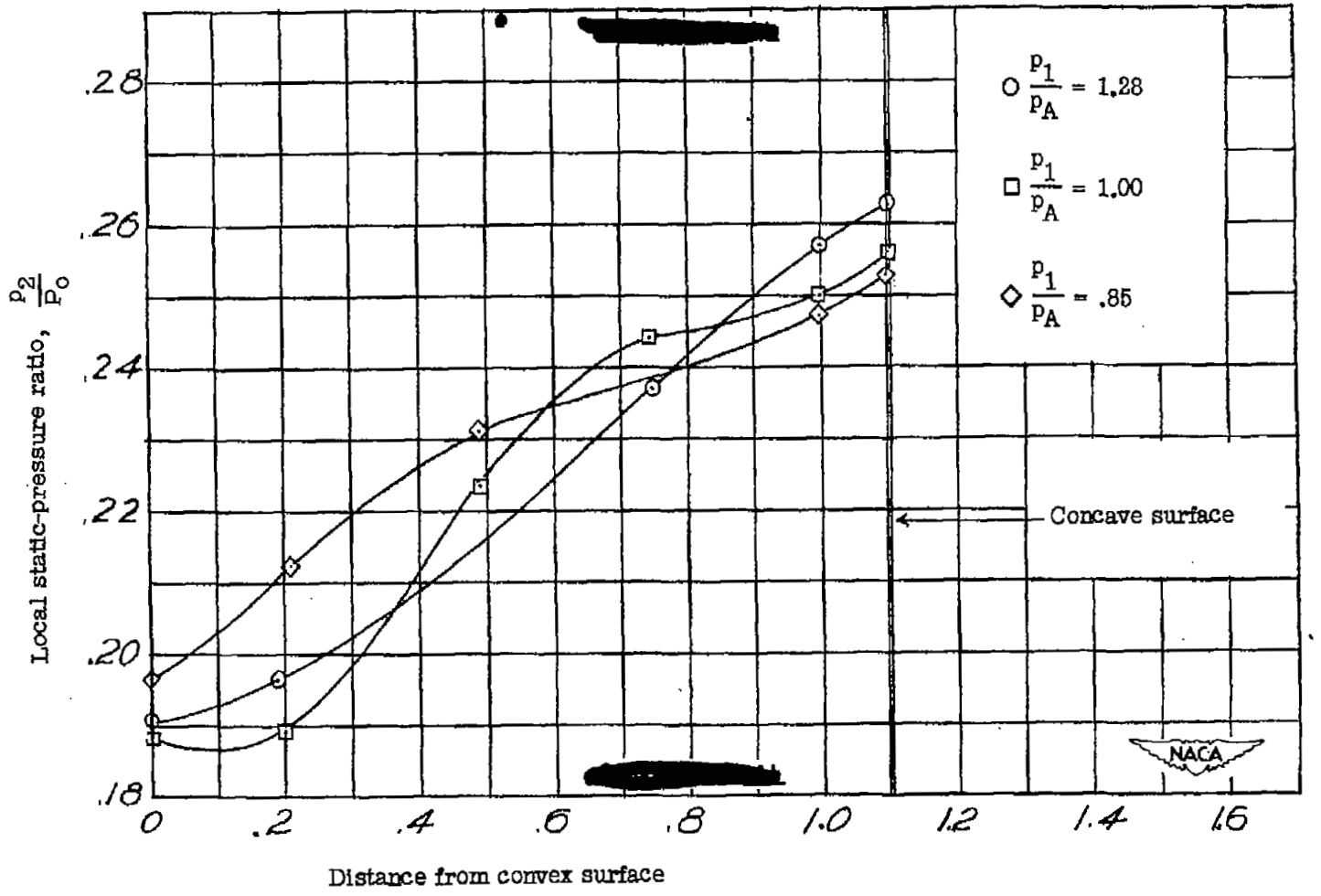

(a) Local static-pressure ratio.

Figure 24.- Pressure distribution at 50-percent-span station for three static-pressure ratios at an area ratio of 1.077 for model 2.

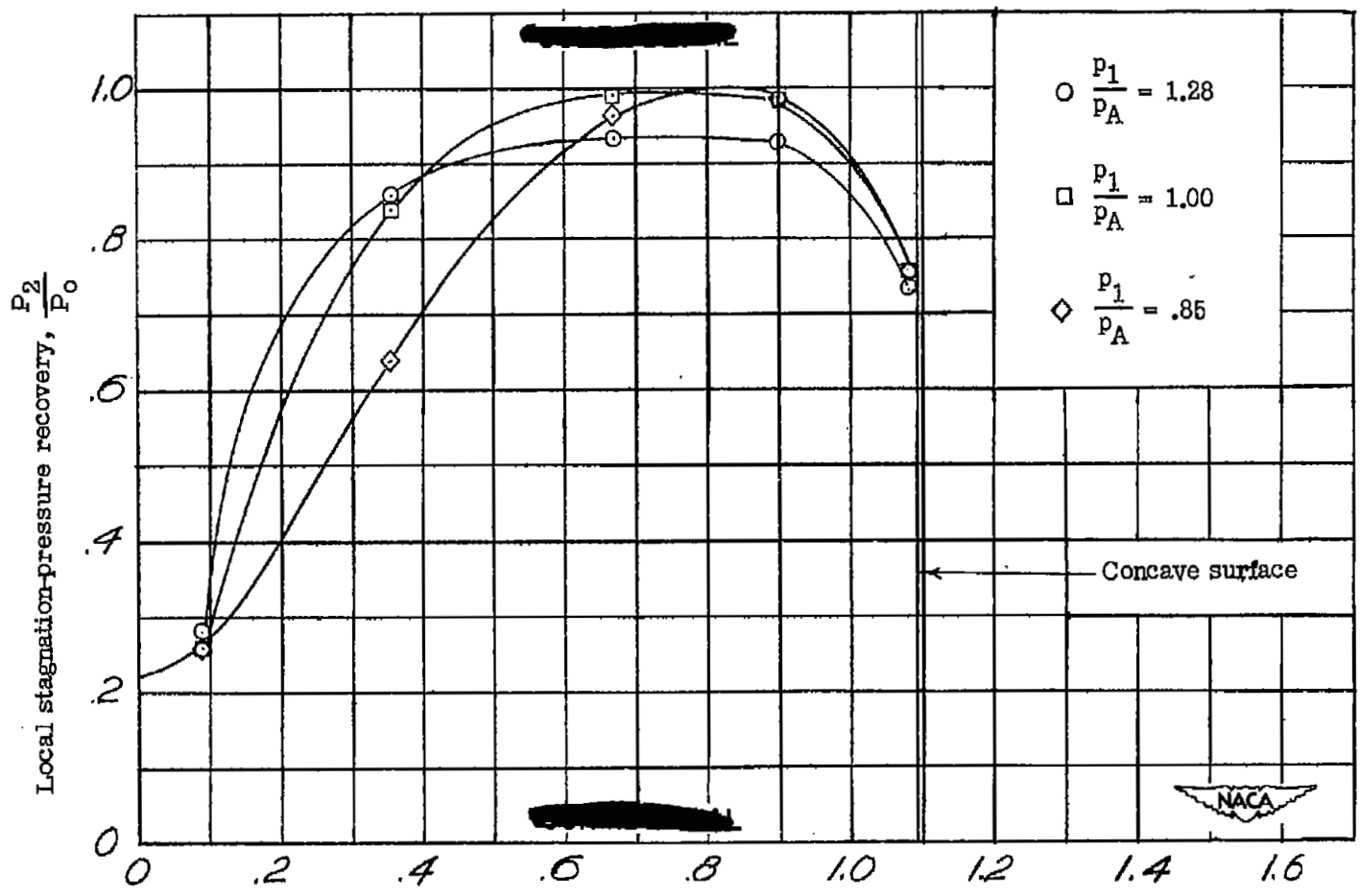

(b) Local stagnation-pressure recovery.

Figure 24.- Concluded.

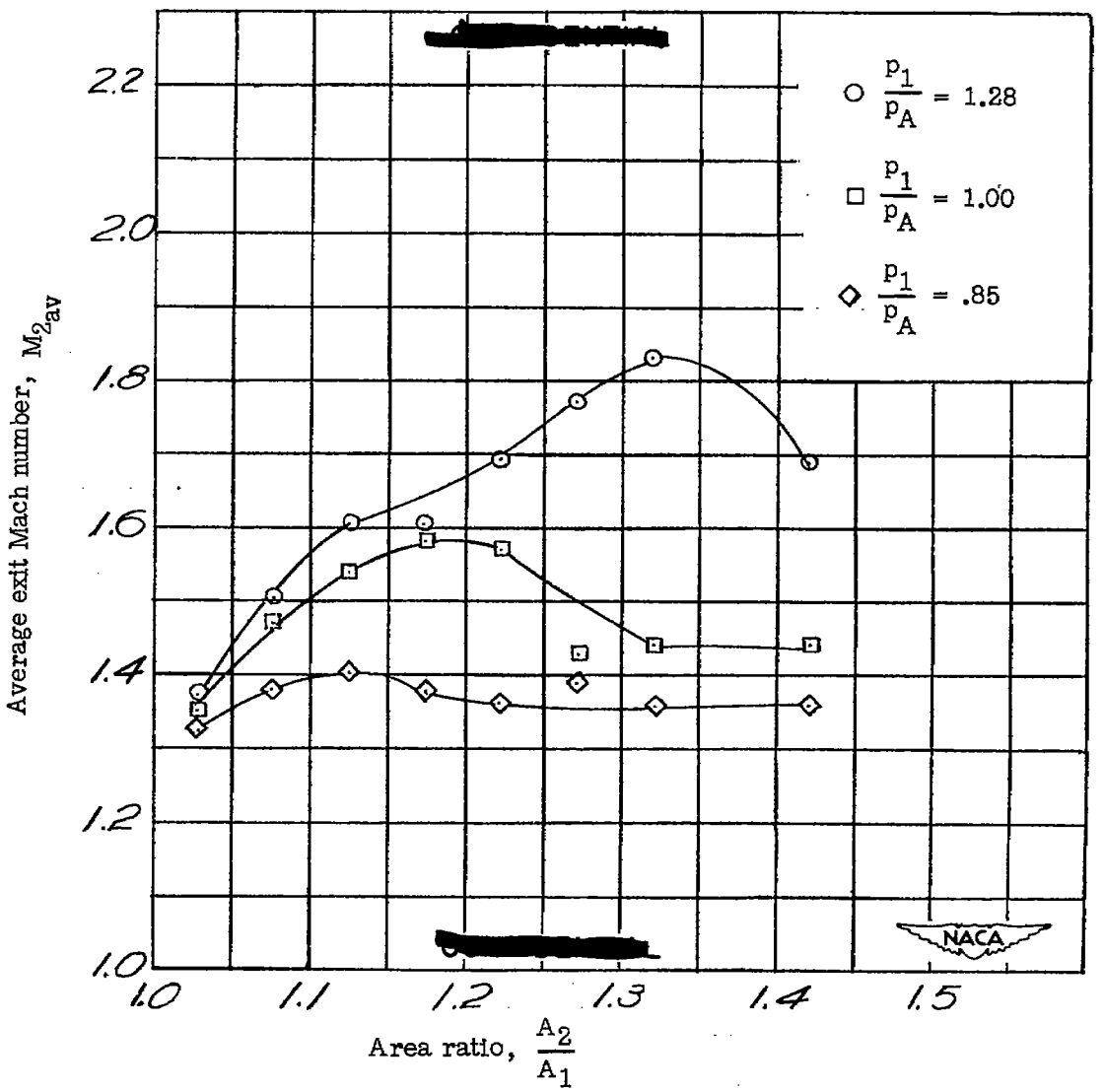

(a) 50-percent-span station.

Figure 25.- The variation of the average Mach number with area ratio for three static-pressure ratios for model 2.

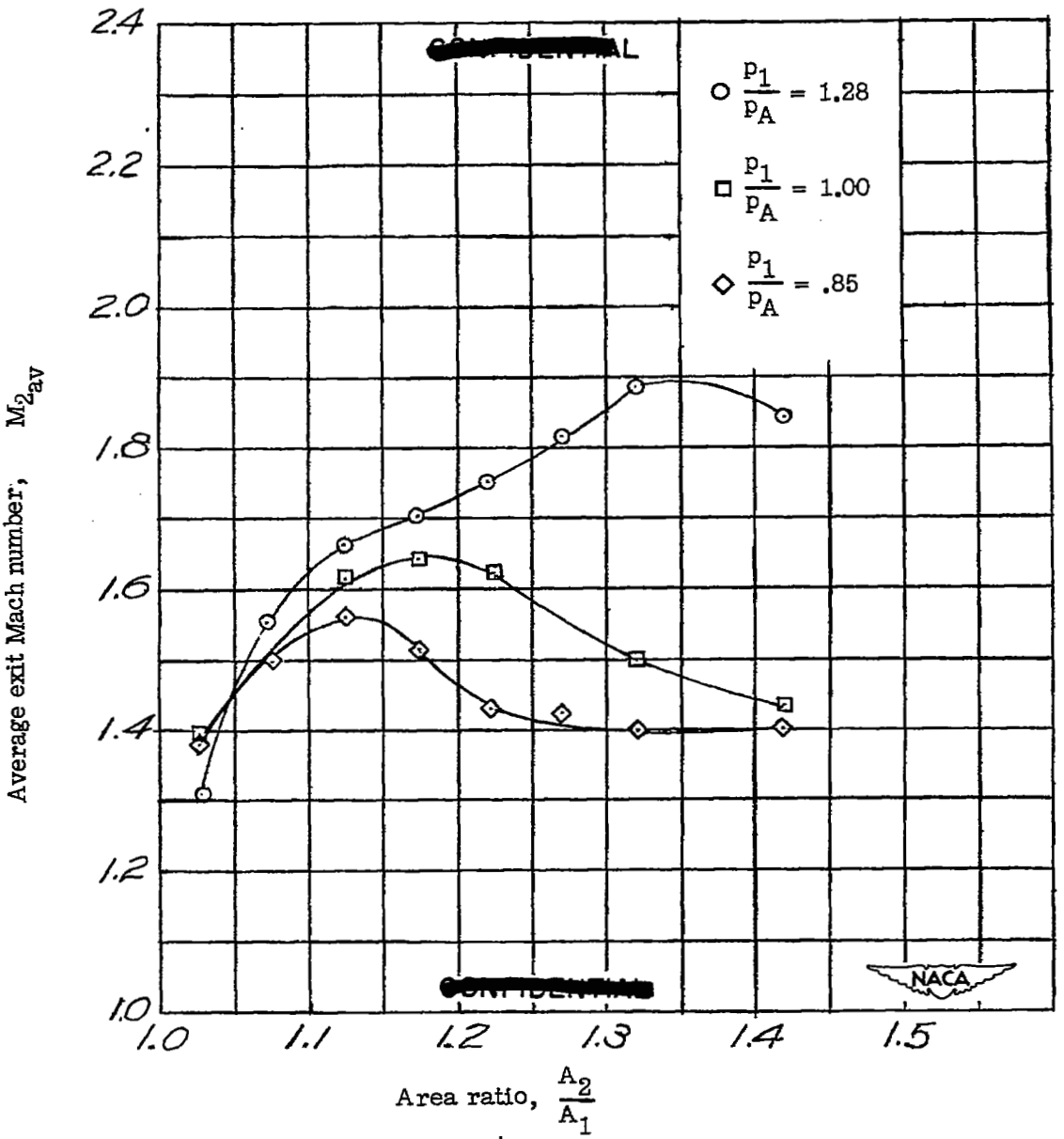

(b) 10.15-percent-span station.

Figure 25.- Concluded.

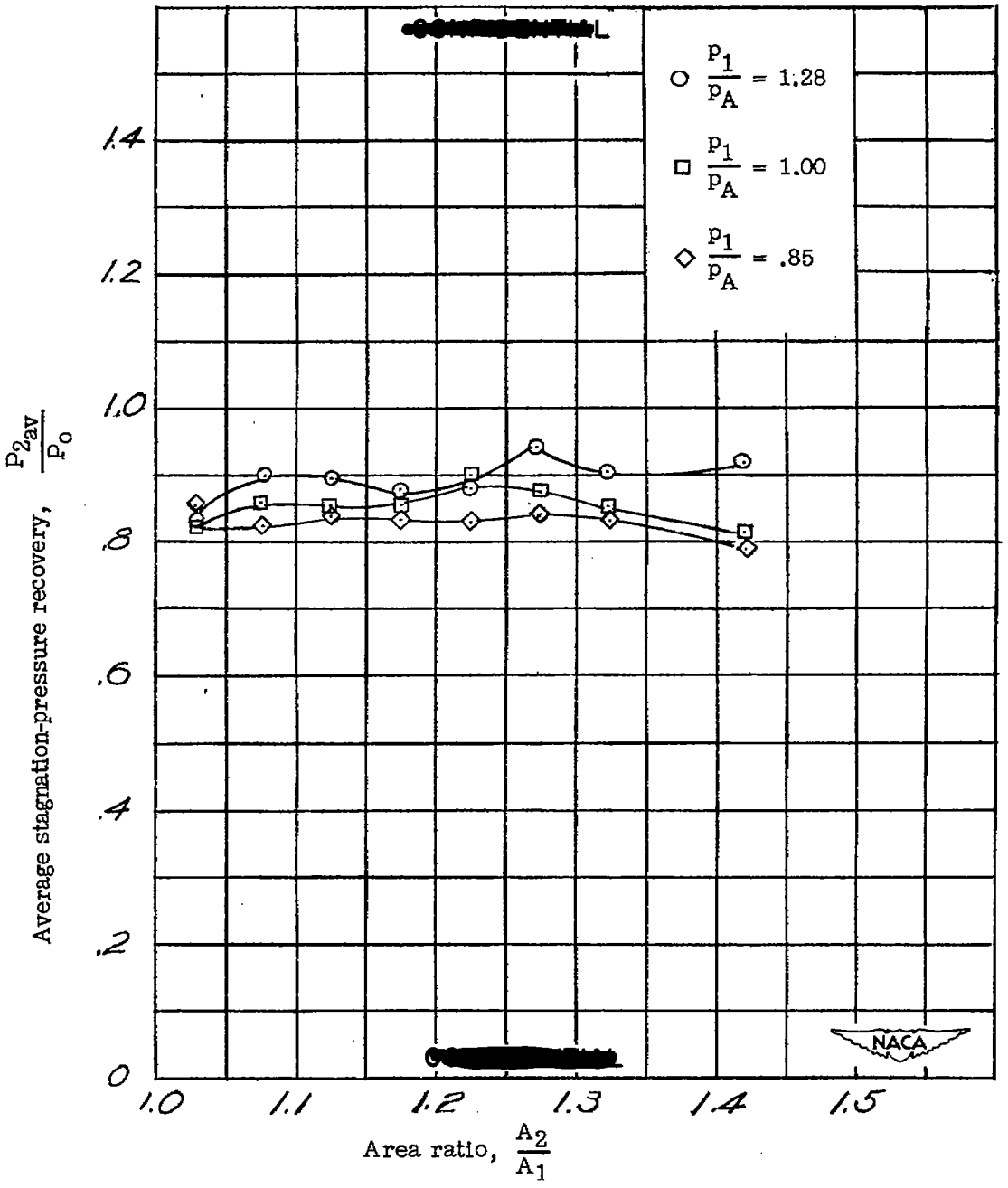

(a) 50-percent-span station.

Figure 26.- The variation of the average stagnation-pressure recovery with area ratio for three static-pressure ratios for model 2.

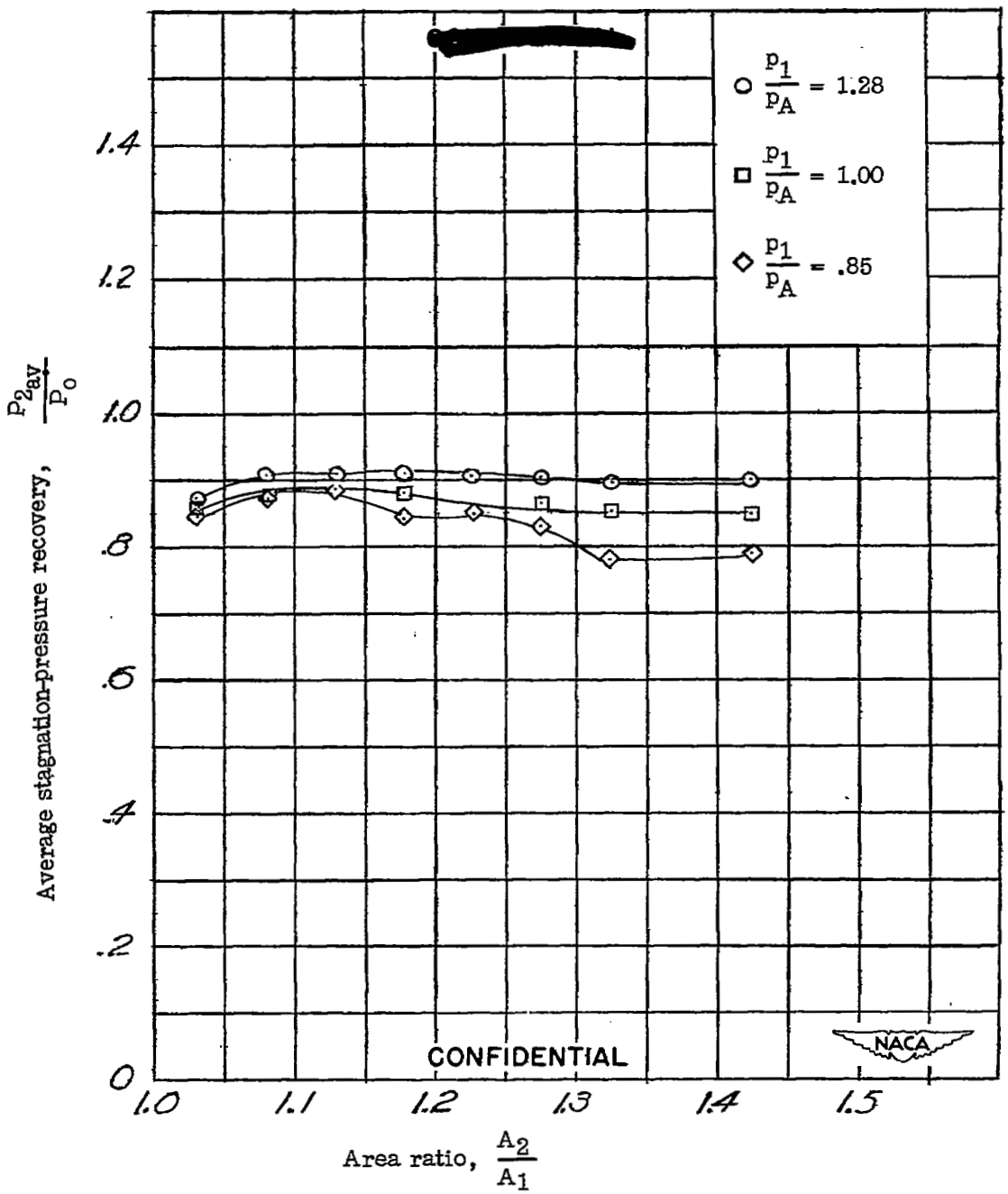

(b) 10.15-percent-span station.

Figure 26.- Concluded.

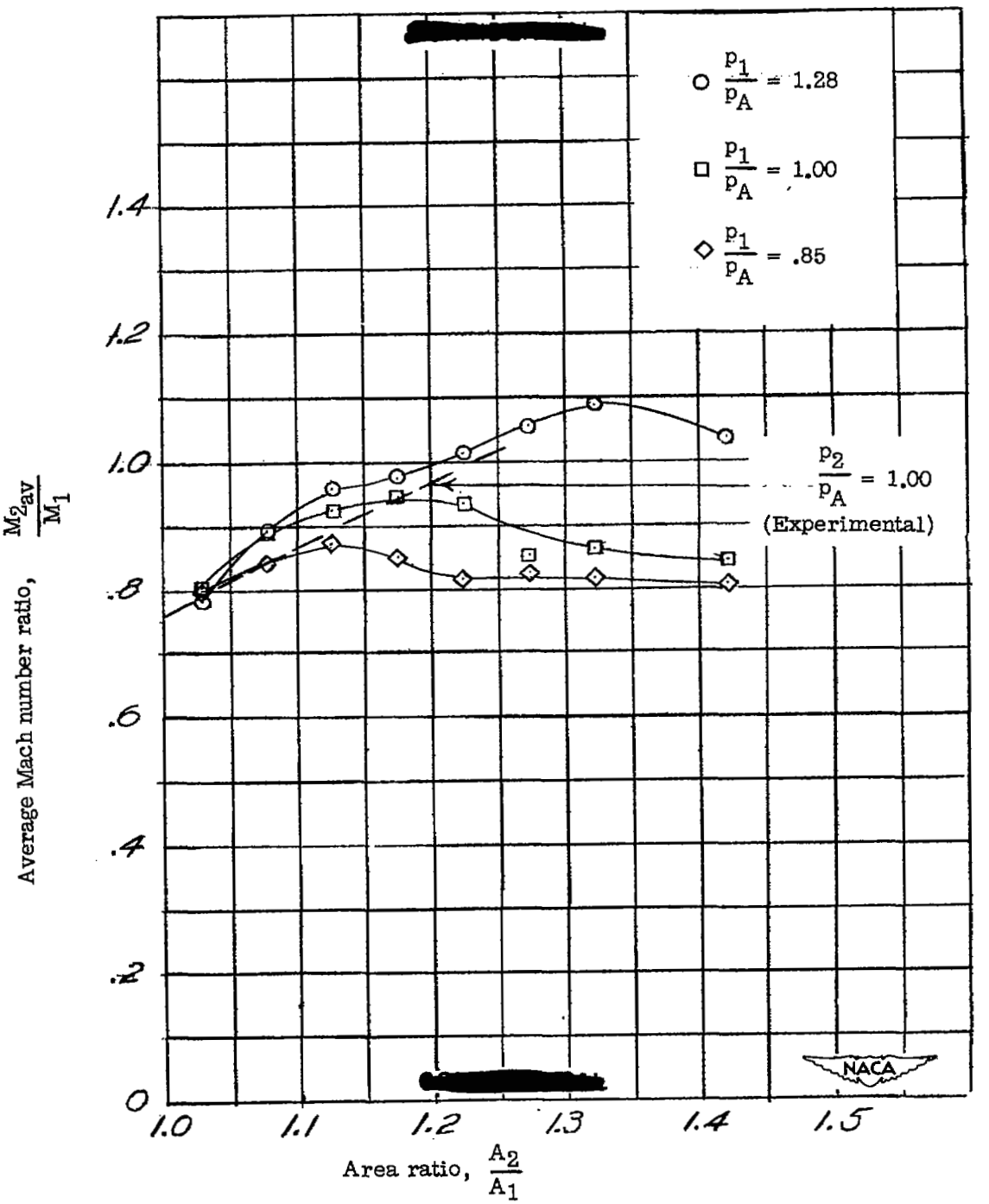

Figure 27.- The variation of the average Mach number ratio with area ratio at three static-pressure ratios for model 2.

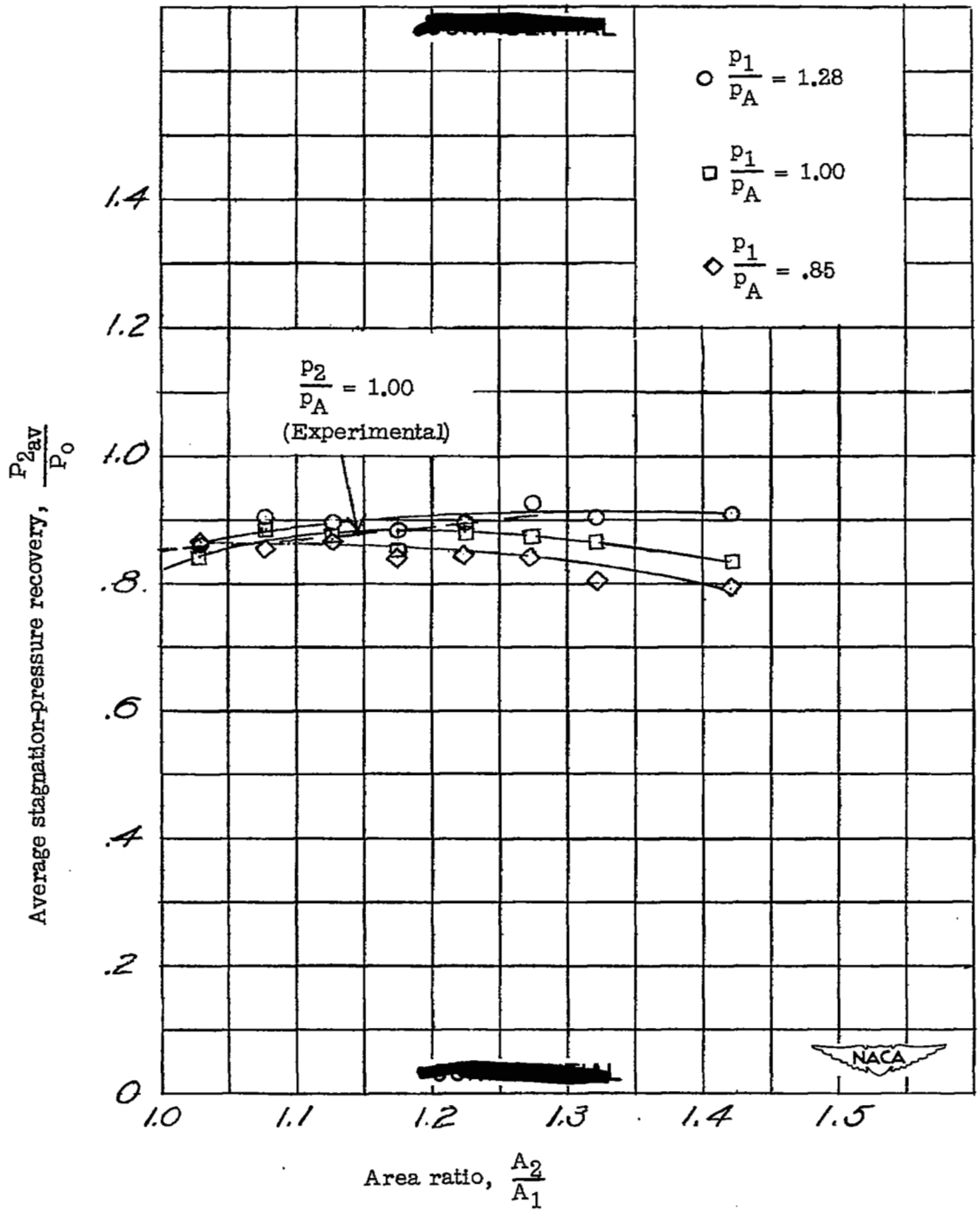

Figure 28.- The variation of the average stagnation-pressure recovery with area ratio at three static-pressure ratios for model 2.

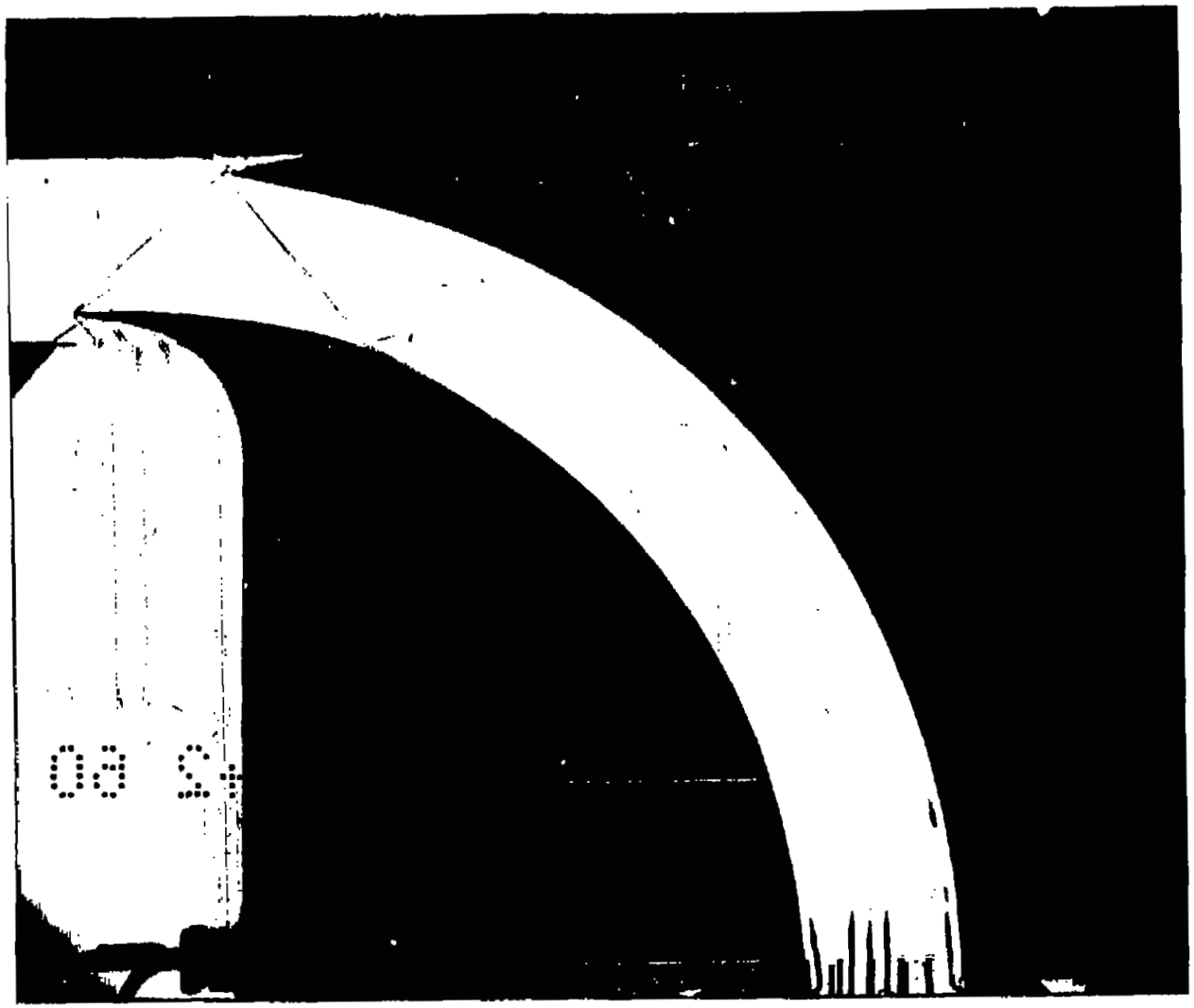

Figure 29.- A shadowgraph of the flow in the passage at an area ratio of 1.273 for model 2.

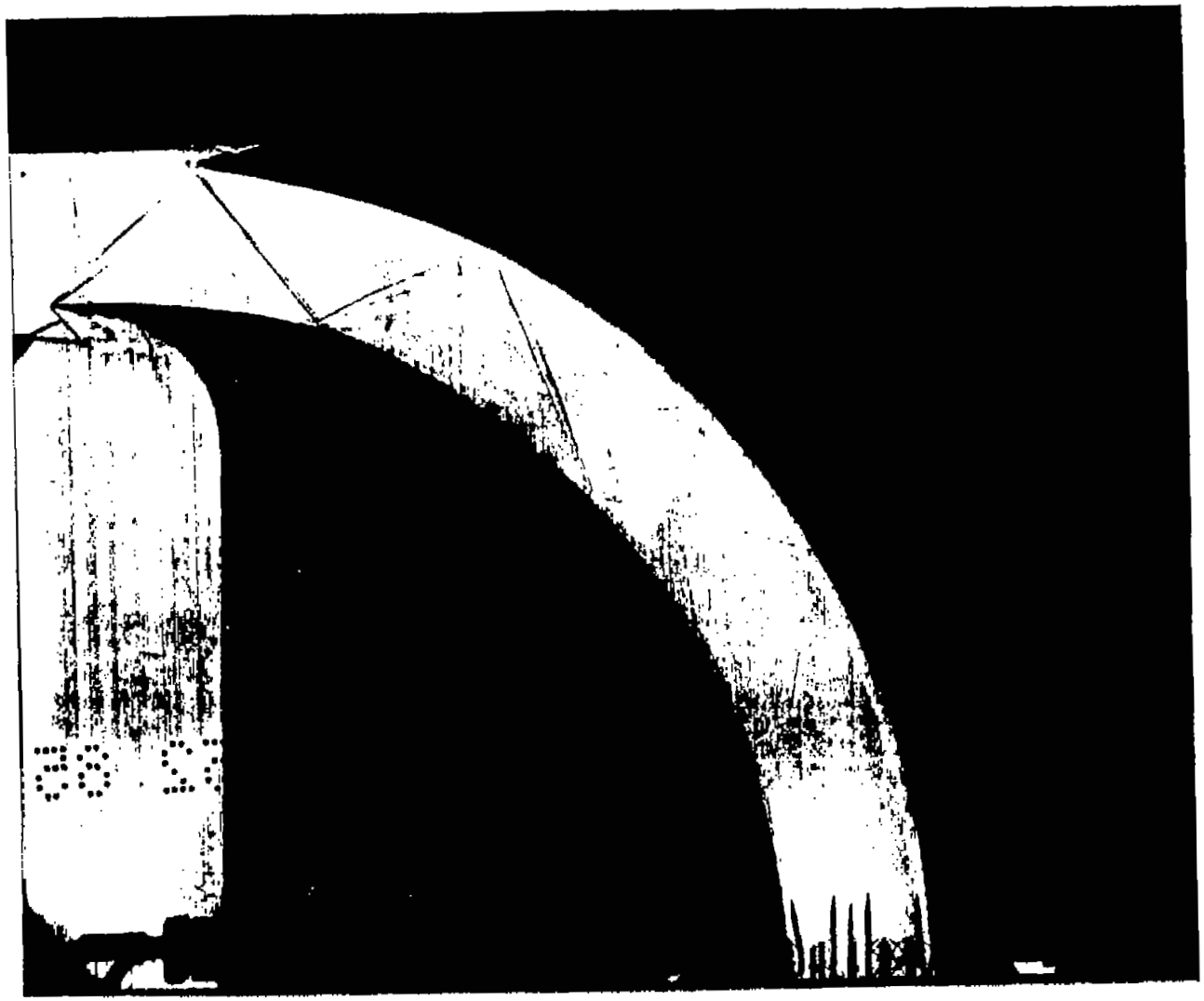

Figure 30.- A shadowgraph of the flow in the passage at an area ratio of 1.175 for model 2.

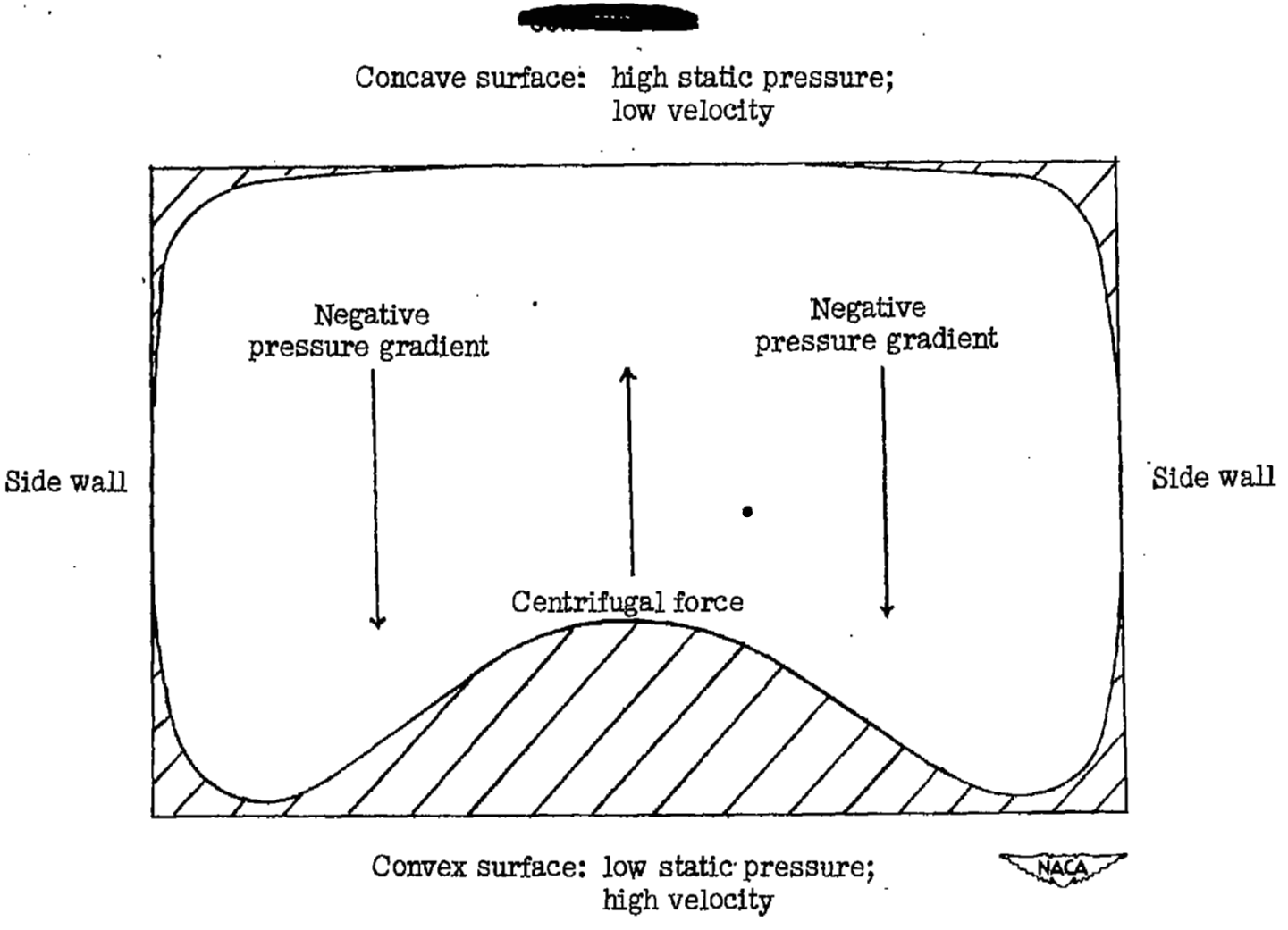

Figure 31.- A schematic diagram of the boundary layer and the secondary flow.

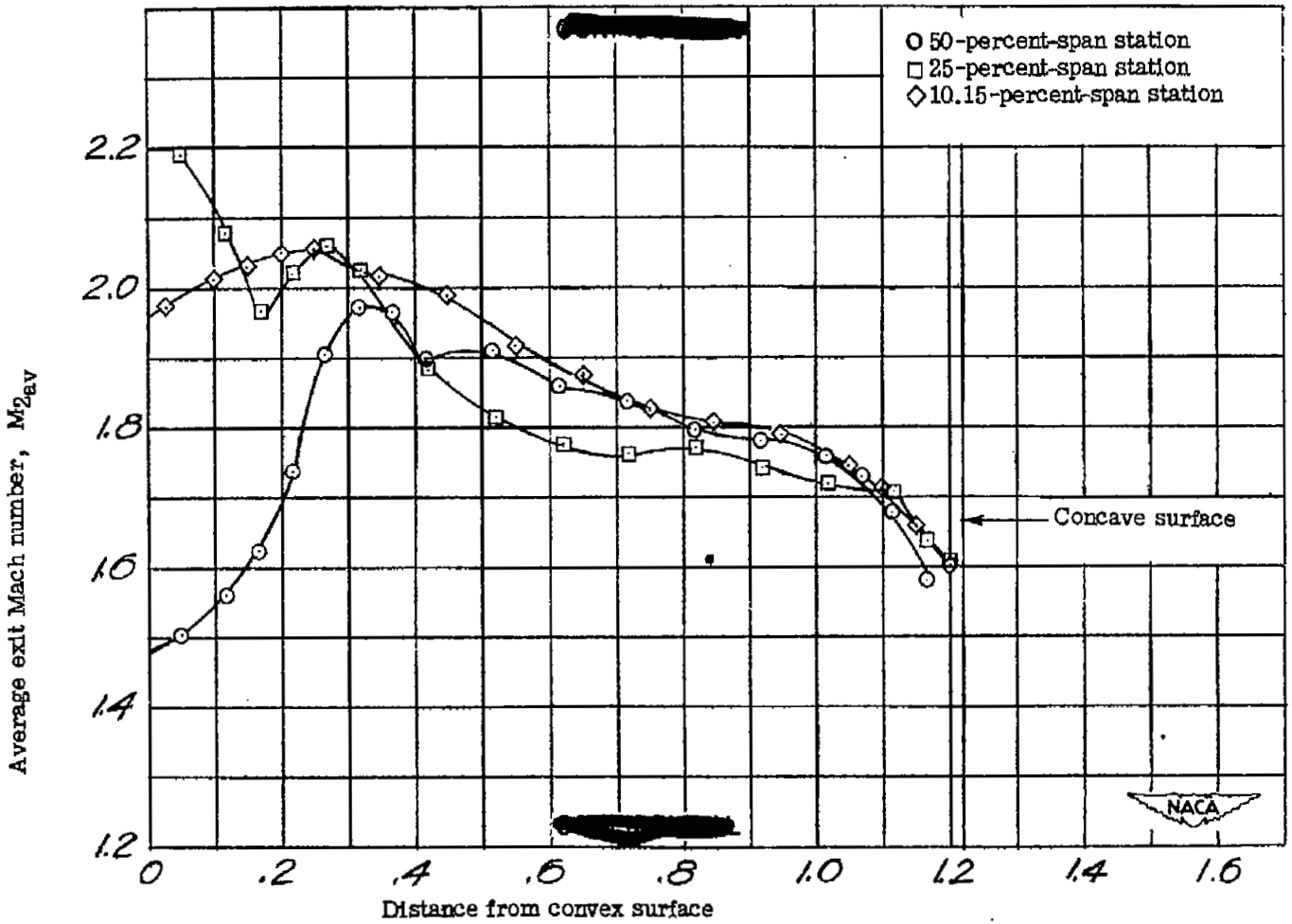

Figure 32.- The variation of the average exit Mach number with distance from convex surface for model 3.

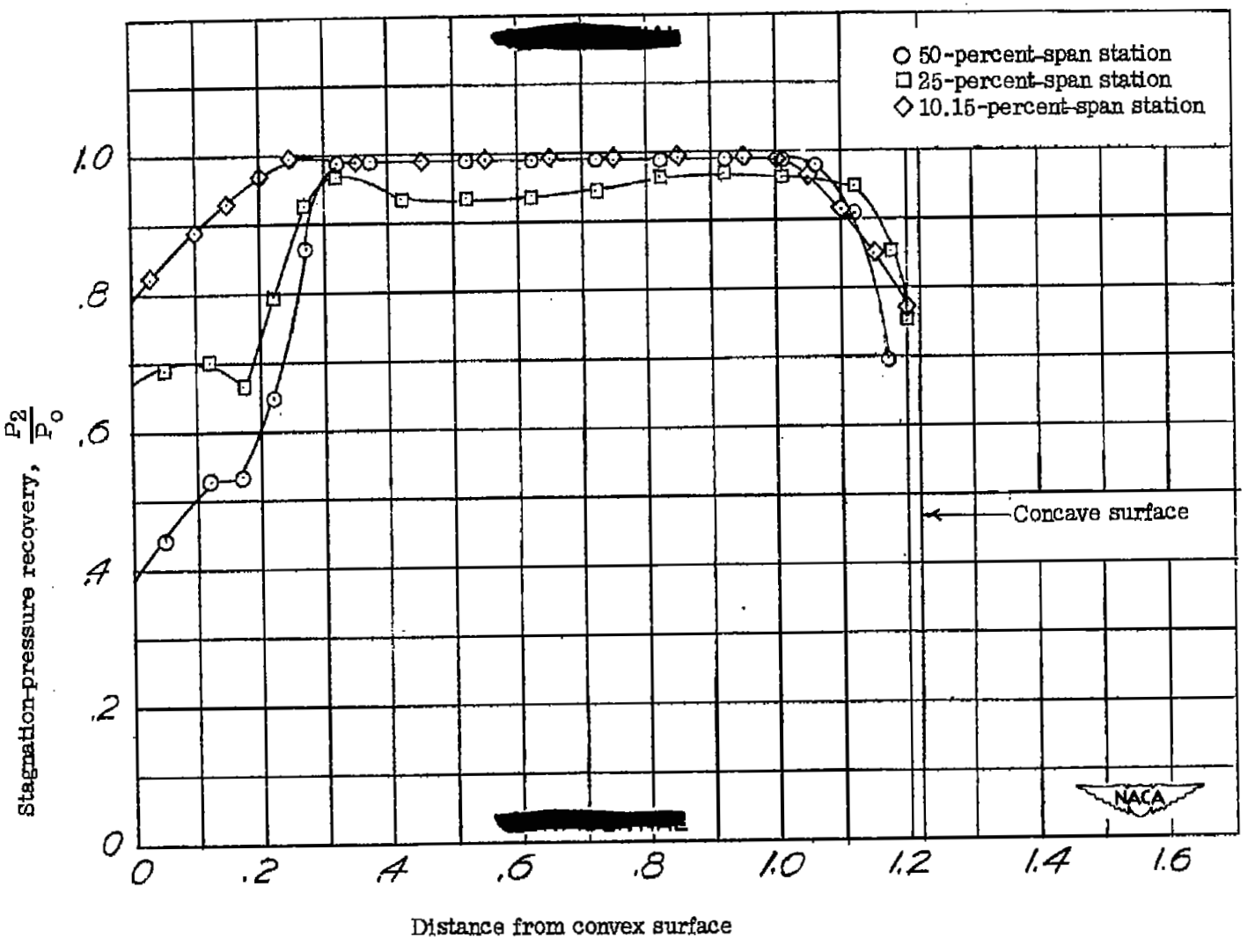

Figure 33.- The variation of the stagnation-pressure recovery with distance from convex surface for model 3.

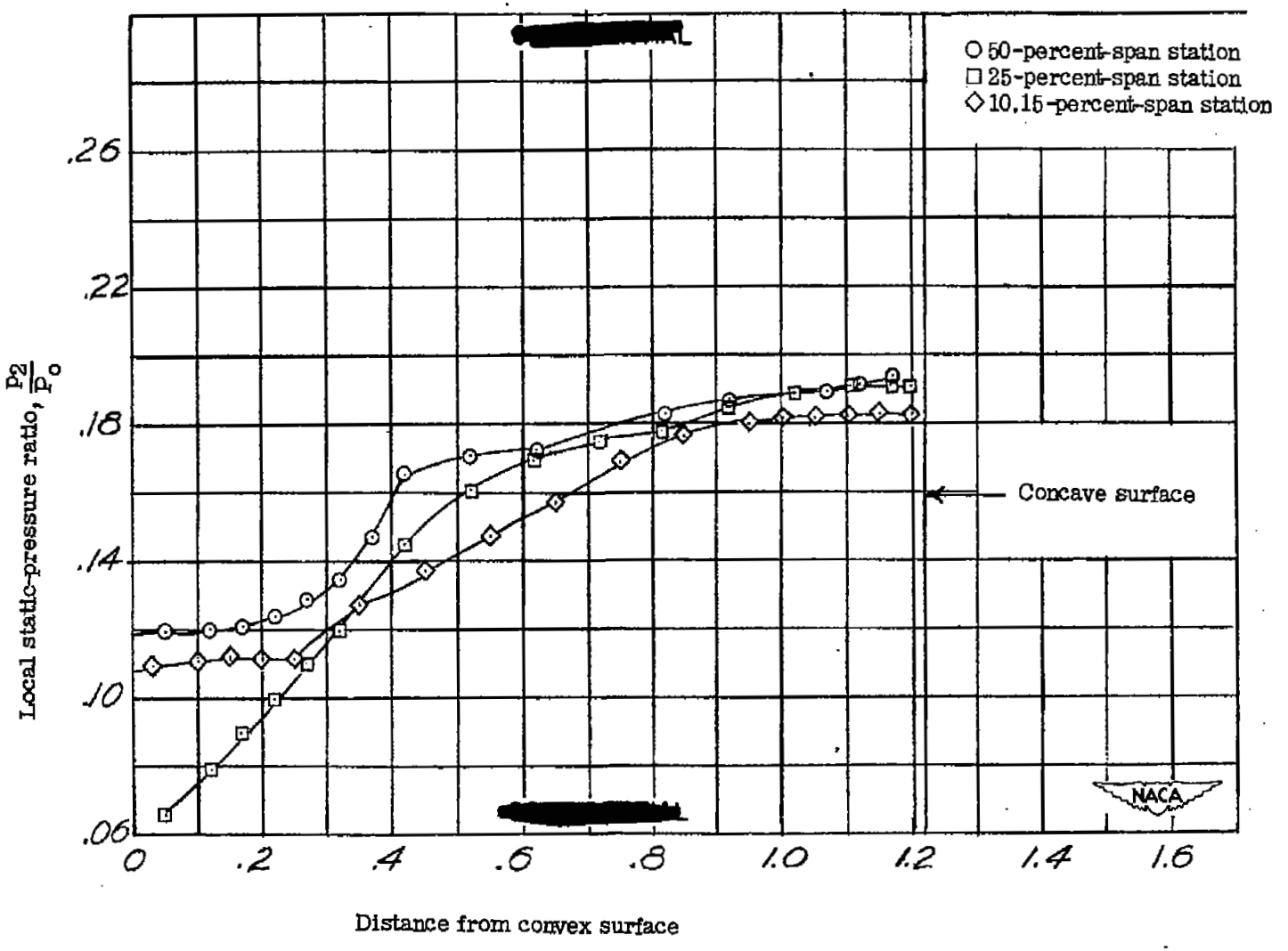

Figure 34.- The variation of the local static-pressure ratio with distance from convex surface for model 3.

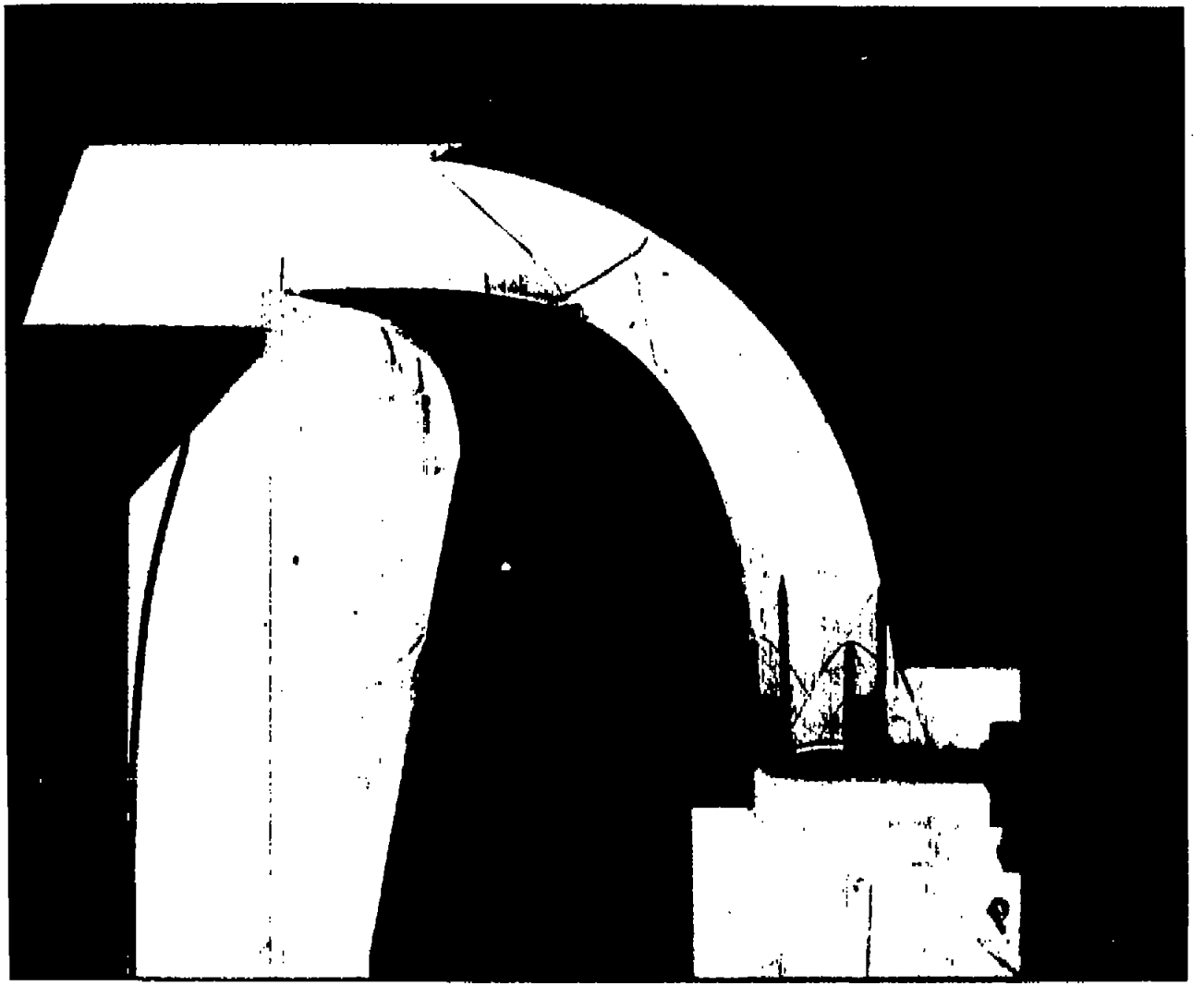

Figure 35.– A shadowgraph of the flow in the passage at an area ratio of 1.208 for model 3.

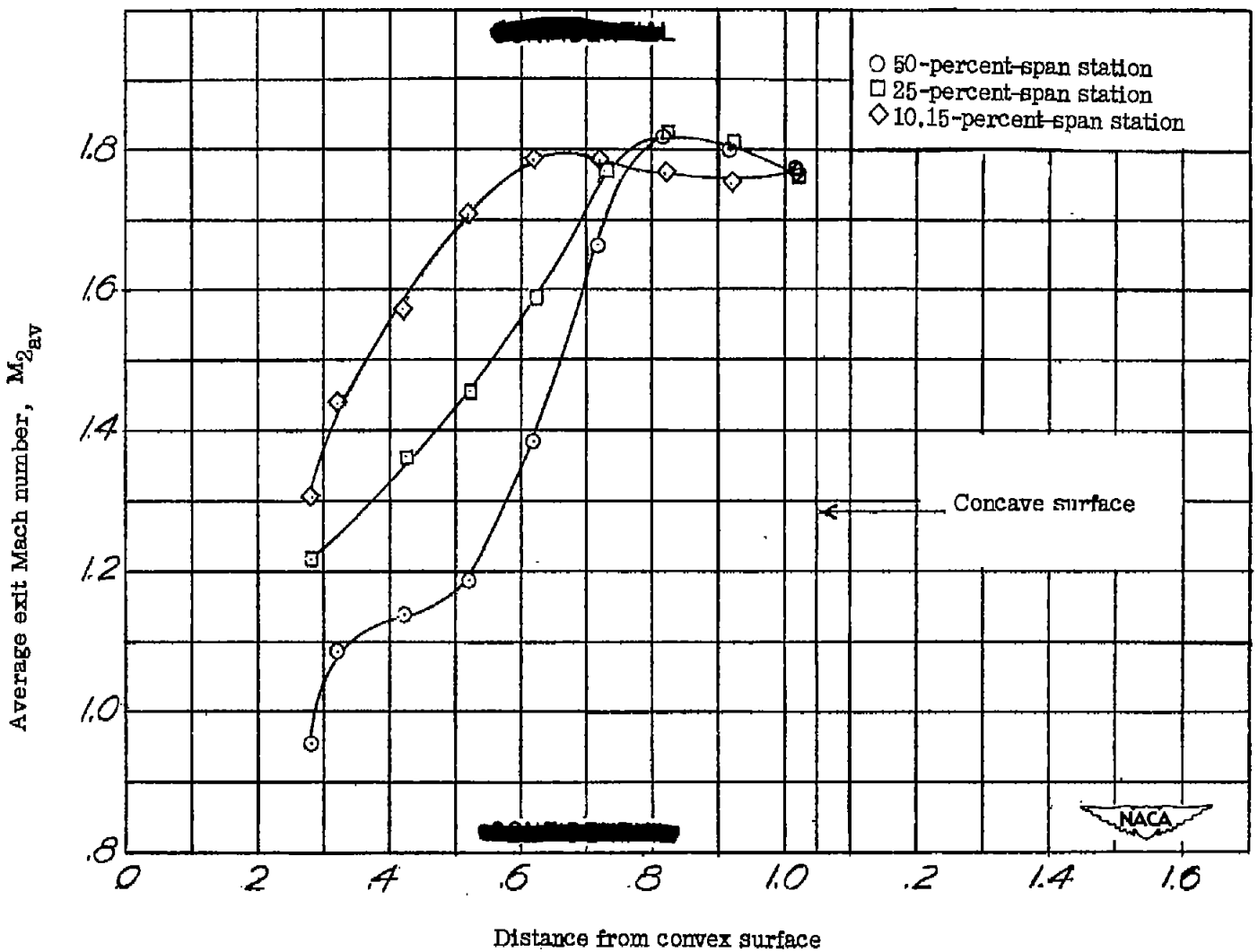

Figure 36.- The variation of the average exit Mach number with distance from convex surface for model 4.

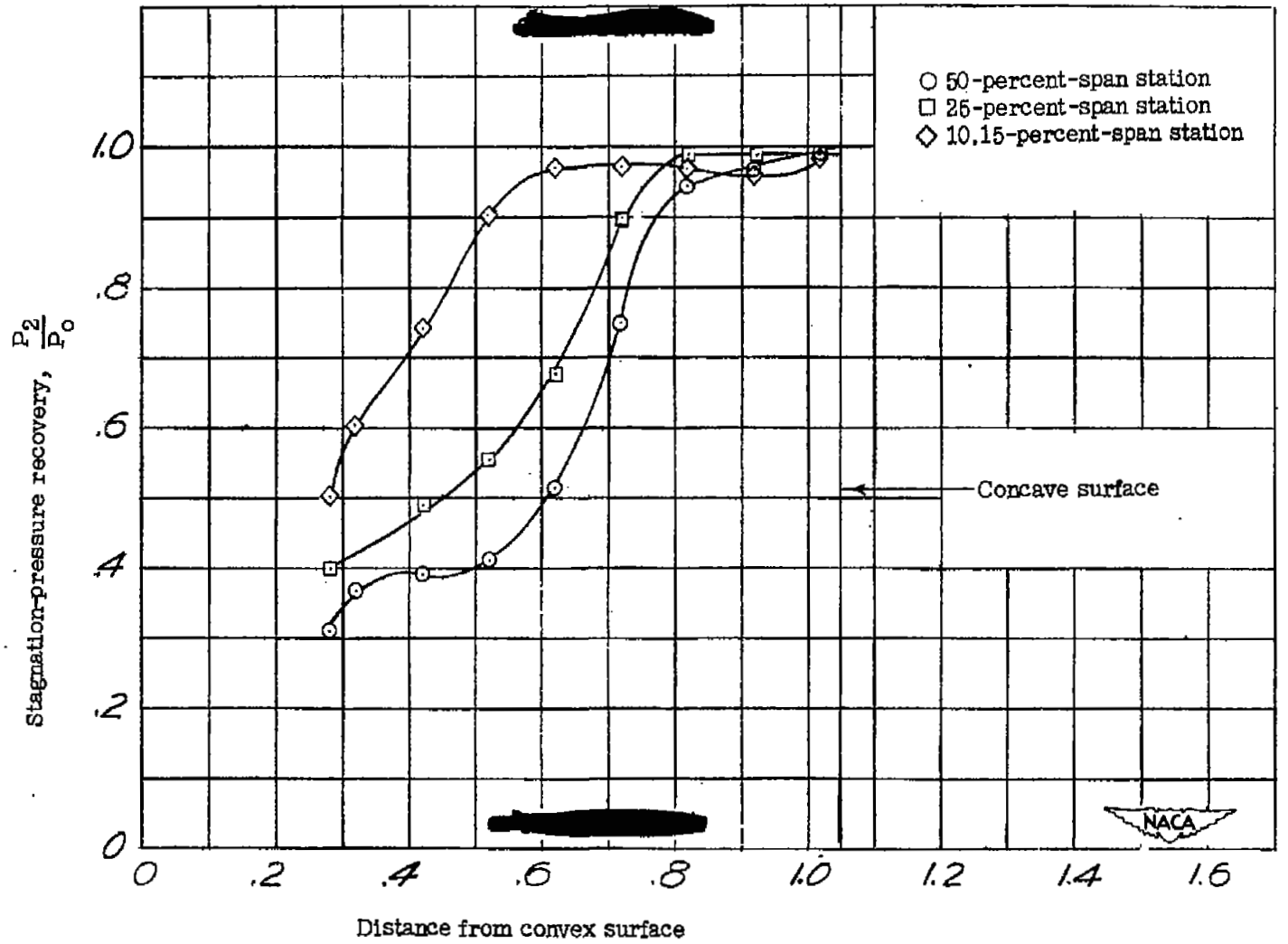

Figure 37.- The variation of the stagnation-pressure recovery with distance from convex surface for model 4.

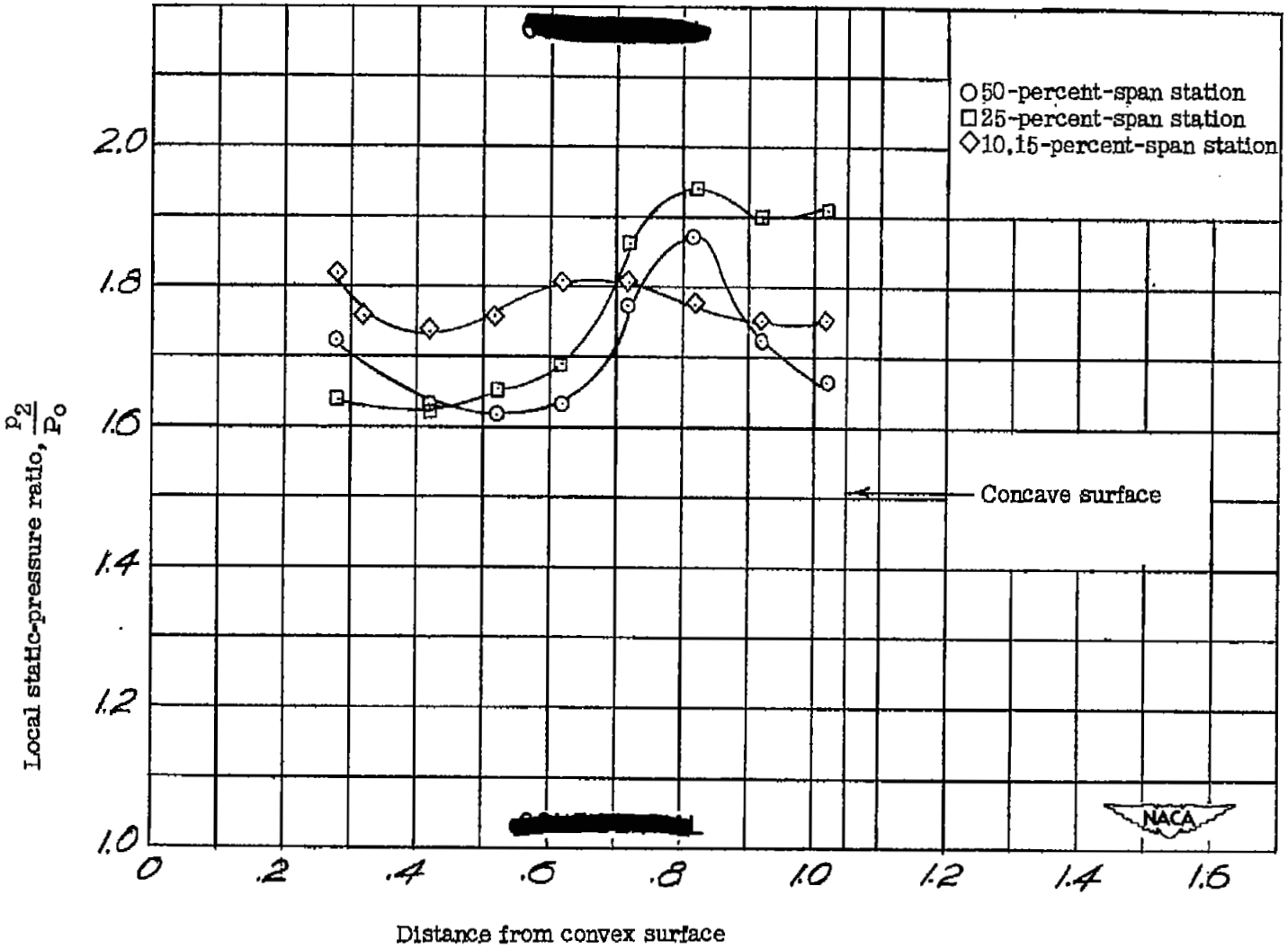

Figure 38.- The variation of the local static-pressure ratio with distance from convex surface for model 4.

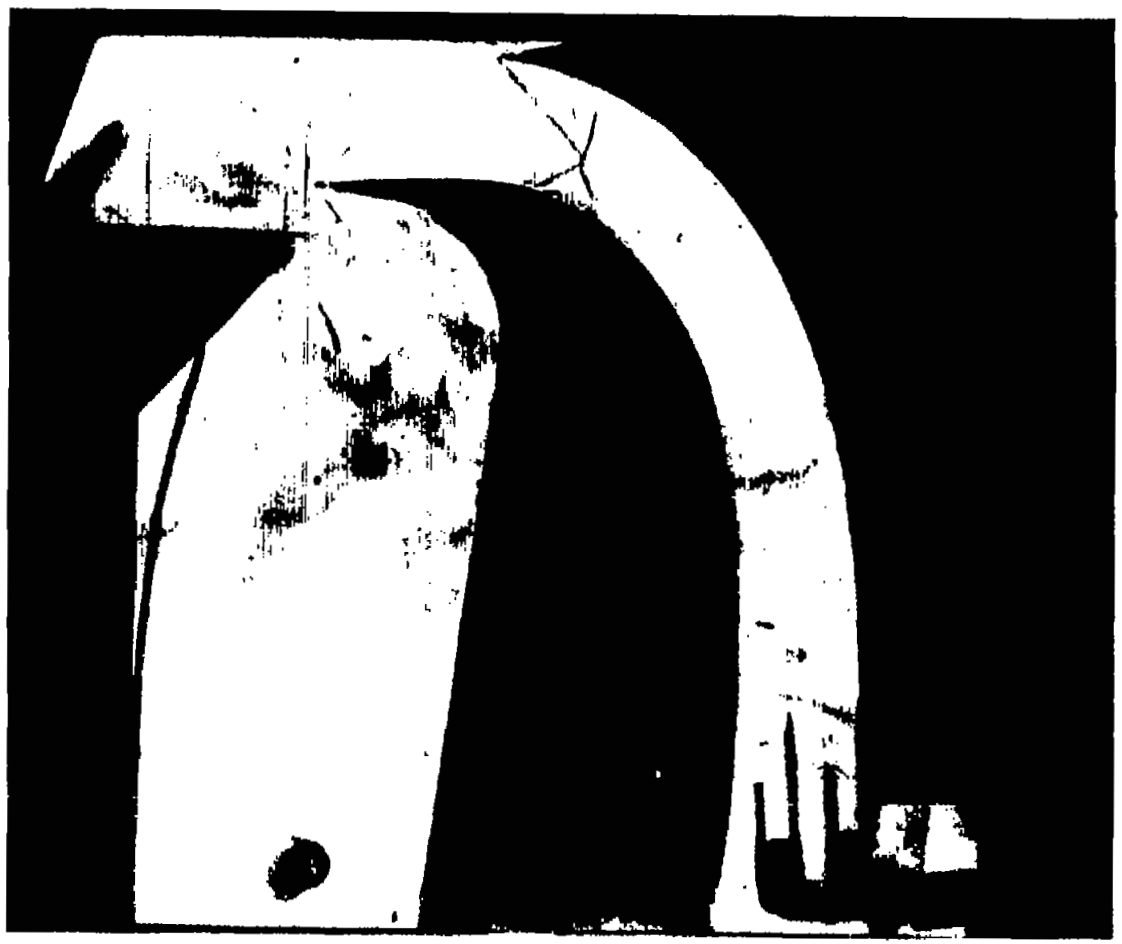

(a) Passage corresponding to characteristics net shown in figure 10(a).

Figure 39.- A shadowgraph of the flow in the passage for model 4.

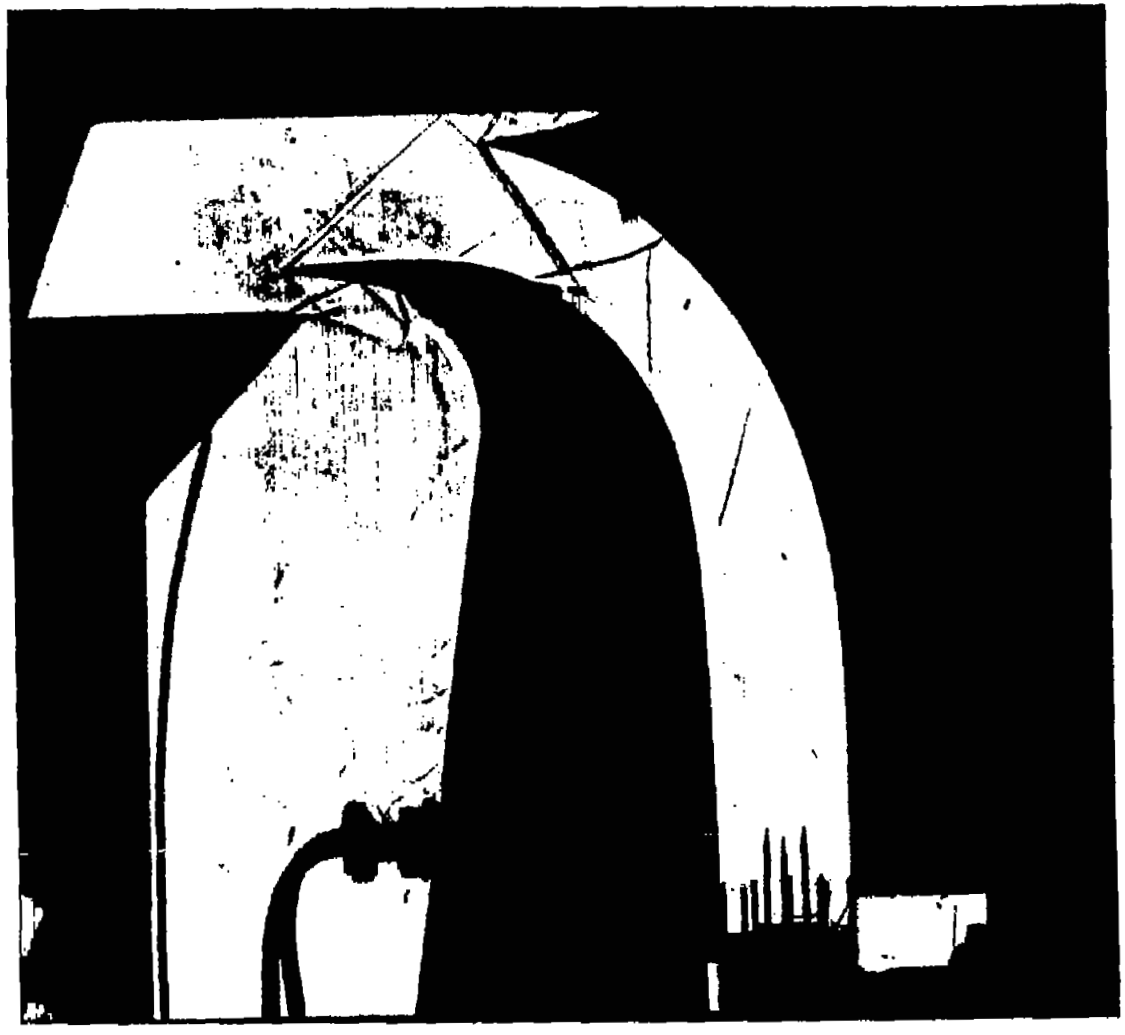

(b) Passage corresponding to characteristics net shown in figure 10(b).

Figure 39.- Concluded.

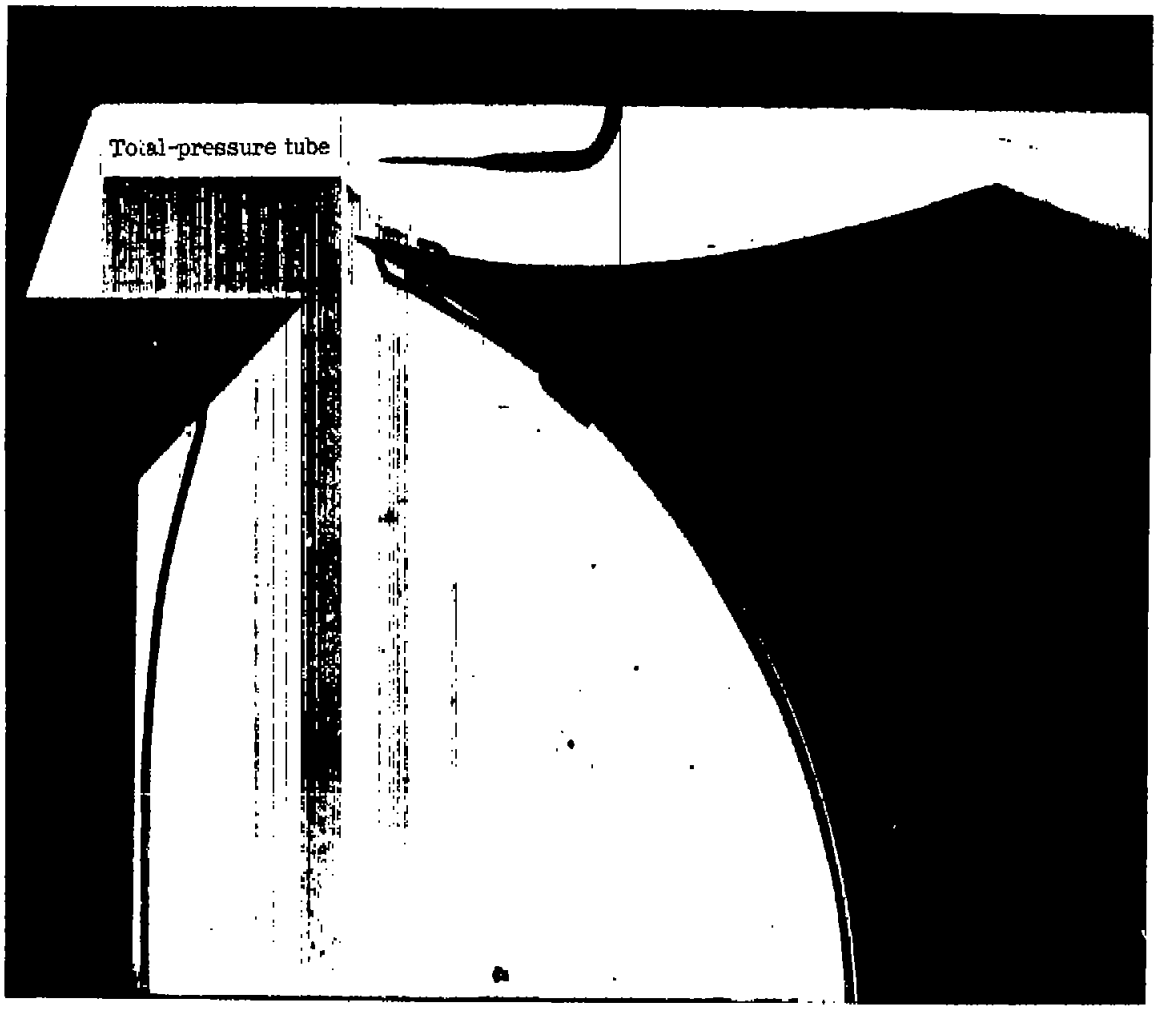

Figure 40.- A photograph of the angle of attack setup without flow.

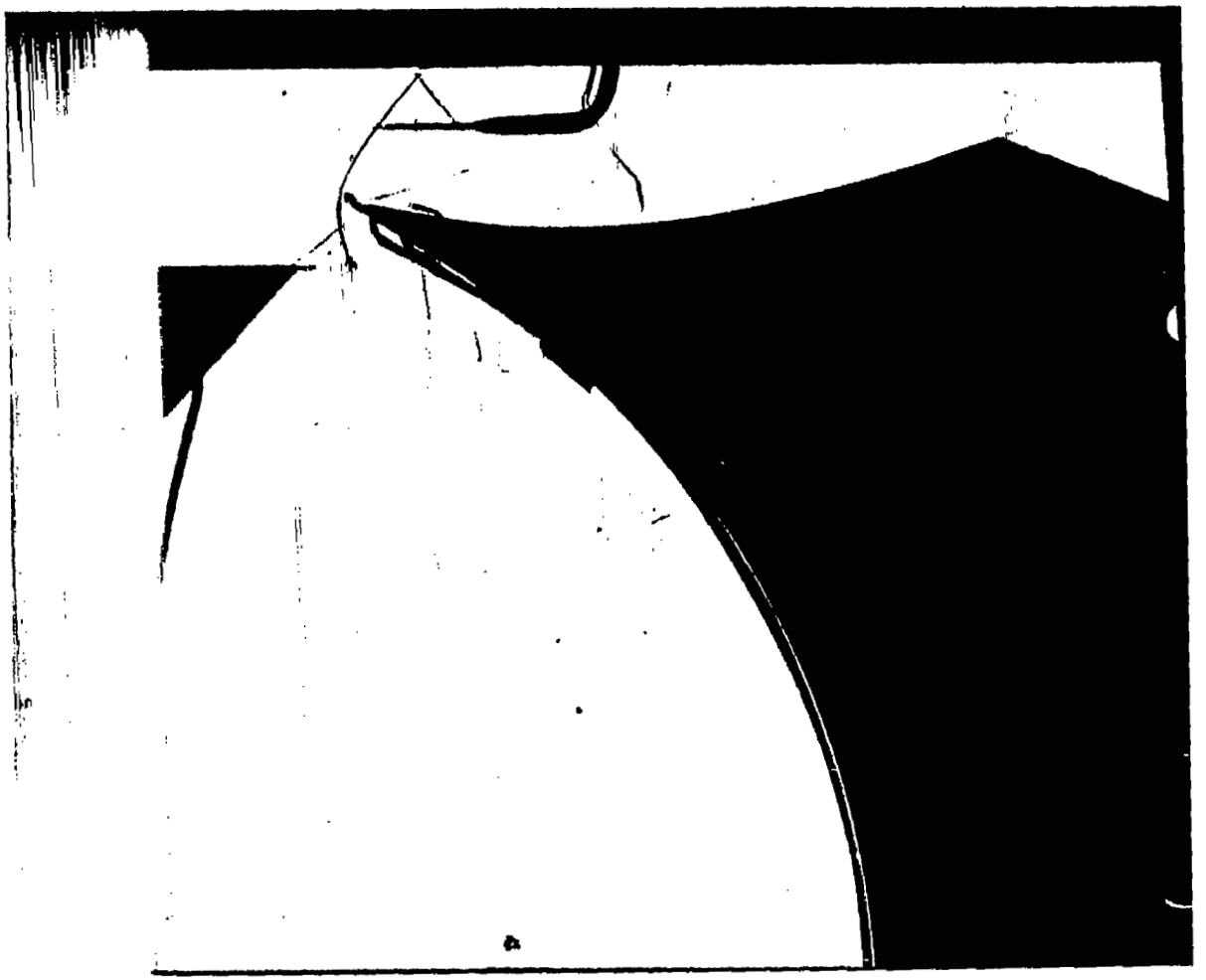

Figure 41.- A shadowgraph of the flow at an angle of attack of 29.83°.

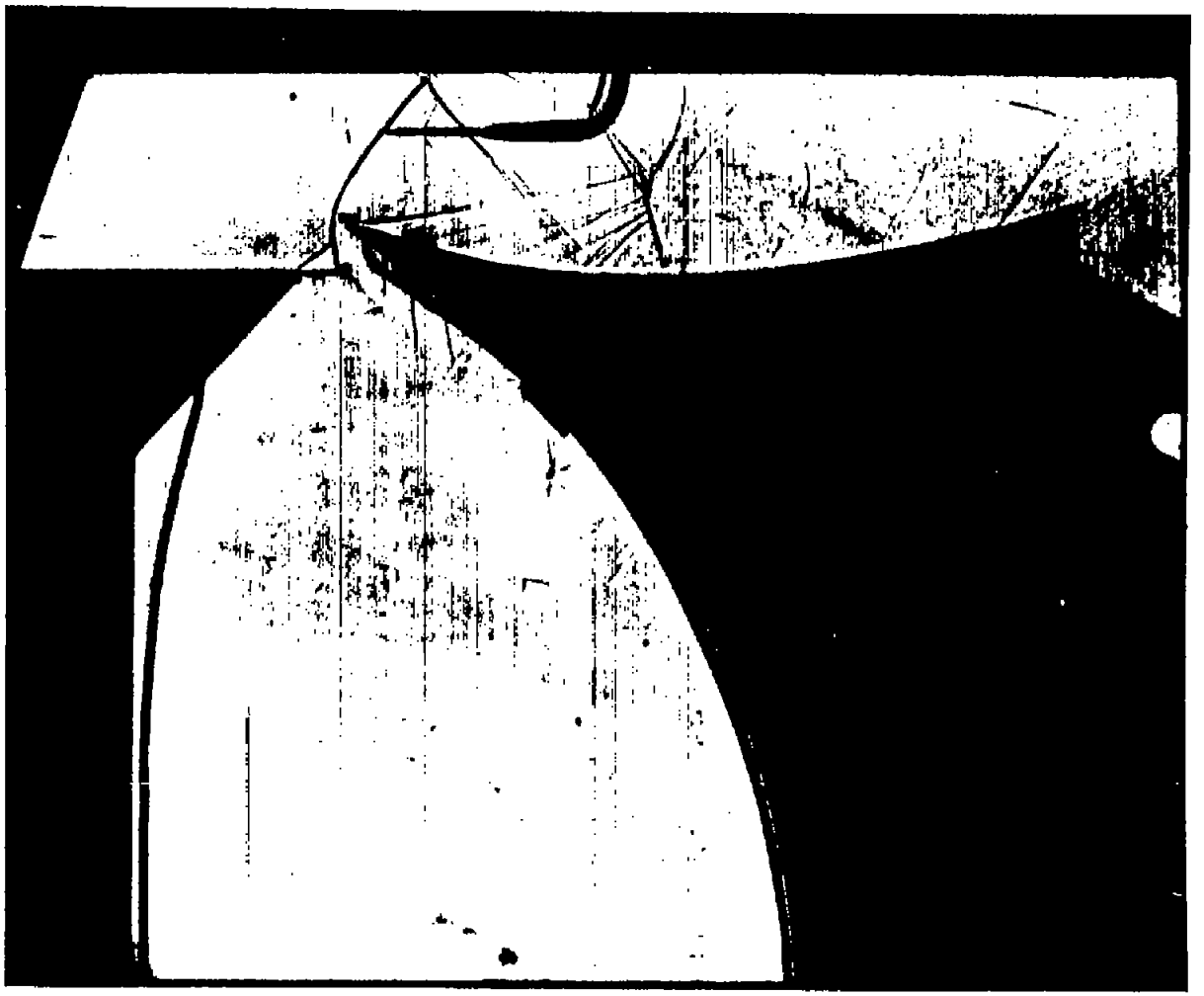

Figure 42.— A shadowgraph of the flow at an angle of attack of 35°.

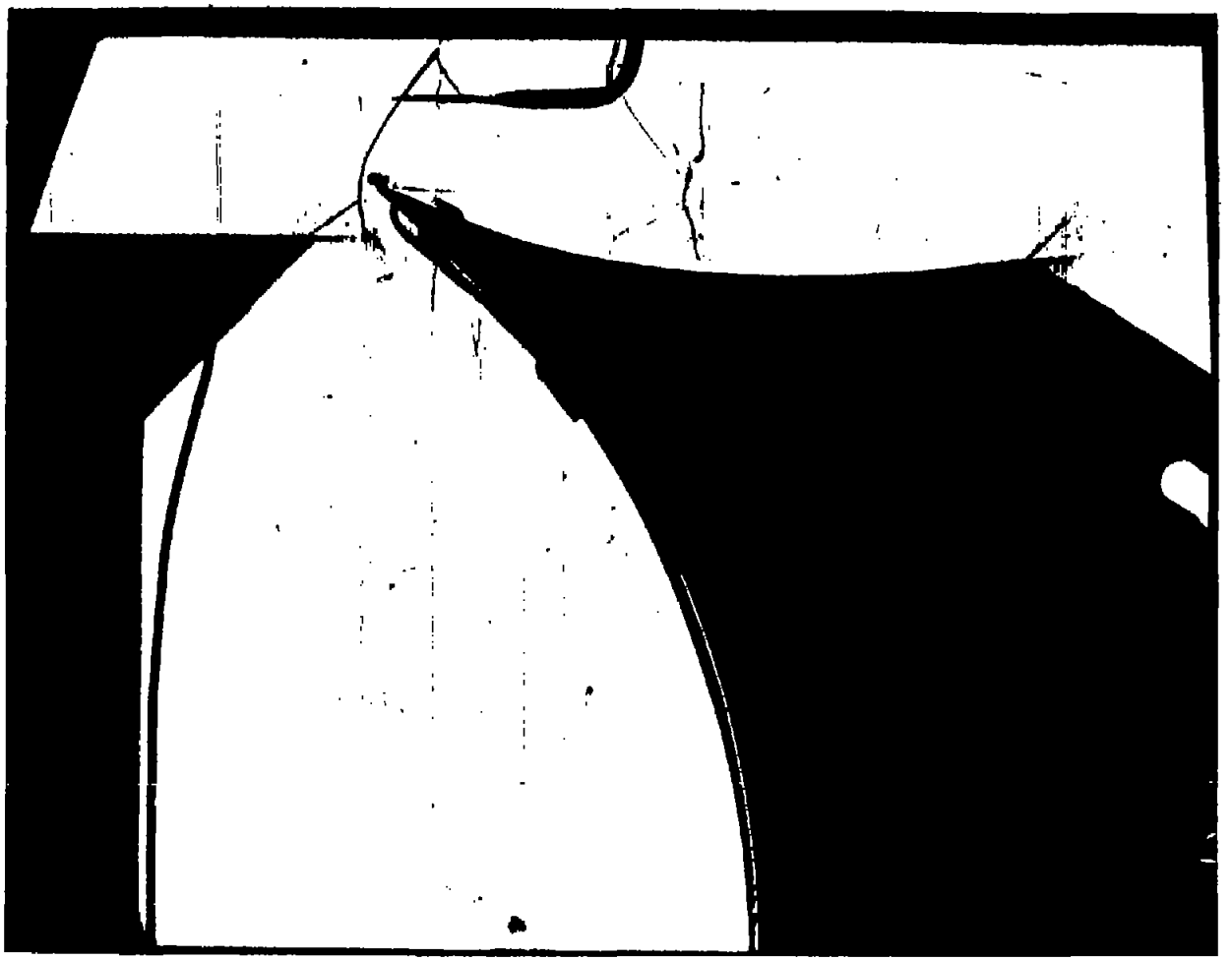

Figure 43.– A shadowgraph of the flow at an angle of attack of 40.08°.

NACA-Langley - 9-12-49 - 300

NASA Technical Library
3 1176 01436 7610